Magnetoreception in *Arabidopsis thaliana*: Effects of geomagnetic fields on transcription and translation

Dissertation
zur
Erlangung des Doktorgrades
der Naturwissenschaften
(Dr. rer. nat.)

dem
Fachbereich Biologie
der Philipps-Universität Marburg

vorgelegt von
Sunil Kumar Dhiman
aus Rae Bareli (Indien)

Marburg/Lahn 2013

Die Untersuchungen zur vorliegenden Arbeit wurden im Zeitraum von April 2008 bis Oktober 2013 am Fachbereich Biologie der Philipps-Universität Marburg unter der Leitung von Herrn Prof. Dr. Paul Galland durchgeführt.

Von Fachbereich Biologie der Philipps-Universität Marburg als Dissertation angenommen am: 24.10.2013

Erstgutachter: Prof. Dr. Paul Galland
Zweitgutachter: Prof. Dr. Alfred Batschauer

Tag der mündlichen Prüfung am:

Table of Contents

List of Abbreviations

µT	microtesla
8-HDF	8-hydroxy-7,8-didemethyl-5-deazariboflavin
ALP	Alkaline phosphatise
APS	Ammonium persulphate
AVTD	anomalous viscosity time dependence
B0	Magnetic field
B_{AC}	ELF magnetic field
BCA	Bicinchoninic acid
B_{DC}	static magnetic field
BSA	Bovine Serum Albumin
cDNA	complementary DNA
cab4	chlorophyll a/b binding protein gene
chs	chalcone synthase gene
COP1	constitutive photomorphogenic 1
CRY1, CRY2	Cryptochrome 1, Cryptochrome 2
cry1cry2	cryptochrome 1 cryptochrome 2 double mutant
Ct	cycle threshold
DTT	Dithiothreitol
EDTA	Ethylenediaminetetraacetic acid
ef1	elongation factor-1 gene
ELF	Extremely low frequency magnetic fields
FAD	Flavin adenine dinucleotide
h	Planck's constant
hemb2	porphobilinogen synthase gene
HIOMT	hydroxyindole-O-methyltransferase
ICR	Ion-cyclotron resonance
IPR	Ion-parametric resonance
ISC	Inter-system crossing
L	Angular momentum
LED	Light Emitting Diode
Ler	Landsberg erecta
Lhca4	Light harvesting complex-4

lyc	lycopene cyclase gene
mT	millitesla
MTHF	5,10- methenyltetrahydrofolate
NBT/BCIP	Nitro blue tetrazolium /5-bromo-4-chloro-3-indolyl phosphate
nos1	nitric oxide synthase gene
pal4	phenylalanine ammonia lyase-4 gene
PCR	polymerase chain reaction
pds	phytoene dehydrogenase gene
PHR	Photolyase Homology Region
phyAphyB	phytochrome A phytochrome B double mutant
PvDF	Polyvinylidene floride
q	ion charge
QPCR	Quantitative Polymerase Chain Reaction
rbcl	large subunit of RuBisCO gene
RBCL	Large Sub-unit RuBisCO
rca	rubisco activase gene
rpm	rotations per minute
rps	rotations per second
RuBisCO	Ribulose-1,5-bisphosphate-carboxylase
SD	Standard deviation
SDS	Sodium-dodecyl-sulphate
SDS-PAGE	Sodium Dodecyl Sulfate Polyacrylamide Gel Electrophoresis
SE	Standard error
SQUID	superconducting quantum interference device
T	Tesla
TBS	Tris-buffered saline
TCA	Trichloroacetic acid
TEMED	Tetramethylethylenediamine
Tris	tris(hydroxymethyl)aminomethane
TRP	Tryptophan
Wb	Weber

Summary

Very little is known about the effects of geomagnetic fields on plants. The present work was undertaken to answer the question whether plants can perceive the geomagnetic fields (Galland and Pazur 2005).

Our findings show that the effects of magnetic fields on various responses in *Arabidopsis thaliana* result in a characteristic multi-peaked pattern in the stimulus-response curves with multiple maxima (peaks) and minima (valleys). These multi-peaked stimulus-response curves display a unique phenomenon in biology. They are distinctively different from the stimulus-response curves, observed in plant physiology, showing a pattern of rising exponential functions, with a plateau finally.

The magnetic response also depended upon the fluence rate of the overhead light, the responses being higher at higher fluence rates. However, the magnetic fields apparently are able to manifest their effects even in darkness. The two double mutants displayed variations in their response to magnetic fields, as compared to *Ler* seedlings, although the basic pattern of effects remained the same. Additionally the effects were enhanced in *phyAphyB* double mutants as compared to *cry1cry2* double mutants indicating suppression of cryptochrome-mediated magnetic effects by phytochromes.

These stimulus-response curves are difficult to explain on the basis of the criteria required by the radical-pair model. The effects of magnetic fields were observed not only in darkness but also in *cry1cry2* double mutants. Experiments also revealed responses of the *Arabidopsis* seedlings to magnetic fields even under red light. Interestingly our data are in good correlation with data obtained by Binhi (2001) while working on DNA of *E. coli*. They got similar stimulus-response curves with similar peak positions as have been observed by us. Binhi and coworkers explained their observations in the theoretical framework of the "ion-interference mechanism".

A comparison of the effects of magnetic fields of the various organizational levels of *Arabidopsis* plant, i.e., on hypocotyl length, anthocyanin accumulation, abundance of specific mRNA's and proteins reveal maximum effects on gene transcription (12-fold approx.), which were reduced to about 6-fold in case of anthocyanin accumulation and were further reduced to only about 2.5-fold in case of suppression of hypocotyl length by blue light in *Arabidopsis*. We, therefore state that the effects at transcriptional level get balanced out at higher levels of organization (biochemical pathway, growth response) in order to provide "Magnetohomeostasis".

1 Introduction

Life on earth has evolved and existed with its magnetic field. With such a low magnitude, its effects on living systems seems to be incomprehensible, but still we have a vast body of literature showing the effects of geomagnetic field on the living organisms, with possible theories of mechanism of the actions and their explanations. Some of these living forms have even put the geomagnetic field to some use particularly in their orientation. Most of these studies have primarily been done on animals. With respect to plants, unfortunately, the issue of the perception of geomagnetic field and its affects on their system, has largely remained ignored, even though there have been some initiatives on the subject quite early (e.g. Ssawostin 1930a,b) The present work was therefore, perceived to look for the answers of the questions put forward by Galland and Pazur, 2005 :

1) Do plants perceive the geomagnetic field?
2) If yes, which biological molecule act as the magnetoreceptor and what is its mode of action?
3) Is the geomagnetic field necessary for the existence of plants?

1.1 Geomagnetic Field

Geomagnetic field is the magnetic field associated with the earth, and is similar to a bar magnet, with the two poles located at a distance from the geographical poles, and tilted at an angle of 11° with respect to the rotational axis of the earth. This geomagnetic field seems to be a critical factor in protecting the life from the solar winds, as these winds have potential, in the absence of geomagnetic field, to strip away the ozone layer and rendering the earth surface exposed to the brutal UV rays (Birk et al. 2004; Quirin Schiermeier 2005).

The magnetic field lines emerge from the earth surface at the magnetic north and re-enter at the earth's surface at the magnetic south, traversing halfway around the globe (Fig.1.1). They are pointing perpendicularly upwards at the magnetic north pole, running horizontally to the magnetic equator, and directed perpendicularly downwards at the magnetic sorth pole. Between the magnetic equator and the magnetic poles, the magnetic lines emerge and re-enter at an angle less than 90° to the earth's surface. This angle at a particular place on earth is known as Magnetic inclination or dip. Therefore the magnetic dip is +90° at the northern magnetic pole, 0° at the magnetic equator and -90° at the southern magnetic pole. Magnetic declination at a place on earth is an angle between the magnetic south and the true north of the earth. The declination is positive or negative when the magnetic sorth is on east or west of

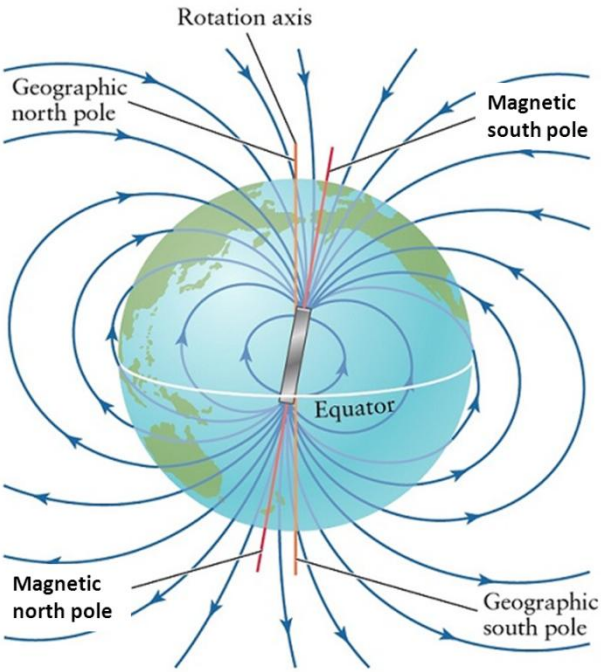

Fig 1.1: The magnetic field of earth. The axis of magnetic field of earth is slightly tilted with respect to the rotational axis, having north Pole and the south Pole on either of its ends. Therefore we have a geographic North pole that is different from magnetic sorth pole and similarly a geographic South pole located differently than the magnetic nouth pole. Magnetic field lines emerge from the magnetic nouth pole, so they are vertical at this position. As we move towards equator these lines gradually bend towards the surface of the earth and finally become parallel to earth's surface at equator. Further ahead towards magnetic sorth pole these magnetic lines are bending more towards the earth and finally enter the earth (modified from patina.ac.th).

true north respectively. The inclination and declination along with the geomagnetic field intensity are very significant in the context of navigation of animals.

The source of geomagnetic field is self-sustaining geodynamo present in Earth's core which is run by the convective forces of the molten iron. This geodynamo is working since 3.5 billion years ago (Tarduno et al. 2010). The intensity of the magnetic field varies on the surface of the globe. It is 25 µT at the equator and as one goes to the poles it gradually increases to 75 µT (König et al. 1981; Merrill et al. 1998). For a particular place the geomagnetic field is static and homogenous, although there may be minute variations due to electromagnetic radiations coming from the sun. Solar winds and magnetic storms can also influence the intensity, but these alterations are usually very small. Paleomagnetic studies for the past 160 milion years suggest that the average field intensity in the past has been about half of the present times (Juárez et al. 1998).

The position of the two magnetic poles is not static. They are wandering independent of each other. Apart from this, there have been instances where the geomagnetic polarity has reversed. The paleomagnetic data indicate that such reversals have occurred hundreds of times

during the magnetic life of the earth. The reversal process can take thousands of years and during these periods there is steep reduction, even below 10% of the average of existing value, of the magnetic field intensity (Birk et al. 2004).

Magnetic field strength is measured as magnetic flux density, which is denoted by 'B' and its SI unit is Tesla (T). The dimension of "magnetic flux" denoted by 'Φ' is Weber (Wb), so the magnetic flux density of one Tesla can defined as one weber per square meter i.e.

$$B = 1\ T = 1\ \frac{Wb}{m^2}$$

The Tesla can also be expressed as

$$1\ T = 1\ \frac{Kg}{As^2} = 1\ \frac{Vs}{m^2} = 1\ \frac{N}{Am} = 1\ \frac{J}{Am^2} = B$$

where, A = ampere
J = joule
Kg = kilogram
m = meter
N = newton
s = second
T = tesla
V = volt

The geomagnetic field has been shown to influence various biological processes. These include orientation, biological rhythms and developments (Galland and Pazur 2005). Out of these the orientation of animals has attracted the most attention from researchers.

1.2 Magnetoreception in Prokaryotes

Magnetotaxis in magnetotactic bacteria is very well understood example of magnetoreception and orientation. Magnetotactic bacteria are a heterogeneous group among prokaryotes which are motile, mostly acquatic, gram negative and possess magnetosomes, exemplified by many species of *Magnetospirillum* (Fig. 1.2). These magnetosomes are the magnetoreceptors which perceive the geomagnetic field and this information is used by the bacteria to orient themselves to their advantage.

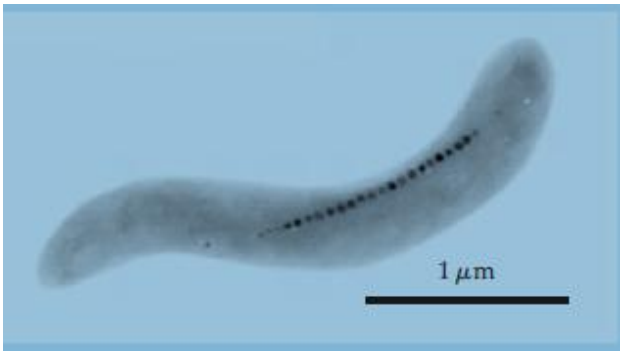

Fig 1.2: Magnetotactic bacteria. Transmission electron micrograph of *Magnetospirillum magnetotacticum* displaying the chain of magnetosomes within the cell (Johnsen and Lohmann 2008).

Magnetosomes are intracellular membrane bound crystals of magnetite minerals which are of a single magnetic domain i.e. either magnetite (Fe_3O_4) or greigite (Fe_3S_4). Within a bacterium, magnetosomes are arranged in one or more chains that provide dipole moment to the cell that aligns the bacteria along the geomagnetic field lines (Bazylinski and Moskowitz 1997). The passive alignment of the cell along with the active swimming of bacteria is known as magnetotaxis (Bazylinski 2004).

Morphology of mineral crystals in magnetosomes is conserved in a particular species or strain of magnetotactic bacterium (Bazylinski et al. 1995) indicating a very precise biomineralisation of these crystals. Crystals of magnetite having morphology similar to those of strain MV 1, a marine magnetotactic bacterium, have also been reported from martian meteorite named ALH84001. These crystals meet almost all the criterions for biogenic Fe_3O_4 indicating ancient presence of life on Mars (Bazylinski 2004).

1.3 Magnetoreception in Protists

Magnetosomes with similar morphology to that of magnetotactic bacteria have also been reported from many protists inhabiting coastal salt ponds which were chemically stratified. These are many biflagellates Cryptomonads, a dinoflagellate and a ciliate, *Cyclidium* (Bazylinski et al. 2000). Magnetosomes were also observed in a phytoflagellate, *Anisonema* belonging to Euglenophyceae. They were isolated from coastal mangrove swamps in northeastern Brazil and had many magnetite crystals arranged in chains (Torres de Araujo et al. 1986).

The origin of magnetosomes in these protists is still unknown as there is no evidence showing the endosymbiotic presence of magnetotactic bacteria and also there were no

observations of engulfment of these bacteria by the protists (Bazylinski et al. 2000). However it has been suggested that magnetosomes might have been acquired by the ingestion of magnetosome-containing bacteria (Neves et al. 2003).

Apart from magnetotaxis, it has been suggested that the magnetosomes in protists, could play a very important role in iron cycling in the chemically stratified anoxic basins (Bazylinski et al. 2000).

1.4 Magnetoreception in Animals

There has been a great deal of work done on the magnetoreception in animals and the research has provided insight in the understanding of the biophysical mechanism behind the phenomenon. In case of invertebrates, the magnetic orientation behaviour studies on nudibranch mollusc *Tritonia diomedea* have indicated that the mollusc orients in the geomagnetic field (Lohmann and Willows 1987). Our understanding on the magnetoreception on eusocial insects such as honey bees, ants, wasps and termites is elevated by a very comprehensive review by Wajnberg et al. (2010). The authors have not only presented the broad survey of the magnetic orientation behavior of these insects but also emphasized on search for the magnetic minerals in their body parts and tissue samples using various techniques like ferromagnetic resonance absorption, electron paramagnetic resonance, magnetometry using high precision SQUID magnetometer and transmission electron microscopy. Apart from studies on eusocial insects, presence of inclination compass has been reported in mealworm beetle *Tenebrio molitor* (Vácha et al. 2008). Similarly very strong evidences have been put forward for the light dependent magnetosensitivity in *Drosophila* (Gegear et al. 2008).

In case of vertebrates, some animals of all the five classes have been shown to be sensitive to the geomagnetic field with the help of behavioral experiments and respond to it as an orientation hint for their migration, homing or moving around their habitat (Wiltschko and Wiltschko 1995). Many fishes have the ability to orient to the magnetic field. Marine elasmobranch fishes like sharks, rays and skates have been demonstrated to show magnetosensitivity through a system of canals and the ampullae of Lorenzini in their heads (Jonsen and Lohmann 2008). Presence of magnetite bearing cells in trout nose of sockeye salmon and the same region innervated by ros V nerve, along with the electrophysiological observations suggest that the magnetite containing cells act as magnetoreceptors and pass the information to brain through ros V nerve (Jonsen and Lohmann 2005).

Experiments with salamanders showed that these animals also have the ability for magnetic field reception which is light dependent. Salamanders could orient normally only in short wavelength (upto 450nm), as the wavelength was increased beyond 450nm, they started disorienting. Under the exposure of light of wavelength of 500nm and above, the animal's disorientation was shifted approximately 90° to the normal (Phillips and Borland 1992b). Comparable light dependent magnetic 90° shift in orientation behavior has also been observed in bullfrog tadpoles (Phillips et al. 2010).

Studies on marine migrations across the Atlantic Ocean by young loggerhead sea turtles (*Caretta caretta*) imply that young hatchlings can sense the inclination angles of the geomagnetic field and can also sense the magnetic field intensity. It indicates that these young ones have the ability to map their location along their navigational route (Cain et al. 2005).

Magnetoreception in birds has attracted attention by many scholars because of its involvement in spectacular long distance migrations of some birds and therefore is widely studied phenomenon which has led to resolving the puzzle of sensing the magnetic field to a certain extent. Wiltschko and Wiltschko (2005) have provided a broad overview on the subject by focusing on its various intriguing aspects. Authors have suggested the presence of two magnetoreceptor systems in birds for assimilating different forms of magnetic field information i e. directional and its magnitude.

Mammals have got very little attention by the researchers in the field. There have been work on subterranean rodents, bats, cattle, deers and hunting foxes and was found that these mammals can sense the geomagnetic field and orient themselves accordingly (Begall et al. 2008; Begall et al. 2013). Ivestigations done with the social giant mole-rat, *Fukomys mechowii*, and the solitary silvery mole-rat, *Heliophobius argenteocinereus*, have revealed that they use light-independent magnetic compass for near space orientation (Oliveriusová L et al. 2012).

There is hardly any evidence that humans are capable of sensing geomagnetic field, however human CRY2 found in the eye. when expressed in *Drosophila* by transgenic method, could function as magnetoreceptor of the magnetoreception system of these flies (Foley et al. 2011)

1.5 Magnetoreception in Plants

Since the research in the field of magnetoreception has been primarily focused on the orientation and navigational aspects of animals, the phenomenon got very little attention in case of plants. But significance of the effects of geomagnetic field on plants can be gauged by the fact that even very minute changes in the geomagnetic fields caused by geomagnetic storms due to increased solar activity leads to nuclear anomalies like polyploidy, giant nuclei or multinucleate cells in the apical meristems of *Allium cepa* (Nanush'yan and Murashev 2003). Let us have a look on the effects of the magnetic field on the plants in a broad perspective. It can be described under the following headings:

- Effects under weak homogeneous magnetic fields
- Effects under zero or very weak magnetic fields
- Effects under strong static homogeneous magnetic fields

1.5.1 Effects on plants in weak homogenous magnetic fields

This also refers to the effects of geomagnetic field on plants as the earth's magnetic field ranges between 25 μT at the equator to 75 μT at either of the poles. Similar to the magnetotaxis shown by magnetotactic bacteria, *Volvox aureus*, a colonial green alga, has the tendency to swim parallel to the horizontal components of the geomagnetic field (Palmer 1963). Such preferences for orientation were also reported in angiosperms, for example, caryopsis of *Hordeum vulgare, Avena sativa, Secale cereale* and *Triticum aestivum* and the seeds of flax germinated and grew faster when they were oriented parallel to the geomagnetic field lines as compared to those which were placed perpendicularly (Pittman 1963a, b). Better germination was also observed in caryopsis of *Zea mays* and *Triticum aestivum*, when their roots were oriented towards the south pole (Krylov and Tarakanova 1960). Experiments with roots of winter wheat, *Triticum aestivum* and Chinook spring wheat showed that they grew preferentially in the plane parallel to the geomagnetic field lines (Pittman 1962, 1964). However the roots of other varieties of wheat and that of *Secale cereale* did not show such magneto-orientation which indicates that not all plants have the capability to respond to magnetic fields.

A surprising and incomprehensible phenomenon was observed that could be related to magnetoreception when plants were subjected to daily rotations (Galland and Pazur 2005). When the plants of *Cyclamen, Phaseolus coccineus* and seedlings of *Avena sativa* were rotated clockwise, they showed suppressed growth and also showed the symptoms of partial senescence. On the other hand when they were rotated counterclockwise, a speedy growth

was noticed (Jones 1960). Brown and Chow (1975) have stated that such observations of affirmative and negative responses in plants due to rotational influence are mediated by geomagnetic field as some of these responses were abolished in the weak field of a slowly rotating (1 rpm, clockwise) bar magnet.

1.5.2 Effects on plants in zero or very weak magnetic fields

The effects of very low magnetic fields are also complex. Some of the notable effects are the ultrastructural changes in the meristmatic cells of plants, for example, *Pisum sativum* plants grown in magnetically shielded boxes showed accumulation of lipid bodies, development of lytic compartment such as vacuoles, cytosegresomes or paramural bodies, reduction of phytoferritins in plastids, increased size of mitochondria with matrix becoming electron transparent along with reduced cristae, in their meristmatic roots cells (Belyavskaya 2001). Similar abnormal morphology of mitochondria was also observed in meristmatic root cells of *Linum usitatissimum* and *Lens culinaris* (Zhadin 2001). A reduced RNA and protein synthesis was also noticed along with reduced proliferation of root meristem by some plants (68-78%) (Fomichjova et al. 1992a, b; Zhadin 2001). Such ultrastructural changes were accompanied by increase in epicotyl growth (Negishi et al. 1999). Branching was also found to be affected at near zero fields (Govorun et al.1992; Zhadin 2001). Experiments with somatic embryos of *Quercus suber* under shielded geomagnetic field, showed that their germination is promoted in weak fields (Celestino et al. 1998). Growth of *Euglena* and *Chlorella* was also accelerated in weak fields (0.1 μT) (Halpern 1966; Halpern and van Dyke 1966).

Hairy roots induced by *Agrobacterium* infection in *Daucus carota* and *Belladona* showed higher growth rates at 5 nT as compared to their growth rate in geomagnetic field (Kato et al. 1989). Roots of *Zea mays* seedlings displayed a bigger gravitropic curvature when maintained under very low magnetic field (5 nT) in contrast to the seedlings grown in geomagnetic field (Kato 1988, 1990). Similarly gravitropism is stimulated in etiolated seedlings of *Linum bienne*, under very low magnetic field conditions (Belova and Lednev 2001a).

In a recent work done on *Arabidopsis* under very low magnetic field show that their hypocotyls were significantly longer as compared to seedlings grown in geomagnetic field. However the same authors observed a delay in flowering in the *Arabidopsis* plants grown in

near null fields as compared to plants that were raised in geomagnetic field (Chunxiao Xu and Tao Song 2012).

1.5.3 Effects on plants in strong static homogeneous magnetic fields

Majority of the experiments done with strong magnetic fields were inspired by the thought that it could help in increasing agricultural yield. For instance, pre-magnetic treatment of seeds of groundnut improved their germination rates and also the vigour of the seedlings (Vakharia et al. 1991). Similar observations were made with seeds of *Oryza sativa* and *Allium cepa* (Alexander and Doijode 1995), *Solanum tuberosum* (Imimoto et al. 1996) and *Lycopersicon esculentum* (Dayal and Singh 1986). Seeds of *Lactuca sativa* showed enhanced water uptake when they were pre-treated with weak and moderate magnetic fields (0-10 mT) (García-Reina et al. 2001). About 70% increase in chlorophyll and protein contents was observed in onion, when grown in strong magnetic fields (505 μT). Such an enhancement was associated with stimulated leaf length of about 40% (Novitsky et al. 2001). Many more examples have been listed by Galland and Pazur (2005) and reviewed by Drobig (1988), which includes primarily the effects of strong magnetic fields on agriculturally important plants. A very dramatic effect of strong magnetic fields is induction or inhibition of cyclosis (cytoplasmic rotational movements) in *Chara, Elodea* and *Vallisneria* (Ssawostin 1930a).

1.6 Effects of magnetic fields on enzyme activity

There are only few reports of enzyme activities in relation to magnetic fields in plants. The enzyme esterase from *Triticum aestivum* shows increased activity to a treatment of 30 mT of magnetic field (Aksenov et al. 2000). The function of peroxidase from horseradish is influenced by the frequency of the applied magnetic fields (Portaccio et al. 2005). Similarly the enzyme carboxydismutase from *Spinacia oleracea* chloroplasts shows an increased activity in strong magnetic fields (2 T) (Akoyunoglou 1964).

With respect to enzymes from animal system, there are far more reports, for example, in vitro studies of Ca^{2+}/calmodulin-dependent cyclic nucleotide phosphodiesterase at low magnetic field (20 μT) shows that its activity gets influenced in Ca^{2+}-dependent manner which also provides a clue that how geomagnetic field could be biologically significant in Ca-dependent reactions (Liboff et al. 2003). The two key enzymes, hydroxyindole-O-methyltransferase (HIOMT) and acetyl-serotonin transferase (NAT) of melatonin biosynthesis pathway in pineal gland and retina react to 50% increase and decrease in geomagnetic field, both in vivo and in vitro (Cremer-Bartels et al. 1984). The activity of cytochrome c oxidase is

shown to be effected by weak and moderate static as well as alternating fields (Nossol et al. 1993). An enhancement in the activity of trypsin (Cook and Smith 1964) and ornithine decarboxylase (Mullins et al. 1999) is reported under the influence of strong magnetic fields. More recently it has been shown that magnetic fields effect enzymatic ATP synthesis by creatine kinase extracted from *Vipera xanthia* venom (Buchachenko and Kuznetsov 2008).

With these examples and many more, particularly in animals, it seems that the enzymes could play the role of magnetoreceptor (Galland and Pazur 2005).

1.7 Effects of magnetic fields on membranes and Ca^{2+} signalling

Many biological effects caused by magnetic fields are supposed to be due to changes in the calcium flux associated with membranes and this is so because the membrane phospholipids possess diamagnetic anisotropic properties, which leads to their reorientation in the magnetic fields. This causes deformation in associated proteins channels (Galland and Pazur 2005). It has been shown that the Ca^{2+}-channels are more effected than Na^{+}-channels (Rosen 2003).

It has been experimentally shown that the static magnetic fields have the potential to influence the electrical behavior of cell membranes, including their ion fluxes (Galland and Pazur 2005). For instance, under the influence of magnetic fields with the magnitude similar to geomagnetic field, the electrical activity of the pineal cells is considerably altered (Semm et al. 1960). Similarly, in vitro radiation induced efflux of Ca^{2+} in brain tissue is also influenced by magnetic fields (Blackman et al. 1985). Static magnetic fields have been shown to inhibit the activity of Ca^{2+}-channels in GH3 cells (Rosen 1996). These observations clearly make the point that Ca^{2+}-channels could be a pivot in magnetic field sensitivity, which further has the potential to control the downstream reactions leading to the final effect.

1.8 Effects of magnetic fields on DNA and DNA-protein complexes

The mechanism of effects of magnetic fields on DNA is poorly understood. But it has been postulated that the magnetic fields may directly affect the physical status of DNA, leading to changes in transcriptional patterns. It has been argued that the current density in the interior of DNA, along the bases can be 0.5×10^{5} Am^{-2}, which is enough for the magnetic fields to interact directly with the DNA and to influence transcription (Blank and Goodman 1997, 1999). In the *E.coli*, it has been shown that weak static magnetic fields could stimulate conformational changes in their genome. The conformational state directly influences the

transcriptional status of the genes within the genome, thereby indicating another possibility of how magnetic fields could influence the gene expression (Alipov and Belyaev 1996).

1.9 Mechanisms and modals of magnetoreception

As we have seen, there are baffling varieties of effects of magnetic fields on living organisms and one needs the explanation to understand the mechanism behind the puzzling phenomenon. There have been some attempts to provide physical and chemical models for elucidating the mechanism.

1.9.1 Ferrimagnetism

This mechanism is based on the presence of ferromagnetic minerals in the living organism. These minerals are magnetite (Fe_3O_4) and greigite (Fe_3S_4) and form single-magnetic domain crystals which are membrane bound and are known as magnetosomes. These magnetosomes are arranged in chains and provide the organism with a permanent magnetic dipole moment that align the cells parallel to the magnetic field lines, similar to what happens to a compass needle (Blackmore 1982). Such a passive magnetic alignment with active swimming is known as magnetotaxis and is very common in magnetotactic bacteria (Bazylinski 2004).

Magnetosomes are the only conclusively demonstrated magnetoreceptors (Johnsen and Lohmann 2008). They are present in magnetotactic bacteria, many protists and variety of animals. Though magnetosomes are synthesized by bacteria themselves, the protists seem to have acquired them by ingestion of magnetosomes containing bacteria (Neves et al. 2003). Additionally, as the biogenic megnetites present in higher organisms are similar to those of magnetotactic bacteria, it is likely that early magnetotactic bacteria have contributed to the origin of magnetoreceptive eukaryotic cells (endosymbiotic theory) (Kirschvink and Hagedorn 2000). Seemingly ubiquitous presence of magnetites in animal kingdom, there presence in plants has not been reported (Lowenstam and Kirschvink 1985; Frankel 1990). Nevertheless ‘botanical magnetite’ was reported to be present in disrupted grass cells (Gajdardziska-Josifovska et al. 2001, 2002). Presence of phytoferritin in plant cells as crystalline magnetite (Fe_3O_4), ε-Fe_2O_3, and hematite (α-Fe_2O_3) has also been documented (McClean et al. 2001). Magnetite seem to be derived from phytoferritin have also been reported from wood ash (McClean and Kean 1993). It has also been found that some photosynthetic phytoflagellates like *Ochromonas* sp., *Chrysochromulina ericina* and

Thalassiosira pseudonana, has the ability to take up inorganic ion colloids by phagotrophy. These colloids also include magnetite (Nodwell and Price 2001).

The best evidence of magnetite based receptors has come from trout and homing pigeons. In trout, techniques like confocal and atomic force microscopy have revealed the presence of single domain magnetite crystals in the cells near to a nerve that is sensitive to magnetic stimuli. Similarly a part of the pigeon's beak, that has a complex array of magnetic minerals, has been found to be coupled to a nerve which is megnetoresponsive (Johnsen and Lohmann 2008).

At the moment the physiological function of these magnetites in plants is elusive. However if magnetites were part of the ionic channels in the cell membranes, they have the potential to generate torque in a weak magnetic field, that would be enough to influence the ionic transport across the membrane. This assumption, at least in theoretical terms, provides the mechanism that how magnetic fields could affect the physiology of plants (Kirschvink et al. 1992). It has also been found that if a single 100 nm magnetite crystal is exposed to 60 Hz, 0.1 mT magnetic field, it can absorb sufficient energy that will supersede thermal background noise manifold (Kobayashi et al. 1995).

1.9.2 Radical-Pair mechanism

It would be very difficult to comprehend that a chemical reaction could be sensitive to geomagnetic field as the energy of interaction of a molecule with an average of 50 μT earth's magnetic field is about 600 times smaller than the strength of a chemical bond (Rodgers and Hore 2009). However there are evidences that the birds can sense the geomagnetic field direction and such a sense is based upon a chemical reaction (Wiltschko 1968; Ritz and Schulten 2000; Wiltschko and Wiltschko 2006). These special chemical reactions involve radical pairs. Radical pairs are simply a pair of molecules having an unpaired electron, produced together in a reaction, with the spin of the unpaired electron being mutually related, and if in such a reaction the products are electron spin-dependent, then there is a possibility for the external magnetic field to influence the relative orientation of the spins of electron, thereby leading to effects caused by magnetic fields. The theory that the Radical pair reactions can act as magnetoreceptors was first proposed by Schulten in 1978. Since then more and more evidences are accruing for the support of the concept.

Fig. 1.3 demonstrates the functioning of the radical-pair mechanism. A molecule 'A-B' after homolysis generates two radicals i.e. $A^{\bullet}$ and $B^{\bullet}$. These radicals can exist together as a

pair having anti-parallel spins of their unpaired electrons (Wigner's conservation rule). Thus, as these radical pairs are formed they exist is the singlet state $^{1}[A^{\bullet}\ B^{\bullet}]$. But with the process of inter-system crossing (ISC), this radical pair can be interconverted to its triplet state, $^{3}[A^{\bullet}\ B^{\bullet}]$ where the electron spins are parallel to each other. The singlet radical pair $^{1}[A^{\bullet}\ B^{\bullet}]$ can recombine to form the parent molecule 'A-B', but the triplet radical pair $^{3}[A^{\bullet}\ B^{\bullet}]$ cannot do so, because electron pair of the chemical bonds in the parent molecule are in antiparallel spins (Pauli's exclusion principle). It must first come into singlet state to form the parent molecule. Such a situation prolongs the existence of the radical pairs and therefore increases the possibility of synthesis of the derivative products. Since the inter-system crossing (ISC) is prone to external magnetic fields, the generation of either singlet or triplet radical pairs could be modulated by applying external magnetic field, leading to an enhancement of the corresponding product. In addition to external magnetic fields, internal magnetic fields generated by magnetic moments of nuclei, also known as hyperfine coupling can modulate inter-system crossing (Galland and Pazur 2005).

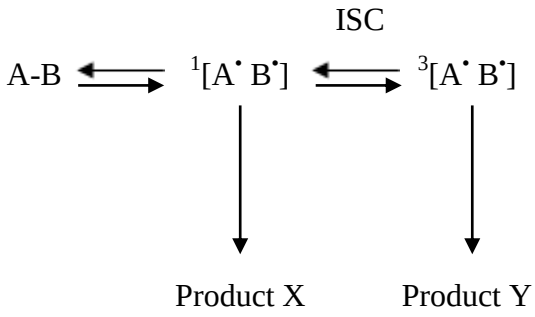

Fig. 1.3: Radical pair formation by the homolysis of 'A-B' and the interconversion of singlet and triplet states by inter-system crossing (ISC) (Galland and Pazur 2005).

A prerequisite for ISC to occur is that the radical pair should be held together for relatively longer time to the order of 10^{-6}s. After this time the spins get randomised (Galland and Pazur 2005). There are experimental evidences and also theoretical predictions which indicate that magnetic fields indeed prolong the lifetime of radicals, increase their average concentrations and also augment the probability of radical reactions with cellular components (Schulten et al. 1976; Scaiano et al. 1994; Walleczek 1995). Such preconditions also apply to enzymatic reaction that encompasses radical pair formation and recombination (Grissom 1995; Eichwald and Walleczek 1996).

It has also been made clear that in several organisms radical-pair mechanism is also light-dependent i.e. the radical pairs are photogenerated. Light is essential for magnetic

compass orientation in birds and salamanders, as when examined in total darkness, they were totally disoriented with respect to their directional movement (Wiltschko and Wiltschko 1981). Further evidences indicate that the cryptochrome, a FAD containing blue-light photoreceptor is responsible for magnetoreception in not only migratory birds but also in other organisms (Möller et al. 2004; Mouritsen et al. 2004; Gegear et al. 2008). Though formation of radical pairs by cryptochrome in birds eyes have not been shown yet, indirect evidence from *Arabidopsis thaliana* cryptochrome suggests that flavosemiquinone radical formed after photoreduction forms the radical pair in vitro (Giovani et al.2003).

Additional support for the radical-pair mechanism comes again from the work on *Arabidopsis*. Cryptochrome dependent responses like inhibition of growth of hypocotyl were found to be magnetic field sensitive. Plants grown in magnetic field strength of 500 μT grew remarkably slower as compared to the plants grown at 50 μT geomagnetic field. Such an effect was found only under blue light (Cryptochrome responds to blue light only) and was absent under red light as well as in darkness. Experiments with plants lacking cryptochrome genes (*cry1cry2* double mutants) did not show the inhibitory effect in either of the magnetic fields (Ahmad et al. 2007). Though these findings could not be replicated independently (Harris et al. 2009), but if turn out to be true, they provide a very strong support to radical-pair theory.

1.9.3 Ion-Cyclotron Resonance

In 1985 Liboff came up with another idea to explain the effects of low-frequency magnetic fields on living systems which he called ion-cyclotron resonance. This mechanism is based on the influence of Lorentzian forces on moving charged particles. When these moving charged particles are exposed to magnetic field which is oriented perpendicular to their path of movement, the particles experience the Lorentz force. Such a force keeps these particles moving in a circular path. However when the angle between the moving trajectory of moving particles and the magnetic field lines becomes less than 90°, the particles then take a helical path.

Movement of electrons around the nucleus creates magnetic moment that is proportional to angular momentum, L, of the electron, much like the momentum experienced by any circular moving object. When these electrons are subjected to external magnetic fields, that cause a torque on electrons, leads to a change, ΔL, of angular momentum of electrons (Fig. 1.4). Such a change results in precession of electrons around the magnetic field, B_0. The precession angular velocity also known as Larmor precession, (ω_{Larmor}) is given by:

$$\Omega_{\text{Larmor}} = \frac{d\phi}{dt} = \frac{B_0 \bullet e}{2 \bullet m_e} \quad (1)$$

Ion cyclotron resonance model assumes that many effects due to magnetic fields require the presence of static magnetic field (B_{DC}) as well as alternating magnetic field (B_{AC}). Accordingly the ICR formula is given by

$$f = \frac{B_{DC} \bullet q}{2\pi \bullet m} \quad (2)$$

where *q* is the ion charge and *m* is the ion mass.

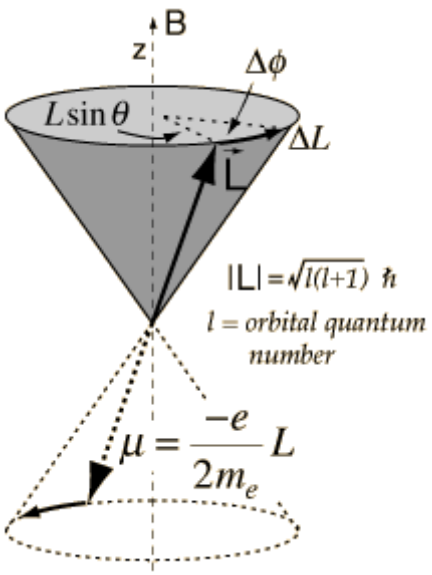

Fig 1.4: The Larmor precession of a charged particle around a magnetic field **B,** with the rotating angular momentum vector, **L** that circumscribes the surface of the cone. When the charged particles like electrons are subjected to external magnetic field **B,** which causes a torque on the particles, it leads to a change, Δ**L**, of angular momentum of the particles. Such a change results in precession of electrons around the magnetic field. This precession angular velocity is known as Larmor precession.

The equation 2 describes magnetic flux density, B_{DC}, of the static field and frequency, *f*, of the alternating magnetic field, B_{AC}, indicating that the resonance frequency depends upon the mass and the charge of the ion in question. So, alternating magnetic fields having frequencies specific for given ions, for instance, Ca^{2+}, K^{+}, Mg^{2+}, etc. can be given to the biological system under question. Resulting biological response would be expected to depend upon the ratio of the frequency of alternating magnetic field and the flux density of the static magnetic field. The effects due to ICR have been observed in vitro, even with the simple

electrolytes, for instance, experimenting on aqueous solutions of glutamic acid with a combination of static and alternating magnetic fields, investigators detected narrow resonance frequency bands for magnetically induced ion currents which obeyed Eq. 2 (Zhadin et al. 1998).

As explained by Liboff (1985) Ca^{2+} ions moving in a helical pathway, within membrane-bound proteins that constitute ion channels, when exposed to geomagnetic fields lines are accelerated due to cyclotron resonance (as a consequence of superimposition of ELF magnetic field and geomagnetic field) , and the result is increased influx of these ions. Such a condition potentially can alter the equilibrium of the biochemical reactions and therefore explains the cause of the effects of ELF magnetic fields. Using the superimposition of two magnetic fields ($\mathbf{B}_{AC}$ and $\mathbf{B}_{DC}$), many in vitro effects (Zhadin et al. 1998; Pazur 2004; Baureus Koch et al. 2003) and physiological responses (Smith 1987) were found, which showed frequency and ion-specificity (Del Guidice et al. 2002). So, the ICR model provides a frequency-specific absorption of electromagnetic fields by ions and their movement in weak magnetic fields, for example, with respect to Ca^{2+} ions, near 50-60 Hz, frequency-specific absorption is predicted, which also is frequency of power lines worldwide (Sandweiss 1990; Durney et al. 1988).

Ion-parametric resonance (IPR) model (Lednev 1991; Blanchard and Blackman 1994) was also presented which is a modification of ICR model, to overcome some drawbacks of ICR model. In case of ICR model, ELF magnetic field effects and their narrow frequencies are predicted at cyclotron frequencies and their harmonics (Liboff 1997), whereas in IPR model, the magnetic effects are predicted at cyclotron frequencies and their subharmonics (Lednev 1991; Blanchard and Blackman 1994). The IPR model takes into account the real conditions of the ion in the cell, such as its binding to the proteins ligands, so it allows the description of ion in its natural environment within the cell. Otherwise the IPR model is same as ICR, as it requires the presence of both static magnetic field ($\mathbf{B}_{DC}$) and ELF magnetic field ($\mathbf{B}_{AC}$) and their superimposition. The probability of the biological effect depends upon the magnitudes of $\mathbf{B}_{AC}$ and $\mathbf{B}_{DC}$ and also on their angular frequency (Galland and Pazur 2005).

The ion-resonance models could explain the effects of magnetic fields on the biological system to certain extent and their strength lies in the fact that they are able to make specific predictions about the type of ions, which are interacting with the magnetic fields to show the response. ICR model have been put to test for Ca^{2+}, K^{+} and Mg^{2+} ions in germinating seeds experiments in radish (Smith et al. 1995) and the IPR model was also tested in the

experiments with bioluminescence of dinoflagellate, *Gonyaulax scrippsae* (Berden et al. 2001)

A major drawback of the ion-resonance model is that they take into account the presence of ELF magnetic field ($\mathbf{B}_{AC}$) as well as static magnetic fields ($\mathbf{B}_{DC}$) and their superimposition for the resulting response. Contradictorily, it has been shown that static magnetic fields alone can have the same effects as those observed with simultaneous application of AC/DC magnetic fields (Belyaev et al. 1994).

1.9.4 Ion-Interference mechanism

To explain the biological effects of static magnetic fields ($\mathbf{B}_{DC}$), that were unexplainable by ion-cyclotron or ion-parametric resonance mechanism, Binhi (1997a), came up with another model known as ion-interference mechanism. It is a quantum-mechanical mechanism that is based on interference of quantum states of ions bound to protein inside an idealized cavity. As explained by Binhi et al. (2001), the superposition of ion states due to interference brings about a non-uniform pattern of probability density of the ion. Such a pattern is in the form of a row of almost dense segments. When exposed to DC fields, such a pattern rotates within the cavity with the cyclotron frequency. However when exposed to AC fields of specific parameter impedes the rotation and promotes the escape of the ion from the cavity. This escape potentially can bring about changes in the equilibrium of biological reactions to show a biological effect eventually.

The theoretical predictions calculated for the ion-interference mechanism were in good agreement with some effects due to exposure to combined DC/AC magnetic fields (Binhi 1997b). However, in the presence of DC fields alone, the mechanism predicts only one peak which should be observed at ‘‘zero’’ static magnetic field. In contrast, the experimental observations with *E. coli* cells revealed several peaks when exposed to only DC magnetic fields (Belyaev et al. 1994). To explain such anomaly, Binhi et al. (2001) made an assumption that these additional peaks are achievable, if the static DC magnetic field exposed ion-protein complexes are rotating inside the cell.

Binhi et al. (2001) showed the effects of static magnetic fields experimentally on the confirmation of DNA-protein complexes (nucleoids) in *E.coli* cells and compared the experimental observations with theoretical calculations based on ion-interference mechanism. The results of the theoretical calculations for Ca^{2+}, Mg^{2+} and Zn^{2+} showed a remarkable consistency with the experimental data. The logic for this comparison was based on the well-

known fact that the conformational state of chromatin substantially depends on the concentration of different ions. For instance, in V-79 cells, Na^+ ion concentration relaxes the chromatin whereas Mg^{2+} ion concentration leads to condensation of chromatin (Heussen et al. 1987). Inhibition of ELF magnetic field effects were also observed when EGTA, the specific chelator of Ca^{2+} ions was used in the growth medium (Belyaev et al. 1999).

The effects due to static magnetic fields in *E. coli* cells were shown in terms of changes in the conformational state of the genome, which was measured using the method of anomalous viscosity time dependence (AVTD). The anomalous viscosity time dependence strongly depends on the conformational state of the genome, which further is dependent on various other factors, important being the number of proteins bound to DNA. Another assay, called comet assay has directly confirmed that the increase in AVTD peaks are due to relaxation of DNA loops, whereas the decrease in peaks is as a result of condensation of chromatin (Belyaev et al. 1999a).

The results showed increased maximum relative viscosity in four windows, 0 ± 1, 43 ± 2, 72 ± 3, and 96 ± 3 μT magnetic field and a decrease of relative viscosity was observed in other four windows, i.e. 26 ± 2, 61 ± 2, 83 ± 3 and 105 ± 3 μT magnetic field. Taken together the effects showed a multi-peaked pattern as shown in Fig. 1.5 along the increase of magnetic flux density. Theoretical calculations based on the model, using different values of model parameters, were performed for many ions of biological relevance, including Li, K, Na, Mg, Ca, and Zn. Only one combination of ions, namely Ca, Mg and Zn led to a good overlap (coincidence) of peaks and valleys with the experimental data. Other combinations did not confirm to the observed graph. The overlap (coincidence) was found to be good when the model parameter, angular velocity (Λ), i.e. 'the same speed of rotation' was chosen for all ion-protein complexes and the considered 'Λ' was 110/s which was equal to 18 rps. The calculated results, for individual ions and for linier superposition of the three ions,

$$P_{sum} = P_{Ca} - P_{Mg} + P_{Zn}$$

have been shown in Fig. 1.5 together with the experimental observations.

As we can observe in the Fig. 1.5, there is a remarkable consistency in the theoretical calculations for Ca^{2+}, Mg^{2+} and Zn^{2+} and the experimental observations. This consistency was noticeable, provided all the ion-protein complexes rotate with the same speed

of 18 revolutions per second which strongly suggests that all these ion-protein complexes are present on the same carrier which is rotating at a peculiar speed. And the carrier is believed to be DNA (Binhi et al. 2001).

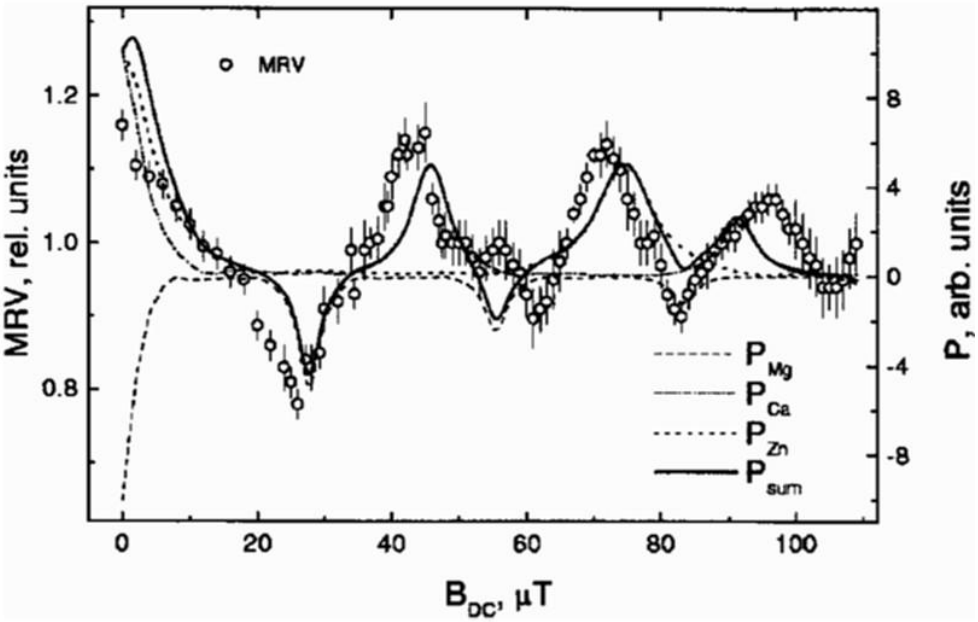

Fig 1.5: Concurrence in the experimental data with results of computer simulations. Points represent experimental observations, which is maximum relative viscosity in cell lysates after exposure of *E. coli* cells to static magnetic field. Lines indicate the magnetic part of dissociation probability of Ca, Mg, Zn and linear superposition of these probabilities (Binhi et al. 2001).

As put it by authors, DNA replication and transcription could be the processes where static magnetic fields could make an effect. However, the process of replication could be excluded as the *E. coli* cells were kept in M9 buffer before exposing the cells to magnetic fields. During transcription there is a relative rotation of DNA and the RNA polymerase (Cook et al. 1992), which could result in periodic rotation of RNA polymerase and several proteins from transcription complexes about DNA.

Enzymes which take care of maintaining the topology of DNA, by removing supercoils in it, such as topoisomerase I and topoisomerase II, may also allow for the rotation of DNA. For example, Vacinia topoisomerase I rotates the cleaved DNA strand with the rate of 20 rps, to remove supercoils from the DNA (Stivers et al. 1997).

Taken together, transcription and the activity of topoisomerase provides the necessary conditions for the proposed ion-interference model to work and account for the effects of the static magnetic field on biological systems.

1.9.5 Electromagnetic induction

Electromagnetic Induction as a mechanism for magnetoreception has been suggested for marine animals (Fig. 1.6). When the marine fishes from the group elasmobranchs, for example, shark and rays, swim in different directions in the sea, they are crossing the geomagnetic field lines at different angles, then it induces variable voltages at their electric organs known as ampullae of Lorenzini (Murray 1962). Electromagnetic induction is quite common and could be observed in animals ranging from aquarium fish to duck-billed platypus. However, due to the fact that the earth has a very low magnetic field, the animals moving at a moderate speed require a highly sensitive electroreceptive system to detect such minute induced electromotive force.

Elasmobranchs like shark and rays have several long canals in their head, which begin as a small pore at the surface of the skin (Fig. 1.6a). These canals have very resistive walls and are filled with highly conductive jelly-like fluid, and could function as electric cables for transmission of voltages. At the other ends of these canals are present ampullae of Lorenzini, which is a group of cells that is very sensitive to even minute changes in the voltage (Kalmijn 1978). According to a conservative estimate the ampullae of Lorenzini have the ability to detect about 2 µV/m of voltage (Johnsen and Lohmann 2008).

It is clear that induction as a model can explain magnetoreception in a limited number of animals and for plants it has no relevance.

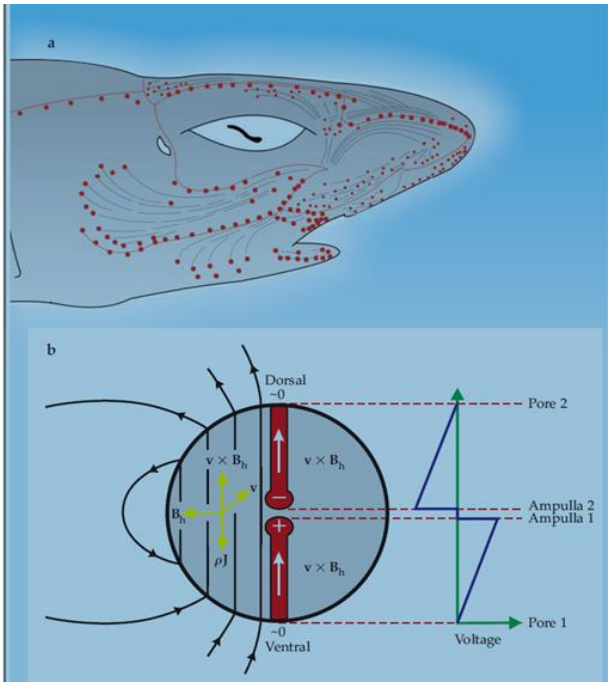

Fig 1.6: Magnetoreception via electromagnetic induction. (a) shows the side view of the shark's head, displaying jelly-filled conductive canals (grey lines) with ampullae of Lorenzini (red dots) at the end of the canals. (b) shows schematic representation of two ampullae with their canals. When the shark swims towards east or into the page with a velocity 'v', the horzontal magnetic field of earth, B_h, leads to generation of electromotive force of magnitude vB_h. However, the voltage drop due to the current density ρJ results in no potential difference between the dorsal and ventral surfaces of the animal, on account of its highly resistive body and skin. But due to high conductivity of the canals, there occurs a large drop of voltage across ampullae (Kalmijn 1981).

1.10 Cryptochrome and radical-pair mechanism

The blue light photoreceptors, cryptochromes are central to the radical-pair mechanism as they are the only photoreceptors which form a radical pair after photo excitation (Liedvogel et al. 2007a). Though remained cryptic for a long time, cryptochromes were discovered as blue-light and ultraviolet-A (UV-A) photoreceptors in *Arabidopsis thaliana* (Ahmad and Cashmore 1993). Apart from light-dependent magnetoreception, they have been identified to be involved in various other important blue-light dependent roles in both plants and animals.

Structurally, cryptochromes are very similar to photolyases, which are flavin containing light-dependent enzymes that are involved in repair of the UV light-damaged DNA through electron transfer process. Owing to structural similarity to photolyases, cryptochromes are widely considered to be the descendants of photolyases, though devoid of photolyase activity (Cashmore et al. 1999). The first cryptochrome (CRY1) is the product of the gene *hy4* from *Arabidopsis* and have 681 amino acids (Ahmad and Cashmore 1993). The N-terminal domain of this protein shares a marked sequence similarity to photolyases and is known as PHR (Photolyase Homology Region). The PHR of cryptochromes also have a three dimensional structure similar to photolyases which is characterized by an N-terminal α/β domain and a C-terminal α-helical domain. What separates cryptochromes from photolyases is the presence of C-terminal extensions of varying lengths (Fig. 1.7). These extensions are usually longer in most of the plants cryptochromes than in animal cryptochromes (Liedvogel and Mouritsen 2010) and are likely regions that provide specific properties to cryptochrome that are responsible for its special functions, for example, in *Arabidopsis* CRY1, it mediates the signalling mechanism of constitutive blue-light response (Yang et al. 2000).

In addition to amino acids, the protein structures of cryptochromes have two non-covalently bound cofactors (Fig. 1.7). One of them is FAD (Flavin adenine dinucleotide), and is necessary for the function of cryptochromes. The other one is a light harvesting chromophore, which has been assumed to be either 8-hydroxy-5-deazariboflavin (8-HDF) or 5,10- methenyltetrahydrofolate (MTHF), on the basis of sequence and structural similarity of both photolyases and cryptochromes (Malhotra et al. 1995; Hsu et al. 1996). That the function of second cofactor is an antenna molecule which harvests light to initiate photoreaction process is thoroughly established (Klar et al. 2007). The antenna molecule, after excitation, can transfer its energy to the catalytic cofactor, as there is a spectral overlap in the absorption spectra of FAD and the florescence of the antenna cofactor (Park et al. 1995). The efficiency

of such energy transfer depends upon the distance between the donor and the acceptor molecules, and has been demonstrated to be very high (70-100%) in photolyases (Payne and Sancer 1990; Kim et al. 1992). In case of *Arabidopsis* CRY3, it has been shown to be 78-87% (Song et al. 2006). On account of absorption of energy and the subsequent excitation of the electron, and its transfer from FAD to amino acids residues of cryptochrome forms a significant process for the radical-pair mechanism (Ritz et al. 2000).

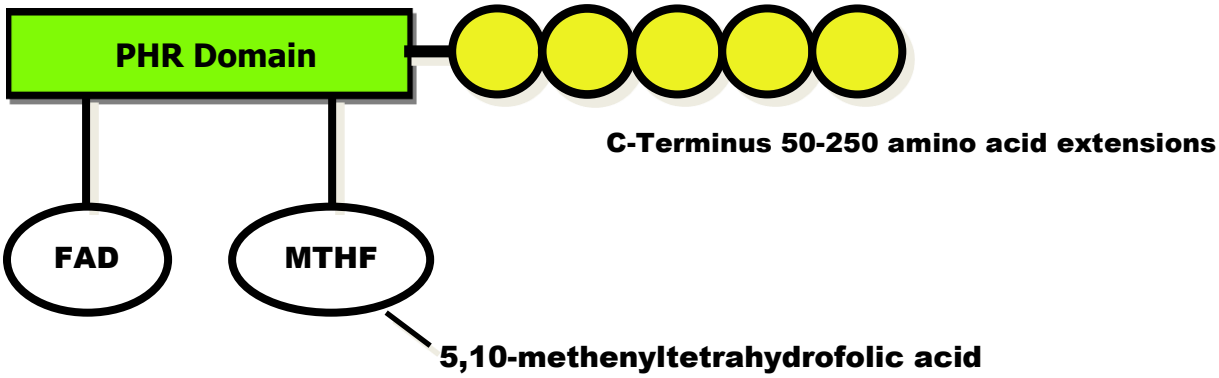

Fig 1.7: The schematic structure of cryptochrome.

The two cofactors in photolyases and cryptochromes are the same, nevertheless the cryptochromes lack DNA repair function, which suggests evolution of novel functions for the cryptochromes, particularly in signalling (Liedvogel and Mourtsen 2010). It has also been suggested that both plant and animal cryptochromes, in spite of their high structural similarity and functional analogy, seems to have evolved independently from different ancestral photolyases. This is based on the fact that animal cryptochromes are more similar to type 6-4 photolyases whereas the plants cryptochromes show closer sequence similarity to type I microbial photolyases (Kanai et al. 1997).

Cryptochromes have been shown to be associated with many blue-light dependent functions in both plants and animals. In plants, they are involved in inhibition of hypocotyl growth (Ahmad and Cashmore 1993), in anthocyanin accumulation (Ahmad et al. 1995), in leaf and cotyledon expansion (Cashmore et al. 1999; Lin and Shalitin 2003), transition to flowering (El-Din El-Assal et al. 2003), regulation of blue-light regulated genes (Jiao et al. 2003) apart from their role in magnetoreception (Ahmad et al. 2007). Animal cryptochromes have been implicated to play a direct role in circadian rhythms as part of circadian pacemakers (Miyamoto and Sancar 1998; Zhu et al. 2008), An indirect role in circadian

rhythm by way of feeding light information to circadian clock, has been found to be associated with cryptochromes in *Drosophila* (Stanewsky 2002; Busza et al. 2004). Additionally it has also been reported that the *Drosophila* circadian clock is magnetically sensitive and this sensitivity is cryptochrome-dependent (Yoshii et al. 2009). Cryptochromes have also been suggested to play a role as core clock element in monarch butterflies (Zhu et al. 2008). In migratory birds, cryptochromes are considered to be a receptor molecule for light-dependent magnetic compass orientation.

The role of cryptochromes as a receptor for light-dependent magnetic compass orientation depends upon the formation of radical pairs by it (Fig. 1.8). Before light activation of cryptochrome, the flavin cofactor is present in its fully oxidized FAD state. When FAD absorbs blue light photons, it is promoted to the excited $FAD^{\bullet}$ state. $FAD^{\bullet}$ is then protonated, possibly by gaining one proton from nearby aspartic acid, generating $FADH^{+}$. As the electronically excited flavin cofactor enters in its $FADH^{+}$ state, a light induced electron transfer is induced. This electron transfer process involves three tryptophans, numbered Trp400, Trp377 and Trp324 in the *Arabidopsis* cryptochrome structure (Solov'yov et al. 2007).

At first an electron jumps from the nearby tryptophan, Trp400 (Fig. 1.9) into the hole left by the excited electron in $FADH^{+}$ that forms FADH + $Trp400^{+}$. Thereafter another electron jumps from Trp377 to Trp400, forming, FADH + $Trp377^{+}$. Similarly once again another electron jumps from Trp324 to Trp377, forming FADH + $Trp324^{+}$. Eventually $Trp324^{+}$ becomes deprotonated to Trp324dep, forming FADH + Trp324dep, fixing the electron on the FADH cofactor. The cryptochrome is considered to be in its active signalling state, when its flavin cofactor is in semiquinone state i.e., FADH form. The external magnetic field can influence the three radical pair states (FADH + Trp400+, FADH + Trp377+ and FADH + Trp324+) formed as a result of the photoreduction process (Solov'yov et al. 2007).

Each of these three radical pair states can exist in either singlet state [↑↓] or in triplet state [↑↑]. The external magnetic field regulates the interconversion of these states, and as both these states lead to production of a different product eventually, we have a case where the external magnetic fields shows up its influence on the biological system.

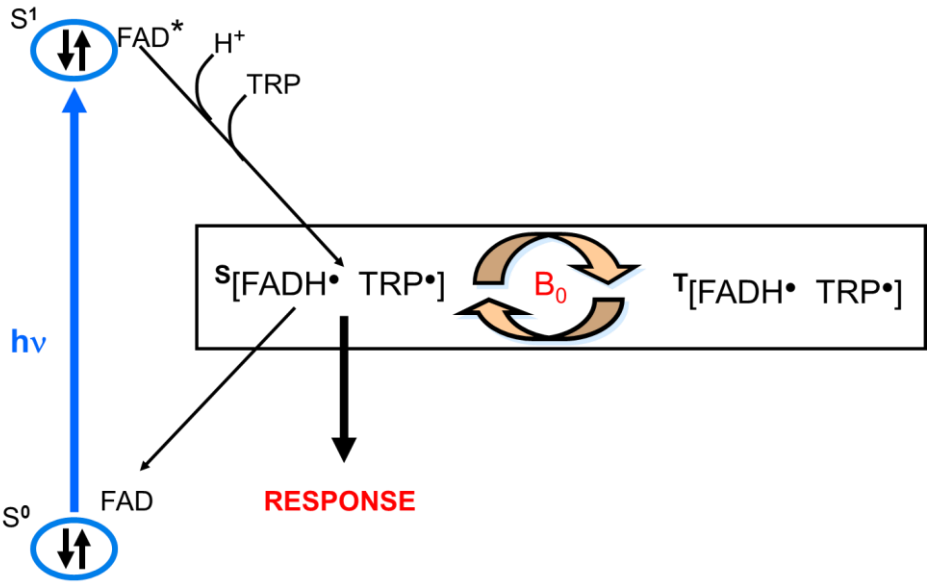

Fig 1.8: Radical-pair mechanism in cryptochrome. After absorption of the blue light photons the fully oxidized cofactor FAD of cryptochrome, becomes excited $FAD^{\bullet}$. Its excited state promotes its protonation that results in formation of $FADH^{+}$. But once electronically excited flavin is in $FADH^{+}$, an electron from the nearby tryptophan enters into the hole left by the excited electron which results in semiquinone FADH form of the cofactor. The FADH form is biologically active state of the cofactor and together with tryptophan forms the radical pair, which could be in singlet state (responsive) or triplet state (non-responsive). The interconversion of these two states is modulated by external magnetic field, thereby showing its effects on the biological systems.

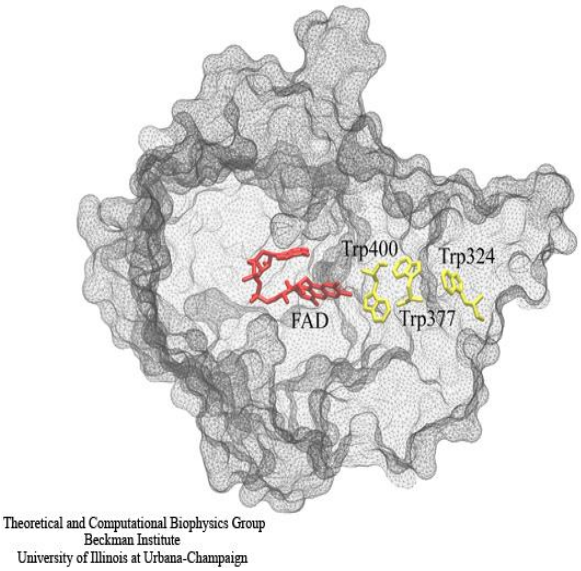

Fig 1.9: Cryptochrome showing the positions of cofactor FAD and the nearby chain of three tryptophans which are involved in the light induced photoreduction pathway. Cryptochrome in its semi-reduced state (semiquinone form) is in active signalling state. This state is achieved by the photoreduction pathway which involves a chain of three tryptophans, namely Trp400, Trp377 and Trp324. (Solov'yov et al. 2007)

Radical-pair mechanism based on cryptochrome makes certain predictions about the responsiveness of *Arabidopsis* to static magnetic fields. These predictions are based upon preconditions that are required for the functioning of radical-pair mechanism. These are as follows:

1. The response should be observed only in near UV and blue light
2. There should be no response when plants are exposed to red light
3. No response should be observed in darkness
4. The responses should be absent in cryptochrome mutants
5. A single optimum should be displayed by the stimulus response curves similar to the stimulus response curves for the radical yield in dependence of the magnetic flux density.

These questions formed the basis of our experiments and the responsiveness of *Arabidopsis* seedlings was evaluated using following responses:

1. Hypocotyl length
2. Light induced anthocyanin accumulation
3. Chlorophyll accumulation
4. Gene expression (transcription)
5. Protein expression (translation)

2 Materials and Methods

2.1 Materials

2.1.1 Culture medium

Solid medium consisting of Murashige-Skoog Medium 2.165 g/l (Duchefa Biochemie, Netherlands), MES buffer 0.5 g/l (Roth, Karlsruhe) cotaining 1.5% sucrose (Roth, Karlsruhe) with the gelling agent Phytagel 3 g/l (Sigma) in standard petri plates (diameter 92x16 mm) form Sarstaedt, Germany.

2.1.2 Plants used

Three strains of *Arabidopsis* were examined. They are as follows:-

a) Wild type strains of *Arabidopsis thaliana* (L.) Heynh. the ecotype Landsberg erecta (*Ler*)(Redei, 1962)(Originally obtained from LEHLE SEEDS, Tuscon, AZ, USA)
b) *cry1cry2* double mutant, a double mutant with alleles hy4-3 fha1 is defective in the photoreceptors cryptochrome 1 and cryptochrome 2 (Ahmad et al., 2007).
c) *phyAphyB* double mutant, a double mutant with alleles phyA-201 phyB-5 is defective in phtoreceptors phytochrome A and phytochrome B (Reed et al., 1994).

2.1.3 Magnetic fields generation and seedlings irradiation

a) Helmholtz coils- Magnetic fields of desired magnitudes were generated in Helmholtz coils. The body of these coils were made of a cylinder of acryl glass (diameter 18 cm and height 9 cm) from Thyssen Krupp Plastics GmbH, Köln and coils were of enamelled magnetic copper wire (diameter 2 mm from HELLENIC CABLES Athens, Greece). Each cylinder had a pair of windings, one on each edge, but made up of a continuous wire. The numbers of coils in the pair, for a given Helmholtz coil, were the same. Attached to the plastic cylinder of these coils were two stands of the same plastic material. One of these stands was cylindrical in shape whereas the other one was in the form of elongated rectangle. Clamped to the cylindrical stand were the set ups for holding two LED arrays meant for illuminating the seedlings. The rectangular stand along with the stand for LED set ups was meant for supporting the lid of the Mu- metal box.

b) LED Arrays- Seedlings were irradiated with the desired light using LED arrays. Both blue and red LED arrays were designed and prepared by our biology workshop for providing

a homogenous light to experimental seedlings in the Helmholtz coils. Each array had 10 LEDs soldered in series on a rectangular plastic plate (6x3 cm). Blue LEDs had spectral radiance peak at 475 nm and red LEDs had at 660 nm.

c) Mu-metal box- Each Helmholtz unit with its illuminating set up was kept in tightly closed Mu-metal cylindrical box with a lid (25 cm diameter x 40 cm height) prepared from 0.5 mm Mu-metal sheets (Henry Electronic, Bopfingen, Germany).

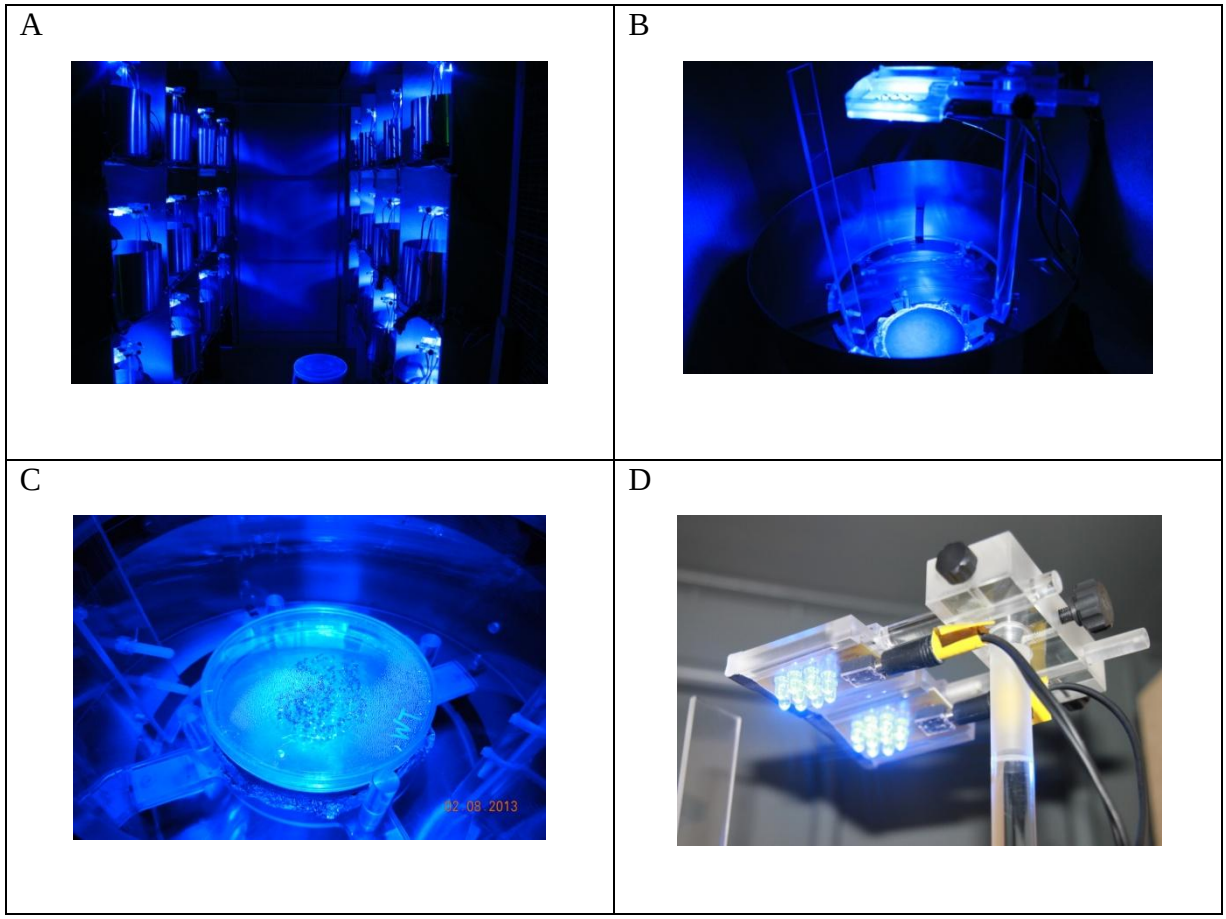

Fig 2.1: Experimental room with Mu-metal boxes. **A.** 24 Mu-metal boxes placed on the 2 shelves (12 on either side) in the experimental room which is known as faraday cage. The faraday cage shields the room against any outside magnetic fields, which results in an average magnetic flux density of 3 µT within the room. **B.** A single Mu-metal box with a Helmholtz coil within it. Note the two stands attached to the body of Helmholtz coil. On the top of one stand is attached the assembly of LED arrays. At the center of the Helmholtz coil is present a stage for keeping the experimental petri plates. **C.** The stage of the Helmholtz coil with a petri plate on it. The petri plate has five days old *Ler* seedling grown on it under the blue light irradiation from the overhead LED array set up. This figure shows the typical conditions in which the seedlings are grown within Helmholtz coil for five days. **D.** The LED array set-up of the Helmholtz coil for irradiating the growing seedlings.

2.1.4 Materials and Reagents

Material	Manufacturer
Anthocyanin Extraction	
a) Propanol	Merck, Darmstadt
b) HCl (conc.)	Merck, Darmstadt
Protein Extraction and quantification	
a) Amido black	MERCK Schuchardt, Munich
b) Acetic acid	Applichem GmbH, Darmstadt
c) Na-P buffer	Chemicals from MERCK, Darmstadt
d) Methanol	MERCK, Darmstadt
e) NaOH	Roth, Karlsruhe
f) BSA	Sigma, USA
Quantitative PCR	
a) RNA Extraction	
i)RNeasy mini kit	QIAGEN, Hilden, Germany
ii) ß-Mercaptoethanol	Roth, Karlsruhe
b) cDNA synthesis	
i) 10X reaction buffer for DNase I	Fermaentas life sciences
ii) DNase I	Fermaentas life sciences
iii) EDTA	Fermaentas life sciences
iv) Oligo$(dT)_{18}$ Primer	Fermaentas life sciences
v) dATP's, dCTP's, dGTP's, dTTP's	Fermaentas life sciences
vi) RiboLock Rnase Inhibitor	Fermaentas life sciences
vii) M-MLV Reverse Transcriptase	Promega, Madison, WI
viii) RNase free water	QIAGEN, Hilden, Germany
c) Quantitative PCR	
i) ABsolute QPCR SYBR Green Mix	Thermo Scientific, Germany
ii) RNase free water	QIAGEN, Hilden, Germany
iii) Primers	Eurofins, MWG Operon, Ebersberg
Western Blotting	
a) Sample Preparation	
i) Trichloroacetic acid (TCA)	Roth, Karlsruhe

ii) Acetone	Roth, Karlsruhe
iii) ß -Mercaptoethanol	MERCK-Schuchardt,Munich
iv) Sodium-dodecyl-sulphate	United States Biochemical, OH
v) Dithiothreitol	Applichem, Darmstadt
vi) Glycerol	Roth, Karlsruhe
b) Protein quantification	
i) Bicinchoninic acid (BCA), Reagent A and Reagent B	Pierce, Thermoscientific, USA
ii) Bovine Serum Albumin (BSA)	Sigma, USA
c) Separation Gel and Stacking Gel	
i) Acrylamide	Serva, Heidelberg
ii) N.N´-Methylene-bis-Acrylamide	Sigma, USA
iii) Tris	Sigma, USA
iv) Sodium-dodecyl-sulphate	United States Biochemical, OH
v) Ammonium Persulphate	Serva, Feinbiochemica, Heidelberg
vi) TEMED	Serva, Feinbiochemica, Heidelberg
vii) Isopropanol	Merck, Darmstadt
d) Gel Staining	
i) Coomassie	Serva, Feinbiochemica, Heidelberg
ii) Ponceau	Sigma, USA
e) Protein Transfer to PvDF Membranes	
i) Glycin	Applichem GmbH, Darmstadt
ii) Methanol	MERCK, Darmstadt
iii) Tris	Sigma, USA
iv) Sodium-dodecyl-sulphate	United States Biochemical, OH
v) PvDF membranes	Millipore Corporation, Bedford, MA
vi) Blotting paper	Biorad Laboratories, München
f) Membrane Analysis	
i) Tris	Sigma, USA
ii) NaCl	Roth GmbH, Karlsruhe
iii) Tween 20	Fisher Scientific, USA
iv) Non-fat dried milk powder	Applichem GmbH, Darmstadt
v) NBT/BCIP Tablets	Roche Diagnostics GmbH, Mannheim

Arabidopsis culture medium	
a) Murashige-Skoog Medium	Duchefa Biochemie, Netherlands
b) MES buffer	Roth, Karlsruhe
c) Phytagel	Sigma
d) Sucrose	Roth, Karlsruhe
Arabidopsis seed sterilization	
a) Ethanol	Lenz-Chemie, Westerburg
b) Sodium hypochlorite	Roth, Karlsruhe
c) Top agar	Sigma, USA
d) Parafilm'M'	Bemis, Neenah,WI

2.1.5 Primers for QPCR

Gene/ Locus	Primer	Sequence
Chalcone Synthase/ AT5G13930	Forward- Chsy_72_f Reverse-Chsy_226_r	5`-ATAATGGTGATGGCTGGTGCT-3` 5`-CTGTTGGTGATGCGGAAGTAG-3`
Porphobilinogen synthase/ AT1G44318	Forward- HEMB2_734_f Reverse-HEMB2_984_r	5`-GTGAGATGTTGGATGGTCGC -3` 5`-GAGAGATGGGAGTGCTGGCTT-3`
Phenylalanine ammonia lyase/ AT3G10340	Forward- Pal_265_f Reverse-PAL_417_r	5`-AAACAATCACATCACCGCCG-3` 5`-CCAATCGTCAAAGTCTCACCTC-3`
Nitric oxide synthase/ AT3G47450	Forward- Nos_124_f Reverse- Nos_273_r	5`-TTCCTTCTCTTCCTCGTCGC-3` 5`-CCGCCGCAAATCCATCT-3`
RBCL, RuBisCO/ ATCG00490	Forward- Lsu_1026_f Reverse- Lsu_1266_r	5`-TTTGGGCTTTGTTGATTTACTG-3` 5`-TACTCGGTTGGCTACGGCAC-3`
SSU, RuBisCO /AT1G67090	Forward- S1025_179_f Reverse- S1025_330_r	5`-GCTTCCTCTATGCTCTCTTCCG-3` 5`-CTTCCGCCGTTGCTTGT-3`
CAB-1/ AT1G29930	Forward- CAB1_691_f Reverse- CAB1_855_r	5`-GCTGAGTTGAAGGTGAAGGAG-3` 5`-AAAGTTGGTGGCGAAGGC-3`

CAB-4/ AT3G47470	Forward- CAB4_576_f Reverse- CAB4_752_r	5`-GGTGTCGCTGGGATGCTTT-3` 5`-TGGGTTCTTGATGTCTTGCC-3`
Phytoene dhydrogenase/ AT4G14210	Forward- Phytdehy_224_f Reverse- Phytdehy_448_r	5`- GCTGCGTCTCCTGTTTCTCTACTT-3` 5`- ACTCCTCCTCCTTGTTCTTGTCTTA-3`
Porphobilinogen deaminase/ AT5G08280	Forward- Pode_964_f Reverse-Pode_1091_r	5`-TGTCGCATCTATCTTATCTCTCG-3` 5`-TTGTTTCCTCGTGGTTCAGTG-3`
Lycopene cyclase/ AT3G10230	Forward- Lycy_825_f Reverse- Lycy_1028a_r	5`-AGGCTTCCGTGGTTCTTGATG-3` 5`-TCTTGCTGTTCCGTTCTTTC-3`
NAD-kinase/ AT3G21070	Forward Nad_61_f Reverse- Nad_349_r	5`-CTCTCTCTCTTTCTTCTTCGTCTTCG-3` 5`-CGCCTTTCCTTCAGCAGC-3`
Rubisco activase/ AT2G39730	Forward-Ruac_595_f Reverse- Ruac_814_r	5`-TTTACATTGCTCCTGCTTTCAT-3` 5`-TTTGCGGGTTCTCCTGCGT-3`
Cytosolic GAPD/ AT3G26650	Forward- Gapd_40_f Reverse- Gapd_220_r	5`-ACCCTTCTCACTCACCTATCTCAC-3` 5`-GCTCAACATCGTCCCTCTGG-3`
ATP Synthase, ß - Chain/ AT5G08690	Forward- Atps_569_f Reverse- Atps_722_r	5`-CGAAATCAAGACCGAGCAT-3` 5`-ACCGCCAAAGAGACCAATC-3`
Tubilin/ AT4G14960	Forward- Tub_72_f Reverse- Tub_273_r	5`-CGCCCTTCGTCTTCTTCC-3` 5`-CATCACCTCCACCAACAGTCTT-3`
Actin/ AT3G46520	Forward- Act_430_f Reverse- Act_622_r	5`-CCGAAGGCTAACCGTGAGA-3` 5`-GGATTGCGTGTGGAAGTGC-3`
AT4G34270	Forward- HK-1_201_f Reverse- HK-1_366_r	5`-GATTCTCACTTCTCTCGCTGTCG-3` 5`-CCCTTCCTGCTTCCAACCA-3`
AT1G13320	Forward- HK-2_261_f Reverse- HK-2_483_r	5`-TGACGATGACGATGAGGTGC-3` 5`-CTTAGCCAGAGGAGTGAAATGC-3`
AT1G59830	Forward- HK-3_81_f Reverse- HK-3_262_r	5`- CGGCGACTTCTCCTCCTACT-3` 5`-TCTGCTTCACCTAACGGCTT-3`

AT4G33380	Forward- HK-4_143_f Reverse- HK-4_327_r	5`-TGAGAAATGGTGGGATGACG-3` 5-TTGGAATAGATGTGGAGAGAAGAAG-3`
AT2G28390	Forward- HK-5_119_f Reverse- HK-5_331_r	5`-CTTCATCATCCGACACCGA-3` 5`-CTCCATTGCTAACTCCGCC-3`
Elongation factor-1/ AT1G07920	Forward- EF-1_1041_f Reverse- EF-1_1204_r	5`-TGCCGCCAACTTCACCTC-3` 5`-GCTCCTTCTCAATCTCCTTACCAG-3`
D1 Subunit PS I/ ATCG00340	Forward- D1-f-780 Reverse- D1-r-1079	5`-ATTCCATCCACAAACGCAAAG-3` 5`-AACGCATAAGCAGGTAAAGAGTA-3`

2.1.6 Antibodies

Antibody	Immunogen	Antibody Format	Supplier
RbcL, Rubisco large subunit	RbcL protein sequences including AtCg00490 from *Arabidopsis thaliana*	Rabbit polyclonal	AgriseraVännas, Sweden
Lhca4, PSI type IV chlorophyll a/b binding protein	Lhca4 proteins of *Arabidopsis thaliana*(At3g47470)	Rabbit polyclonal	AgriseraVännas, Sweden
Goat anti-rabbit IgG, ALP(Alkaline phosphatise) conjugated(Secondary antibody)	Rabbit immunoglobulins	Goat polyclonal	AgriseraVännas, Sweden

2.1.7 Equipments

Equipment	Name	Manufacturer
Laminar Flow Clean Bench	Faster KBN	Thermo Scientific
Centrifuges	a) Prism microcentrifuge b) Universal 30 RF	Labnet , U.K Hettich zentrifugen, Tuttlingen
Heating Blocks	a) Thermomixer comfort b) Heating Block HLC BT 1302 c) Bio TDB-100	Eppendorf, Hamburg USA/Scientific Plastics Ltd. U.K. MAGV, Londorf.
PCR Cycler	Mastercycler	Eppendorf, Hamburg
pH meter	Digital pH Meter-646	Knick
Power sources	a) Power pac 300 b) Power pac basic c) 6267B DC power supply(3) d) 6274A DC power supply e) 6274B DC power supply f) 6289A DC power supply	Biorad Laboratories, München Biorad Laboratories, München Helwett-Packard Helwett-Packard Helwett-Packard Helwett-Packard
Magnetometer	Fluxmaster Teslameter	Stefan Mayer Instruments, Dinslaken
Optometer	P-2000	Gigahertz-Optik, Germany
SDS-PAGE Apparatus	Mini Protean Tetra Cell	Biorad Laboratories, München
Protein Blotting Apparatus	Transblot SD Semidry Transfer Cell	Biorad Laboratories, München

Spectrophotometer	MPS-2000 Spectrophotometer	Shimadzu, Kyoto, Japan
Nanodrop spectrophotometer	ND-1000 Spectrophotometer	NanoDrop Technologies, USA
Ultrasonicator	Bandelin.Sonerex	Bandelin electronic, Berlin
Plant Miller	MM 200	Retsch, Haan, Germany
Vortex machine	a) VF2 b) Supermixer	Janke & Kunkel, IKA-Labortechnik Lab-line instruments Inc., Illinois, USA
Shaker	Bio Dancer	New Brunswick Scientific, Nürtingen
Water bath	Water bath	Gesellschfts für Labortechnik mbH, Burgwedel
Balances	a)Sartorius handy b)Sartorius c)Sartorius1209MP	Sartorius-werke, Göttingen Sartorius-werke, Göttingen Sartorius-werke, Göttingen
Magnetic Stirrers	IKAMAG RCT	Janke & Kunkel GmbH, Staufen
Autoclave		Technomara Germany, Fernwald

2.2 Methods

2.2.1 Sterilization of Seeds

Appropriate quantity of seeds was taken in the 2 ml eppendorf cups. These were treated with 2 ml 70% ethanol for 2 minutes. After 2 minutes the ethanol was pipetted out and then the seeds were treated with 2 ml of sodium hypochlorite (NaCIO) for 15-20 minutes. The seeds were shaken 2-3 times during this time. After 20 minutes the sodium hypochlorite solution was pipetted out and the seeds were washed with double distilled water 4-5 times to remove sodium hypochlorite thoroughly. After washing the seeds, they were mixed in top agar for inoculating on to the culture medium in the petri plates.

The inoculated petri plates with seeds were then placed in cool room (temp. 5-6°C) for 48 hr to break the dormancy. Before keeping them in the Helmholtz coils they were kept under white light for about 6 hr. A comprehensive picture of the scheme of the protocol for raising the seedlings is shown in Fig. 2.2.

2.2.2 Growing conditions

After the 6 hr light treatment of seeds, they were placed in the Helmholtz coils. Each Helmholtz coil had a specific magnetic flux density, which was set before the start of experiment, by increasing or decreasing the current flowing through the coils. The measurement of flux densities was done using teslameter. These Helmholtz coils were encased in cylindrical Mu-metal boxes. Mu metal is an Iron-Nickel alloy, composed of 77% Nickel, 16% Iron, 5% Copper and 2% Chromium and has a very high magnetic permeability. Due to this property Mu-metal is a very good shield against static or low-frequency magnetic fields. So these boxes protect the Helmholtz coils against any outside pollutant magnetic fields. In addition all the 24 Mu-metal boxes were housed in Faraday cage, where the average magnetic flux is 3 μT approximately. The temperature of the room was set at 22.5°C.

The seeds were also illuminated by light (blue or red) with the help of two LED arrays that were clamped on the top of the stand, fixed to one side of the Helmholtz coils. Each LED array has ten LEDs. So the seedlings in each Helmholtz coil were exposed to more or less uniform light from twenty LEDs.

In these Helmholtz coils the seedlings were allowed to grow for 5 days i.e. 120 hr. After this time the seedlings were harvested with forceps in the 2 ml eppendorf-cups and were flash-frozen in liquid nitrogen for further analysis.

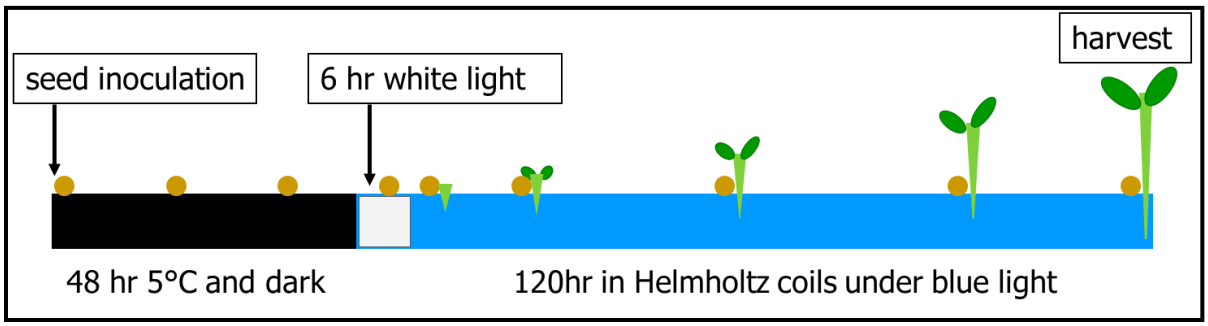

Fig 2.2: The scheme of the protocol for raising seedlings. Inoculated seeds in petri plates were kept in cold dark conditions for 48 hr. Before exposing them to experimental conditions in Helmholtz coils, they were irradiated by white light for promoting their germination. Thereafter the plates were kept in the Helmholtz coils having variable light intensities and magnetic flux densities, and the seeds were allowed to germinate and grow for 120 hr (5 days). This period of 120 hr was found to be necessary for attaining sufficient mass and height by the seedlings so that they could be analyzed further.

2.2.3 Magnetic flux density and Light intensity measurements

Magnetic flux density was measured using teslameter. The teslameter has a range of measuring the flux densities between -200 µT to 200 µT. The sensor of the teslameter was placed in a plastic adapter that fits in the hole at the center of the stage of the Helmholtz coils.

The adapter has three cavities for accommodating the sensor of teslameter. One is in vertical position and the other two are in horizontal positions and at right angle to each other. These cavities are meant for measuring the flux densities in three different vectoral directions. The final flux density was reached by square rooting the sum of the squares of these three values.

The light intensities were measured using the optometer. The optometer provides the possibilities to measure the light of various wavelenths in the visible range. Prior to the actual measurement, the wavelength was set according to experimental requirements. Then the sensor was placed in the central hole of the stage of Helmholtz coils to note the light intensities. The light intesities from the LEDs can be increased or decreased by altering the current supply to it. The current supplier instrument to our LEDs has this facility and the requisite light intensity, as required by the individual experiments was set using this facility.

2.2.4 Hypocotyl length measurement

Five days old seedlings were picked up from the petri plates immediately after the experiments. They were picked one by one and placed on a black plastic plate in 2-3 rows (Fig. 2.3). Altogether 50 seedlings were taken from each petri plate randomly. The plastic

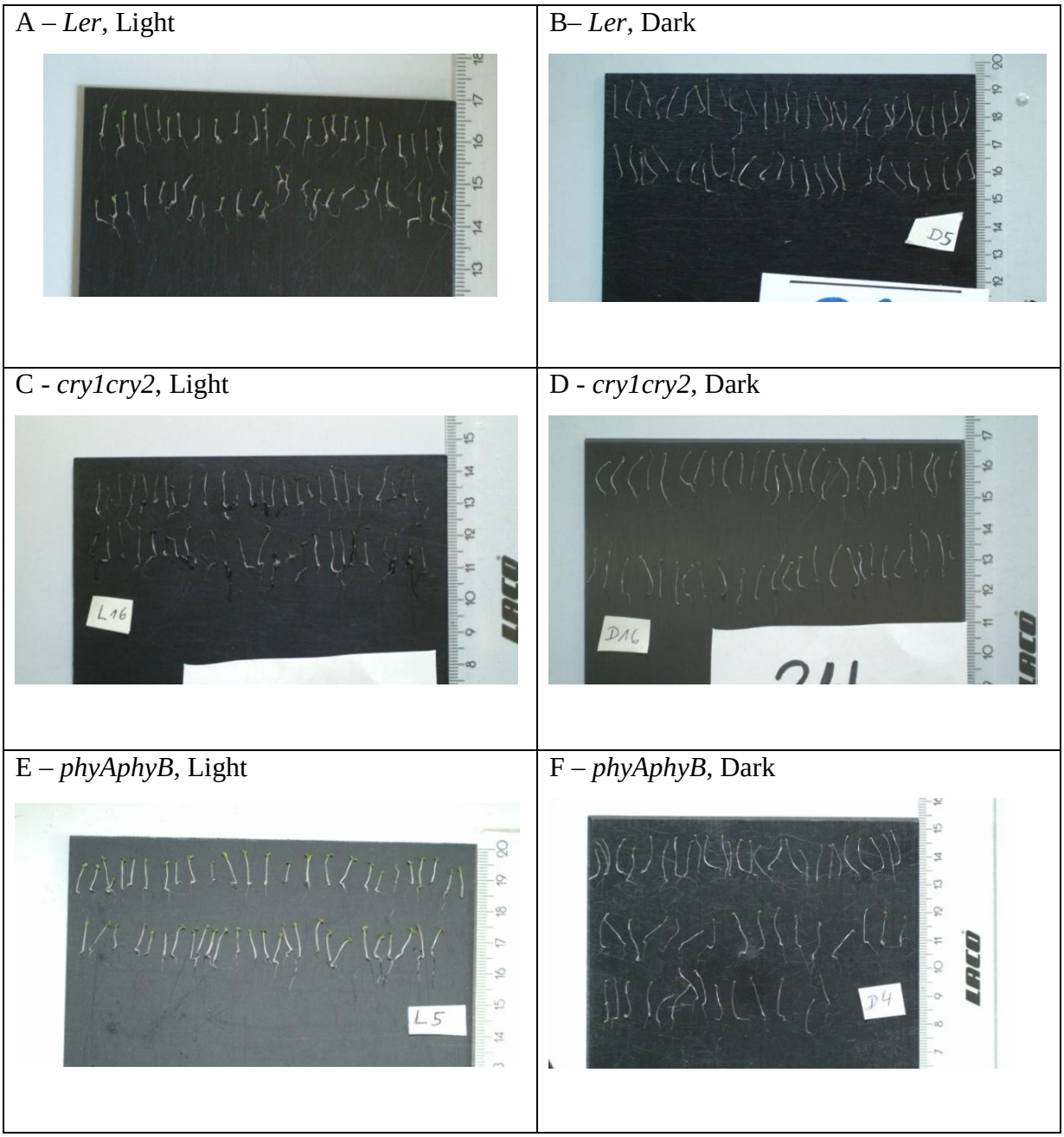

Fig 2.3: Photographs of the harvested five days old seedlings of *Arabidopsis* placed on the dark colored plastic plate for the measurement of the hypocotyl length. **A.** *Ler* seedlings grown under blue light, **B.** *Ler* seedlings grown in darkness, **C.** *cry1cry2* seedlings grown under blue light, **D.** *cry1cry2* seedlings grown in darkness, **E.** *phyAphyB* seedlings grown under blue light, **F.** *phyAphyB* seedlings grown in darkness.

plate with seedlings was photographed with a ruler on one side. This ruler helped in setting the scale while working with the computer programme for measuring the length of the hypocotyls. These photographs were then used for measuring the length of individual hypocotyls with the help of the computer programme known as Image J.

2.2.5 Anthocyanin quantification

For anthocyanin extraction, the five days old seedlings were harvested in 2 ml eppendorf cups. The seedlings were treated with 1 ml of anthocyanin extraction buffer. Thereafter these eppendorf cups were placed in water bath and the contents were boiled for three minutes at 92°C. They were then stored overnight in dark at room temperature. The next morning the samples were centrifuged for 10 minutes at 15000 rpm. The supernatant with anthocyanin was carefully transferred in a new eppendorf cup. Absorbance of these samples was then measured by spectrophotometer at 535 nm and 650 nm. Finally the amount of anthocyanin was calculated using the Raleigh-formula –

$$Abs._{535\ (corr.)} = Abs._{535} - 2.2\ Abs._{650}$$

Buffer

Anthocyanin Extraction-Buffer

81% H_2O

1% Hydrochloric acid (concentrated)

18% Propanol-(1)

2.2.6 Chlorophyll quantification

Five days old seedlings were harvested from the experimental set up, in 2 ml eppendorf cup. 1 ml methanol was added to each cup and then the samples were boiled twice in water bath at 80°C for 30 seconds. Between the two boiling treatments the samples were taken out and shaken properly. Thereafter the samples were centrifuged at 15000 rpm for 5 minutes. After centrifugation the supernatant was transferred carefully into a new eppendorf cup and absorbance was measured by spectrophotometer at 665.2 nm and 652 nm. The amount of chlorophyll was calculated by using the following formula:

Chl A: $18.22\ E_{665.2} - 9.55\ E_{652.0}$

Chl B: $33.78\ E_{652.0} - 14.96\ E_{665.2}$

Chl A + Chl B : $24.23\ E_{652.0} + 3{,}26\ E_{665.2}$

2.2.7 Quantitative PCR

Quantitative Polymerase Chain Reaction (QPCR) was performed on the selected genes to find out the effects of geomagnetic field on their expression. To perform QPCR, five days old experimental seedlings were harvested in 2 ml eppendorf cups and immediately flash-frozen in liquid nitrogen for conserving the metabolic state of the seedlings. From these seedlings, total RNA was extracted using RNeasy kit (QIAGEN RNeasy Mini Kit (250), Catalogue no. 74106) using the protocol prescribed by the manufacturer with little changes for the optimization. Using the total RNA, cDNA synthesis was performed using M-MLV Reverse transcriptase and Oligo $(dT)_{18}$ primer. Real time PCR was performed on this cDNA using the Absolute qPCR SYBR Green mix (Thermo Scientific) following the manufacturer's instruction. Data was assembled and analysed by Ct-method.

2.2.7.1 Isolation of mRNA

About 100 mg of five day old seedlings from the experiments were harvested into the 2 ml eppendorf cups. These samples were immediately flash frozen in liquid nitrogen to arrest and preserve the metabolic state of the seedlings.

Two milling steel balls were added into each cup for the fine grinding of the seedlings. Before the grinding treatment, the samples were precooled in liquid nitrogen. The bead mill homogenizer was used for the milling. Each sample was milled twice for 2 minutes. Between the two millings the samples were taken out from the machine and shaken properly and were cooled again before proceeding for the second round of grinding.

To the finely ground seedlings, 450 µl of RLT buffer (with 1% ß-mercaptoethanol) was added. The samples were again milled one more time for two minutes. The samples were shifted from 2 ml eppendorf cups to 1.5 ml cups to get rid of the milling balls. Now the samples were heated at 56°C for 3 minutes on the heating block. Thereafter they were vortexed and then centrifuged at 15000 rpm for 3 minutes. The supernatant was pipetted out and mixed with 350 µl of 96% ethanol in a 2 ml reaction tube (from RNeasy Kit). The ethanol mixed samples were pipetted onto the column and the column was centrifuged at 10000 rpm for 15 seconds. The filtrate from the column was thrown away. 700 µl of washing buffer (RW1 buffer) was pipetted onto the column, and the column was centrifuged again at 10000 rpm for 15 seconds. This step was repeated with 500 µl of RPE buffer. Finally 500 µl of RPE buffer was pipetted onto the column and then centrifuged for 3 minutes: first at 10000 rpm for two minutes and then the speed was increased to 15000 rpm in the last minute.

For collection of the RNA, the column was placed on 1.5 ml reaction tube (from kit) and 15-20 µl of RNase free water (from Kit) was pipetted onto the column. The columns were centrifuged at 10000 rpm for 1 minute. To collect the remaining RNA on the column, 15-20 µl more RNase free water was added to the column and centrifuged at 15000 rpm for 1 minute. 10 µl of the extracted RNA was separated to a 0.5 ml cup for quantification of RNA and cDNA synthesis. The stock RNA (in 1.5 ml reaction tube) and this separated 10 µl of RNA (in 0.5 ml cup) were flash frozen in liquid nitrogen and then stored at -70°C.

2.2.7.2 cDNA synthesis

RNA samples were first quantified using Nanodrop Spectrophotometer. Accordingly 4 µg of RNA was taken for cDNA synthesis. The first step in cDNA synthesis is to get rid of any genomic DNA that might have been extracted along with the RNA as this will lead to faulty results. To achieve this, RNA was treated with 4 µl of DNaseI (Fermentas). For the activity of DNaseI 2 µl of DNase buffer (supplied with enzyme) was also added. Additional RNase free water was added to the reaction mixture to make a final volume of 20 µl. The DNase was allowed to perform its job at 37°C for a period of 30 minutes on the heating block. The samples were shaken twice in between at the interval of 10 minutes.

After the digestion of any DNA present in RNA samples, the DNaseI was made dysfunctional by adding 2 µl of EDTA (supplied with DNaseI) and heating the samples for 5 minutes at 70°C. For priming the cDNA synthesis, 2 µl of oligo $(dT)_{18}$ primer was added and the samples were heated at 70°C for 5 minutes for better annealing the Oligo dT primer with polyA tail of mRNA. Now the samples were ready for cDNA synthesis. They were stored on ice. In the meantime the mastermix containing all the required constituents (M-MLV 5X buffer, dNTPs, and ribolock) for cDNA synthesis was prepared. In each cup 24 µl of this master mix was pipetted. This 24 µl of master mix has following constituents:

10 µl	M-MLV 5X buffer
2.5 µl	dATP 10 mM
2.5 µl	dCTP 10 mM
2.5 µl	dGTP 10 mM
2.5 µl	dTTP 10 mM
1.2 µl	Ribolock
2.8 µl	RNase free water

Now the total reaction volume is 48 µl and the samples were preheated at 42°C for 2 minutes on heating block. 2 µl of M-MLV reverse transcriptase was added to each cup for the

cDNA synthesis and this increases the total reaction volume to 50 µl. The reaction was allowed to proceed at the 42°C for 1 hr and 15 minutes with moderate shaking. Finally the reaction was stopped by inactivating the reverse transcriptase at 70°C for 10 minutes and the samples were ready for real time PCR.

2.2.7.3 Real time PCR

The real time PCR was performed on the Mastercycler by Eppendorf. A 96-well plate was used for the PCR reaction. The total reaction volume in each well was 25 µl that comprises following constituents:

1.5 µl	Forward primer
1.5 µl	Reverse Primer
2.0 µl	Template cDNA
12.5 µl	SYBR Green Mix
7.5 µl	RNase free water

Forward and reverse primers for the test genes were designed using vector NTI programme. For minimising the pipetting mistakes, a master mix containing forward and reverse primers, SYBR Green mix and RNase free water was prepared for the number of wells to be analysed and out of this master mix 23 µl was pipetted into each well in addition to the 2 µl cDNA.

After preparing the plate, it was subjected to PCR reaction on Mastercycler. Necessary alterations were done in the PCR programme to suit to our needs and the reaction was allowed to go on for the time required for the 40 PCR cycles and developing melting temperature curves. Usually this time is 2 hr and after the run the data was exported to excel file for analysis and making the graphs.

2.2.8 SDS-PAGE and Western Blotting

SDS-PAGE and Western blotting were performed in four steps:

a) Sample preparation and protein quantification
b) SDS PAGE
c) Protein transfer to PvDF membranes
d) Immunostaining

2.2.8.1 Sample preparation and protein quantification

Protein samples to be analysed by western blotting were prepared by TCA-acetone procedure of total protein extraction. To obtain the proteins, about 100 mg five days old experimental seedlings were harvested, in 2 ml eppendorf cups, which were ground in the bead mill homogenizer by using liquid nitrogen, in the same way as was done for the RNA extraction. To the powdered plant material 1 ml of ice cold extraction buffer was added. The mixture was thoroughly mixed by vortexing. The eppendorf cups containing the mixture were allowed to stand at -20°C for 1 hr. After the cold treatment the milling balls were removed and samples were subjected to cold centrifugation (4°C) at 13000 rpm for 15 minutes in a pre-cooled centrifuge. The supernatant was removed thereafter and the pellets were washed with ice cold wash buffer. For the washing, the pellets were shaken properly in the wash buffer using vortex machine. Before centrifuging again, the samples were kept at -20°C for 15-30 minutes. The centrifugation was done in cold conditions at 13000 rpm for 15 minutes. The supernatant was removed again. The washing step was repeated two more times with the same cold centrifugation in between. For the third washing step, the protein samples in wash buffer were treated with ultrasonic waves in cold ultrasonic bath for 7 to 9 minutes for ensuring thorough mixing of pellets in the wash buffer. Again the samples were kept at -20°C for 15 minutes and then they were centrifuged as done previously. The supernatant was removed and the pellets were dried with vacuum centrifuge to remove the last remnants of acetone.

To the dried pellets 200 µl of SDS-PAGE-sample buffer-part I was added and the pellet was properly mixed in the buffer by using ultrasonic bath again for 7 to 9 minutes. The samples were then subjected to boiling at 95°C for 10 minutes on a heating block. The samples were centrifuged 15000 rpm for 15 minutes and the supernatant containing the proteins was transferred into a new cup. This is our stock solution for extracted proteins and was stored at -20°C.

From the stock protein solutions 10 µl was used to prepare the loading sample for SDS-PAGE. For preparing the loading sample equal amount (10 µl) of SDS-PAGE-sample buffer-part II was added to stock protein solution. As the protein concentration was high, the loading samples were diluted in 1:5 ratio by adding 40 µl each of SDS-PAGE-sample buffer-part I and part II to make the final volume 100 µl.

Protein quantification was done using bicinchoninic acid (BCA) assay. The BCA assay is based on the principal that peptide bonds reduce cupric ions (Cu^{2+}) to cuprous ions

(Cu^{+}). The quantity of Cu^{2+} reduced is proportional to the quantity of proteins present in the samples and the two molecules of bicinchoninic acid chelate with the reduced Cu^{+} ion, forming a purple coloured product which absorbs light at a 562 nm. The amount of protein present in a solution can be quantified by measuring the absorption spectra and comparing with protein solutions of known concentration.

For determining the protein concentration the 10 µl of stock protein solution was diluted 100 times and 100 µl of this was used for the protein quantification. An additional 100 µl of water was also added to this protein sample to make a total test volume of 200 µl as this gave better results in our lab. Reagent-A (BCA) and Reagent-B ($CuSO_4$) were mixed separately in the ratio of 50:1 to make the working reagent. 1 ml of this working reagent was added to each of the diluted protein solutions. The mixture was subjected to 37°C for 30 minutes on the heating block. The absorption spectra were measured at 562 nm using the spectrophotometer.

Calibration curve was prepared with 0 µg, 25 µg, 50 µg 75 µg and 100 µg BSA per 200 µl of water. Each calibration sample was prepared in duplicates. These samples were also treated in the same way as the unknown protein samples and absorption was measured at 562 nm. The values were recorded and the calibration curve was prepared using them.

Buffers and Reagents

Extraction buffer

90% Acetone,

10% TCA

0.07% ß-mercaptoethanol

Wash buffer

100% Acetone

0.07% ß-mercaptoethanol

SDS-PAGE-sample buffer-part I

50 mM Tris/HCl

2% (w/v) Sodium dodecylsulphate (SDS)

SDS-PAGE-sample buffer-part II

20% Glycerol

0.02% Bromophenolblue

100 mM Dithiothreitol (DTT)

2.2.8.2 SDS-PAGE

The sodium dodecyl sulfate polyacrylamide gel electrophoresis (SDS-PAGE) was used to analyse the expression of proteins with respect to influence of geomagnetic fields on *Arabidopsis*. SDS is an anionic detergent that binds and denatures the proteins and maintains them in their primary structure. It also gives a net negative charge to them which is proportional to the number of amino acids in the polypeptide chain as one SDS molecule binds to two amino acids in the chain. In the PAGE these denatured proteins are separated as a function of their molecular weight. Small proteins with little retention move faster and are at the bottom of the gel, whereas larger proteins with strong retention move slowly and are at the top of the gel.

Gel Composition

Separating Gel

12% Acrylamide

375 mM Tris-HCl, pH 8.8

0.1% (w/v) SDS

Stacking Gel

5% Acrylamide

125 mM Tris-Hcl. pH 6.8

0.2% (w/v) SDS

Amounts of ingredients for SDS-PAGE minigels

	Stacking Gel		Separation Gel	
	(ONE GEL) 12%	(TWO GELS) 12%	(ONE GEL) 5%	(TWO GELS) 5%
30% -ACRYLAMIDE	2000µl	4000µl	325µl	650µl
1.5M Tris-HCL pH-8.8 1M Tris-HCl pH-6.8	1250µl	2500µl	250µl	500ml
10%-SDS	50µl	100µl	20µl	40µl
Water (Millipore)	1650µl	3300µl	1250µl	2500µl
10%-APS	50µl	100µl	25µl	50µl
TEMED	2.5µl	5µl	2.5µl	5µl

For casting and running the gels Mini Protean® III Cell apparatus was used. The glass plates with 1 mm spacer were properly cleaned and mounted on the casting stand. Solutions for separating and stacking gels except APS and TEMED were added in separate 50 ml falcon tubes. After checking that everything is ready, APS and TEMED were added to the separating gel solution and mixed gently. This solution was carefully poured between the glass plates until enough space (1.5 cm high appox.) was left for the stacking gel. The solution was covered with water saturated isopropanol. The gel was allowed to polymerize for 20 minutes. After checking the polymerization status, the isopropanol was removed and the gel top was washed with water and then dried carefully with filter paper. Now APS and TEMED were mixed in stacking gel solution. After gently mixing about 1 ml of it was poured on the separating gel. The comb (slot-former) was inserted carefully on the top of the stacking gel solution, also allowing air bubbles to escape. The solution was allowed to polymerize for about 10 minutes.

The gel plate with gel was removed from the holder and clipped into the electrophoresis assembly and was placed in the tank. The tank and the gel assembly unit were

filled with the electrophoresis running buffer. The comb was removed carefully from the gel and the pockets were swilled with the running buffer. Now the gels were ready for loading the samples.

The samples were heated at 95°C for 5 minutes before loading and spinned down with the help of centrifuge. Sample lane order was pre planned. Usually the protein marker was loaded in the first lane and the reference standard in the second one. The test samples in the remaining lanes. When loading was finished, the tank was covered with its lid and the current was set 15 mA with the running time of 120 minute.

The run was stopped when the bromophenol front has reached the bottom of the gel. The gel plates were removed and washed with water. The two glass plates were separated gently with a plastic spatula. The gel was taken out and stored appropriately for further analysis.

Solutions required

Electrophoresis Running-buffer

25 mM Tris-HCl, pH-8.3

250 mM Glycine

0.1% (w/v) SDS

2.2.8.3 Coomassie Staining of proteins

Staining the gels by coomassie is the simplest method to visualize the proteins in the gel. Coomassie dye interacts to proteins by ionic interactions between dye sulfonic acid groups and positive protein amine groups as well as by Van der Waals interactions. The alcohol and acetic acid in the stain fix the proteins in the gel by precipitation.

After the electrophoresis, the gels were incubated in the staining solution for 1 hour on the shaker. Excess stain was removed by destaining the gel using destaining solution. Destaining was done for 2 hours. For accelerating the destaining process the gel was cooked in a microwave oven.

Reagents

Staining solution

40% Methanol

7% Acetic Acid

0.025% Coomassie Brilliant blue R250

Destaining solution

10% Acetic Acid

2.2.8.4 Protein transfer to PvDF membranes

The proteins from the gel were transferred to PvDF (Polyvinylidene floride) membrane with the help of Trans-Blot Semi Dry Transfer Cell from BioRad. For the same the PvDF membrane was trimmed to gel size and was pre-soaked in methanol for 2 minutes, washed with water and finally kept in transfer buffer. The filter papers to be used for the transfer were also soaked in transfer buffer.

First, a soaked filter paper was placed on the anode base plate of the transfer cell. The PvDF membrane was placed over this filter paper avoiding any trapping of the air bubbles between the membrane and filter paper. The gel was then placed over the membrane and finally another soaked filter paper was placed on the gel to complete the sandwich unit for the transfer. A glass rod was rolled over the sandwich to remove any trapped air bubble. The lid of the transfer cell was positioned over the cell for completing the circuit. The transfer was achieved by applying 12 volts for 2 hrs. The membrane was retrieved after the transfer and stored in TBS buffer immediately for immunostaining. The membrane was stained with ponceau stain to visualize the transferred proteins on it and to ensure that enough proteins were transferred on the membrane to proceed further. This was done by incubating the membrane in 20 ml Ponceau solution for 5 minutes.

Solutions required

Transfer-buffer

48 mM Tris-HCl

39 mM Glycine

0.01% (w/v)SDS

20% Methanol

Ponceau solution

0.1 % (w/v) in 5% acetic acid

2.2.8.5 Immunostaining

A particular protein transferred on the membrane could be identified by treating the membrane with the specific antibody against this protein and this was achieved in this step. The charged groups on the surface of the membrane were blocked first by incubating the membrane in blocking buffer (non fat milk) for one hour on a shaker with mild shaking. The membrane was washed by TBS-Tween buffer, on the shaker, thrice for a period of 5 minutes each time.

The membrane was incubated with the RBCL (Large Sub-unit RuBisCO) antibody with 1:10000 dilution and the CAB4 antibody with 1:5000 dilution in a total volume of 20 ml. These dilutions were done in TBS-Tween buffer. This incubation lasted for 1 hour on the shaker with mild shaking. The membrane was washed again with TBS-Tween buffer for three times, each time for 5 minutes. The membrane was incubated now in the secondary antibody with 1:1500 dilution in TBS-Tween. The secondary antibody is conjugated to alkaline phosphatase enzyme. This incubation also lasts for one hour and the membrane was washed again in a similar way as described above.

For the detection, the membrane was finally incubated for 10-15 minutes in NBT/BCIP (Nitro blue tetrazolium /5-bromo-4-chloro-3-indolyl-phosphate) solution made from NBT/BCIP ready to use tablets (one tablet in 10ml water) in dark. To stop the colour development the membrane was washed in water. The developed membrane was dried and scanned for record and analysis by image J programme.

Solutions required

Blocking-buffer

5 %(w/v) Nonfat dried milk powder in TBS-Tween

TBS-Tween buffer

100 mM Tris-HCl, pH7.4

150 mM NaCl

0.2% Tween-20

3. Results

Inoculated seeds of different strains of *Arabidopsis thaliana* (*Ler*, *cry1cry2* double mutant and *phyAphyB* double mutant) were kept in cold room (5°C) in darkness for a period of 48 hr. Thereafter the petri plates containing the seeds were brought under white light under normal temperature (25°C) for 6 hr to promote germination. Subsequently the petri plates were exposed to different experimental conditions by placing them in Helmholtz coils having different magnitudes of magnetic flux density. The range selected for this study was 0 µT to 180 µT. This range includes the range of geomagnetic field which is from 25 µT to 75 µT. Within the Helmholtz coils the seeds were allowed to germinate and grow for a period of 120 hr (5 days). Such a time-span for the seedling growth in the Helmholtz coils was found to be necessary for attaining sufficient mass and height by them, so that they could be analyzed further for various responses. Fig. 3.1 depicts this scheme that was followed for all the experiments.

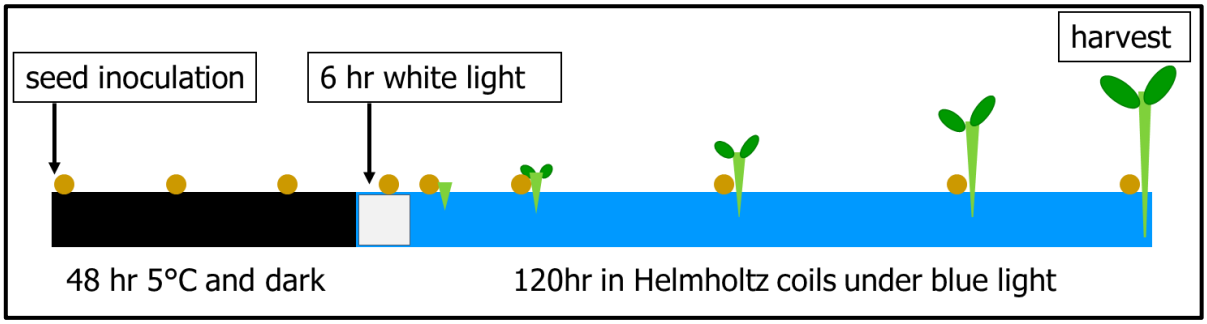

Fig 3.1: The scheme of the protocol for raising seedlings. Inoculated seeds in petri plates were kept in cold dark conditions for 48 hr. Before exposing them to experimental conditions in Helmholtz coils, they were irradiated with white light for promoting their germination. Thereafter the plates were kept in the Helmholtz coils having variable light intensities and magnetic flux densities and under these conditions the seeds were allowed to germinate and grow for 120 hr (5 days). This period of 120 hr was found to be necessary for attaining sufficient mass and height by the seedlings so that they could be analyzed further.

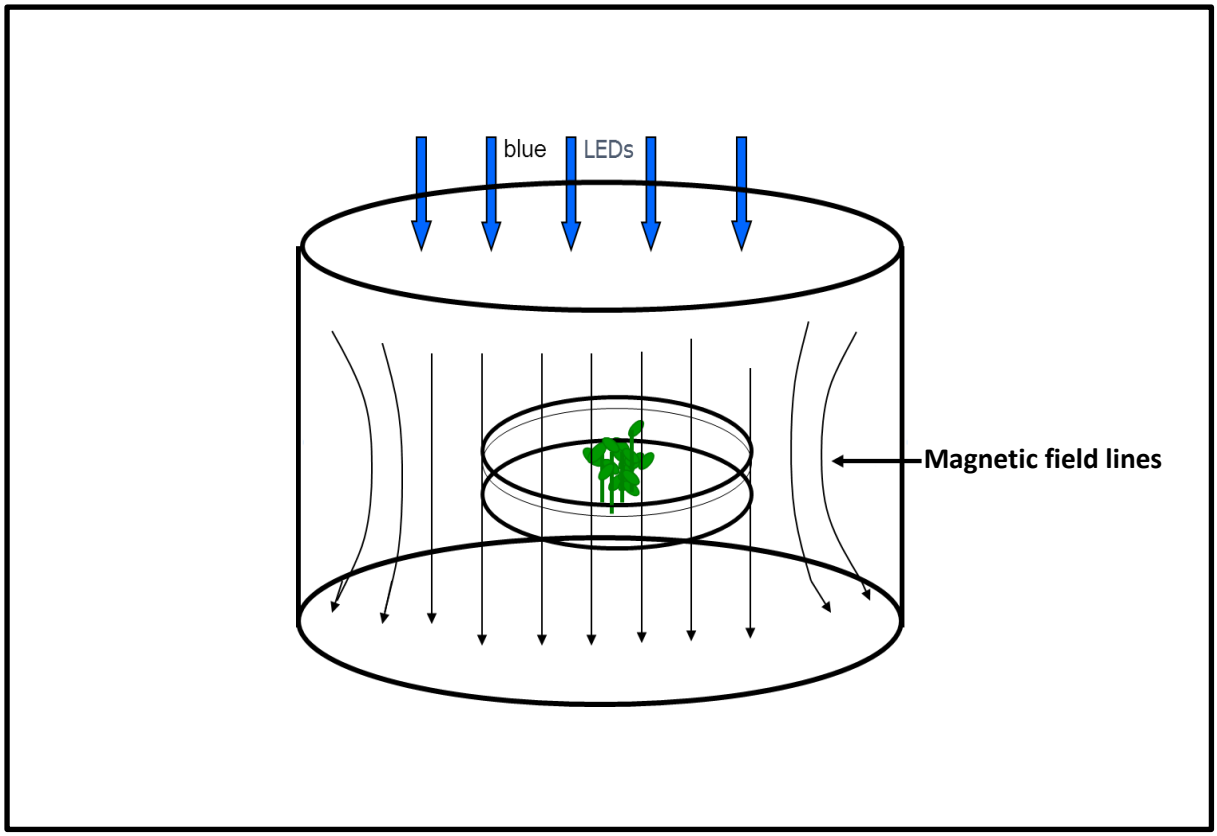

Fig 3.2: Schematic representation of the experimental conditions in the magnetic field. The petri plates with *Arabidopsis* seedlings were placed at the center of the Helmholtz coils for exposing them to uniform magnetic fields of variable flux densities in different Helmholtz coils. At the same time they were also irradiated with the desired quantum of light from the overhead LED arrays.

The petri plates containing the seeds and later on seedlings of *Arabidopsis thaliana* were placed at the center of the Helmholtz coils as shown in Fig. 3.2. Such a position within the Helmholtz coils was very important for the experiments as magnetic fields were found to be homogenous only in the center. After the completion of 120 hr, the seedlings were harvested and analyzed for the effects of magnetic flux density on them (Fig. 3.3). The following attributes were selected for the analysis:

1. Hypocotyl length
2. Anthocyanin quantification
3. Chlorophyll quantification
4. Gene expression
5. Protein expression

A. *Ler*, blue light

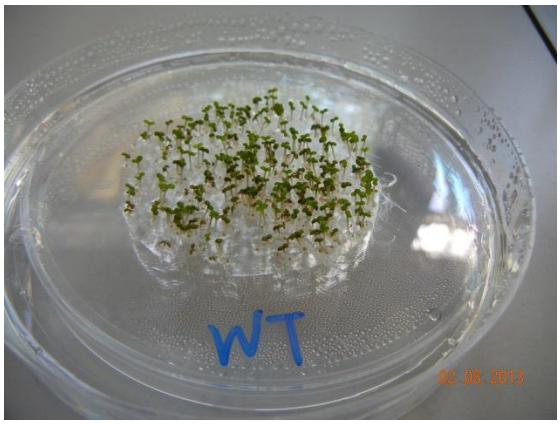

B. *Ler*, dark

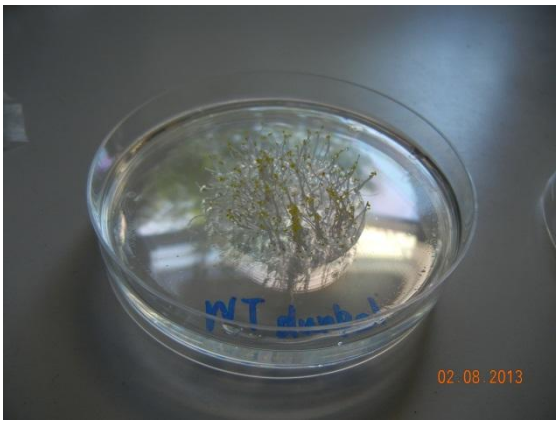

C. *cry1cry2*, blue light

D. *cry1cry2*, dark

E. *phyAphyB*, blue light

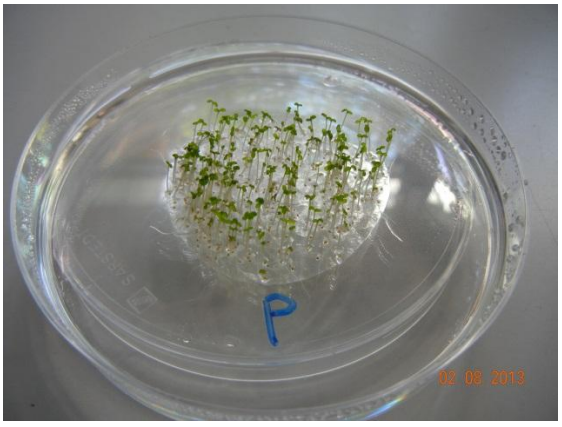

F. *phyAphyB*, dark

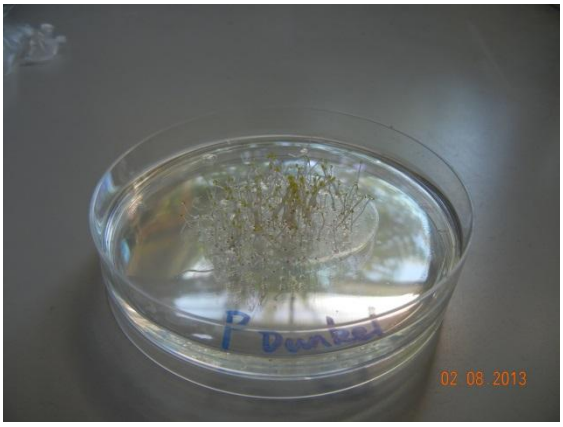

Fig 3.3: Seedlings of *Arabidopsis* ready to be harvested after they have grown in experimental conditions within Helmholtz coils for five days. The light grown seedlings in this figure are from the experiments where they were grown under blue light with the fluence rate of 10 W/m².

Prior to the study of the effects of magnetic flux density on *Arabidopsis* seedlings, we performed some experiments to understand the kinetics of the gene expression of some genes in our experimental system. As gene expression was a very significant parameter in our study,

it was interesting to know how these genes are being expressed in the system as a function of time. It was also important to know whether 120 hr time was appropriate for our study in terms of gene expression. Therefore we began with the study of the kinetics of gene expression at 0, 25, 50 and 90 µT.

3.1 Kinetics of gene expression in blue light in *Ler* from 87 hr to 120 hr of seedling growth at 0, 25, 50, and 90 µT

Some of our preliminary but very interesting experiments were to study the kinetics of gene expression as a function of time at different magnetic flux densities. Such experiments were also significant to determine the developmental stage of the seedlings that provides enough quantity to work on the analysis of the above mentioned attributes. For performing the experiments we selected four points on the magnetic flux density scale. They were 0, 25, 50 and 90 µT. As these experiments were done in the beginning of the study phase, when a clear picture of the stimulus-response curves was not yet available, the flux densities were selected arbitarily. The time span selected was the last 33 hr of the 120 hr duration the experiment i.e. the period of hour 87 to 120. Starting from hour 87 the seedlings were harvested at a 3 hr interval and mRNA levels of different genes were determined. The following figures show the results of these experiments.

Gene *cab4* (Fig. 3.4) presents a very clear picture of the kinetics as it shows a well-marked 24 hr cycle of circadian rhythm in all the four kinetics experiments. The level of mRNA produced at different magnitudes of flux densities was found to be different, being highest at 0 µT and lowest at 50 µT. The large subunit of RuBisCO (*rbcl*) in Fig. 3.5 presents a similar phenomenon. At all flux densities except 25 µT, the gene is expressed more or less at a particular level in individual cases, but there is a difference in the level of mRNA production at different magnetic flux densities, again being lowest at 50 µT.

Rubisco activase gene (*rca*, Fig. 3.6) shows a circadian rhythm like *cab4*, but the rhythm is more prominent at 0 and 50 µT. At 25 and 90 µT, it is difficult to figure out the rhythm. Similar to other genes studied, the levels of mRNA produced at different flux densities are different. Interestingly, the mRNA levels of this gene at 90 µT are lower and similar to the level of 50 µT. At the same flux density (90 µT), the expression levels of other genes are much higher.

In case of the chalcone synthase gene (*chs*, Fig. 3.7), the pattern of transcript levels is similar at all flux densities, being higher from 90 hr to 105 hr, and becoming lower thereafter.

But again the transcript levels are lowest at 50 µT. At other flux densities the levels of mRNA transcripts seem to remain more or less similar.

Somewhat similar results were shown by the genes porphobilinogen synthase (*hemb2*, Fig. 3.8) and phytoene dehydrogenase (*pds*, Fig. 3.9). They show a sudden increase in the transcript levels between 95 hr and 105 hr and subsiding again thereafter. The influence of magnetic flux densities persists in these genes as has been noticed in other genes, being highest at 0 µT and lowest at 50 µT.

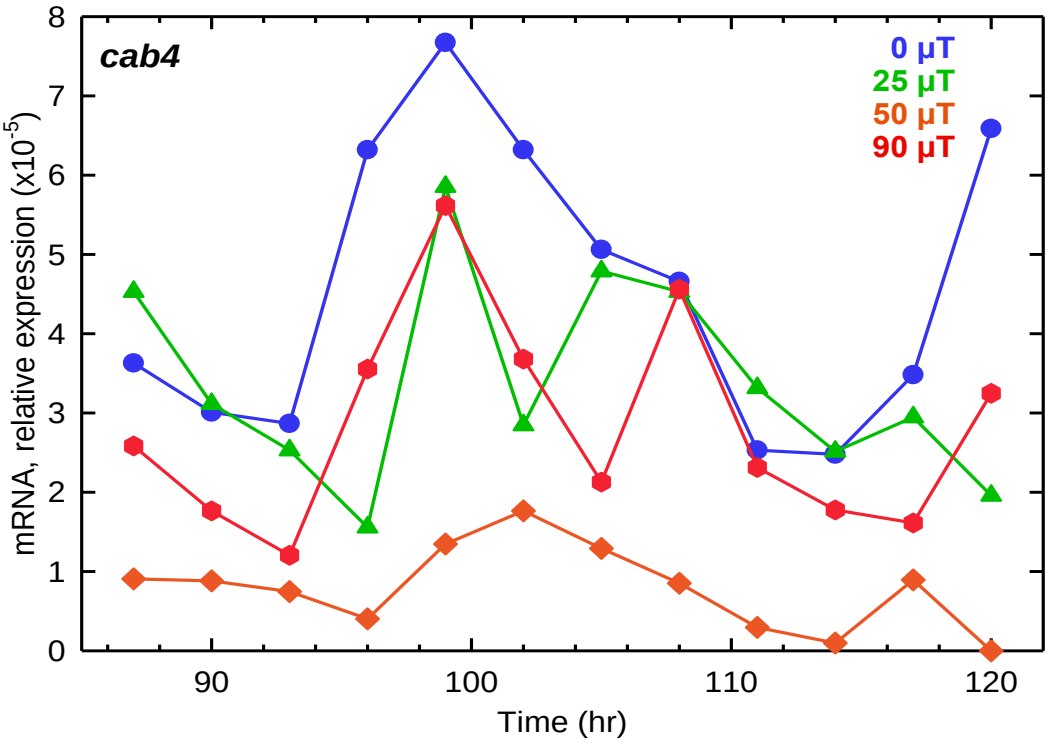

Fig 3.4: Kinetics of the transcription of chlorophyll a/b binding-4 gene (*cab4*) from 87 hr to 120 hr at four different magnetic flux densities (0, 25, 50 and 90 µT). All the original values of mRNA expression were multiplied by 10^5 to present in the graph.

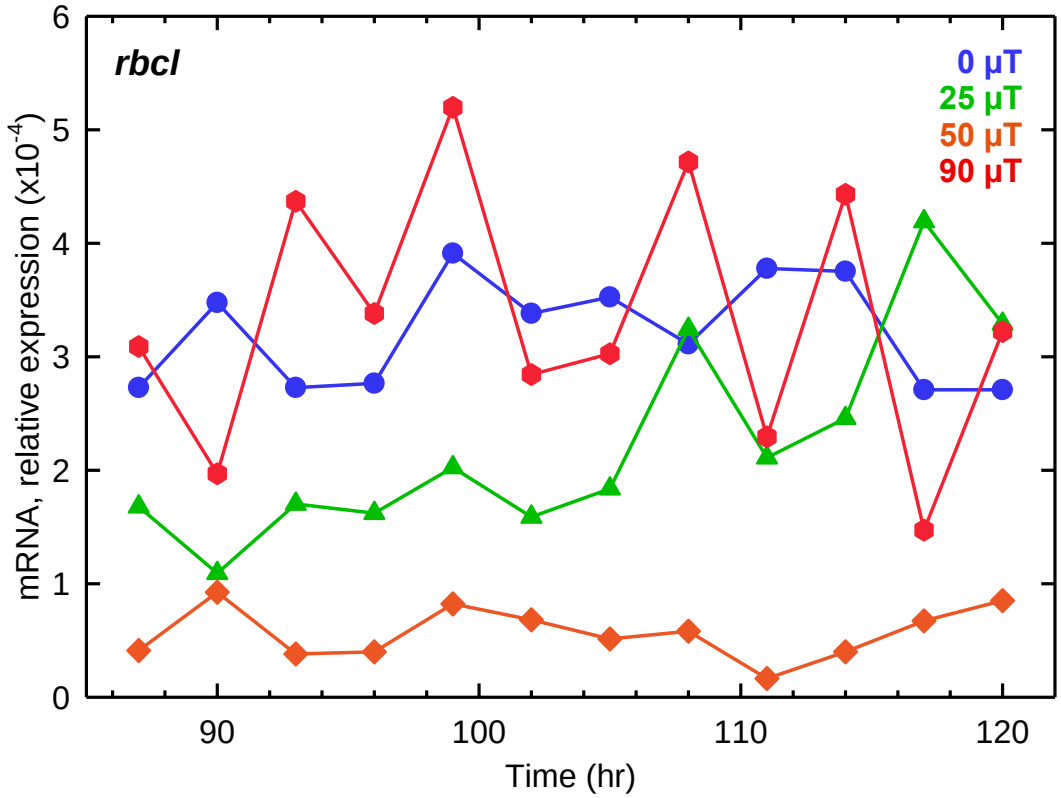

Fig 3.5: Kinetics of the transcription of large subunit of RuBisCO (*rbcl*) from 87 hr to 120 hr at four different magnetic flux densities (0, 25, 50 and 90 µT). All the original values of mRNA expression were multiplied by 10^4 to present in the graph.

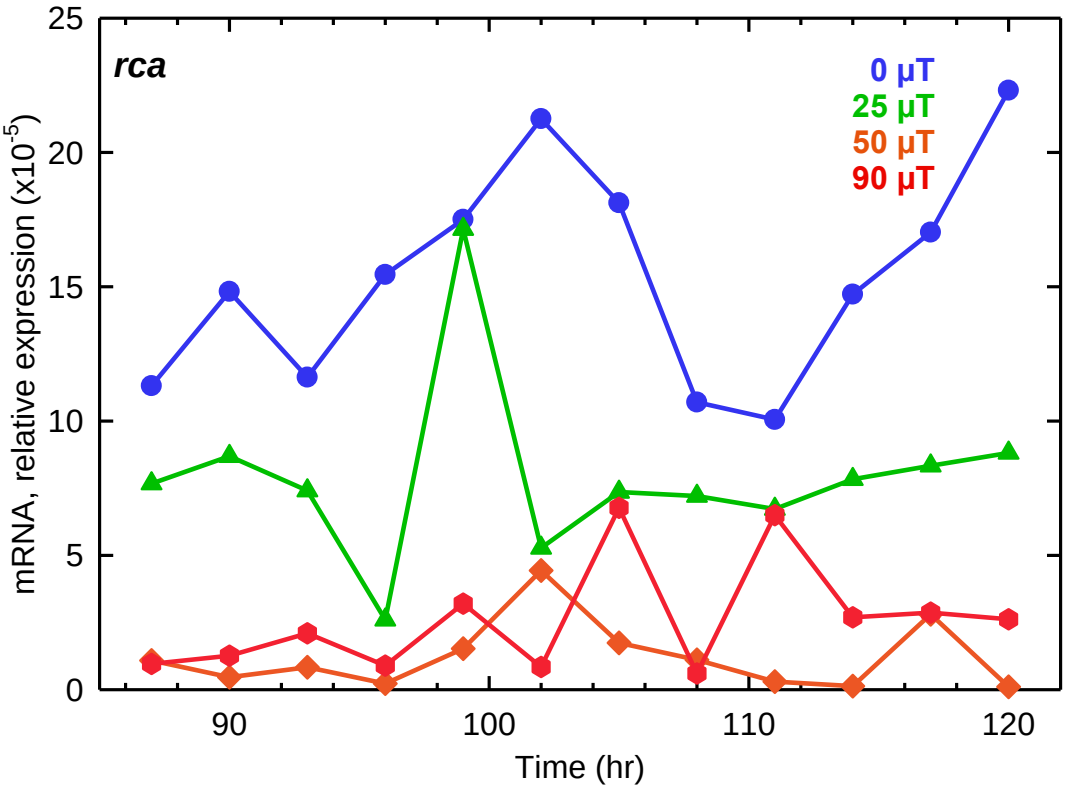

Fig 3.6: Kinetics of the transcription of rubisco activase gene (*rca*) from 87 hr to 120 hr at four different magnetic flux densities (0, 25, 50 and 90 µT). All the original values of mRNA expression were multiplied by 10^5 to present in the graph.

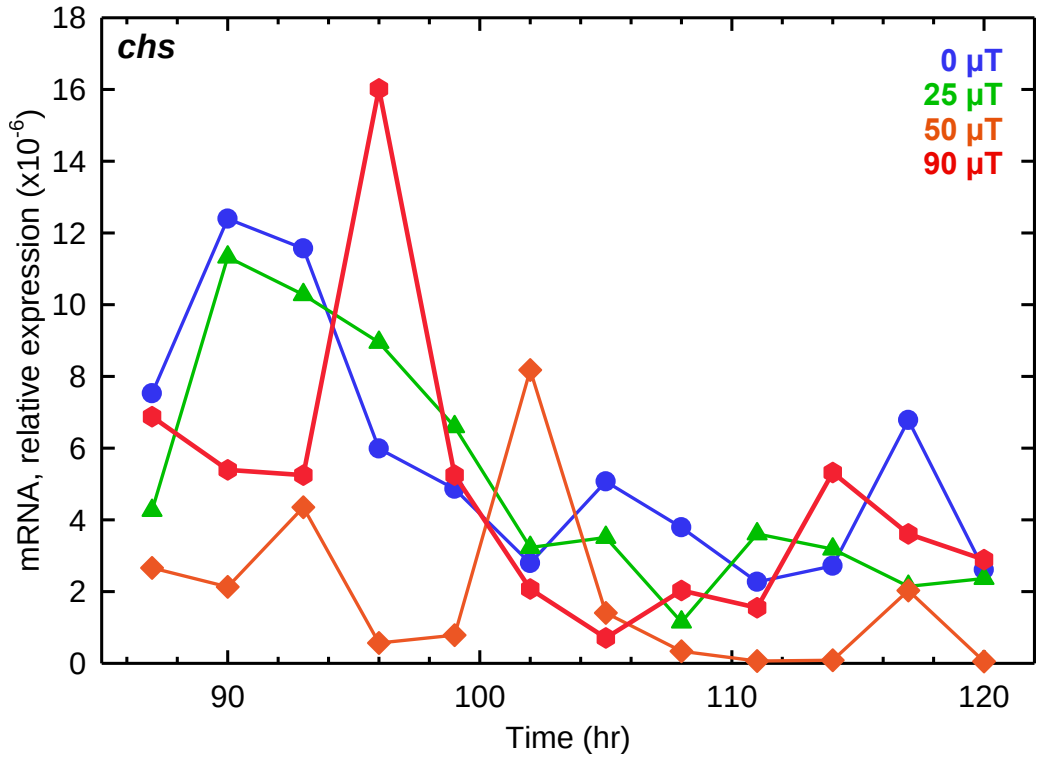

Fig 3.7: Kinetics of the transcription of chalcone synthase gene (*chs*) from 87 hr to 120 hr at four different magnetic flux densities (0, 25, 50 and 90 µT). All the original values of mRNA expression were multiplied by 10^6 to present in the graph.

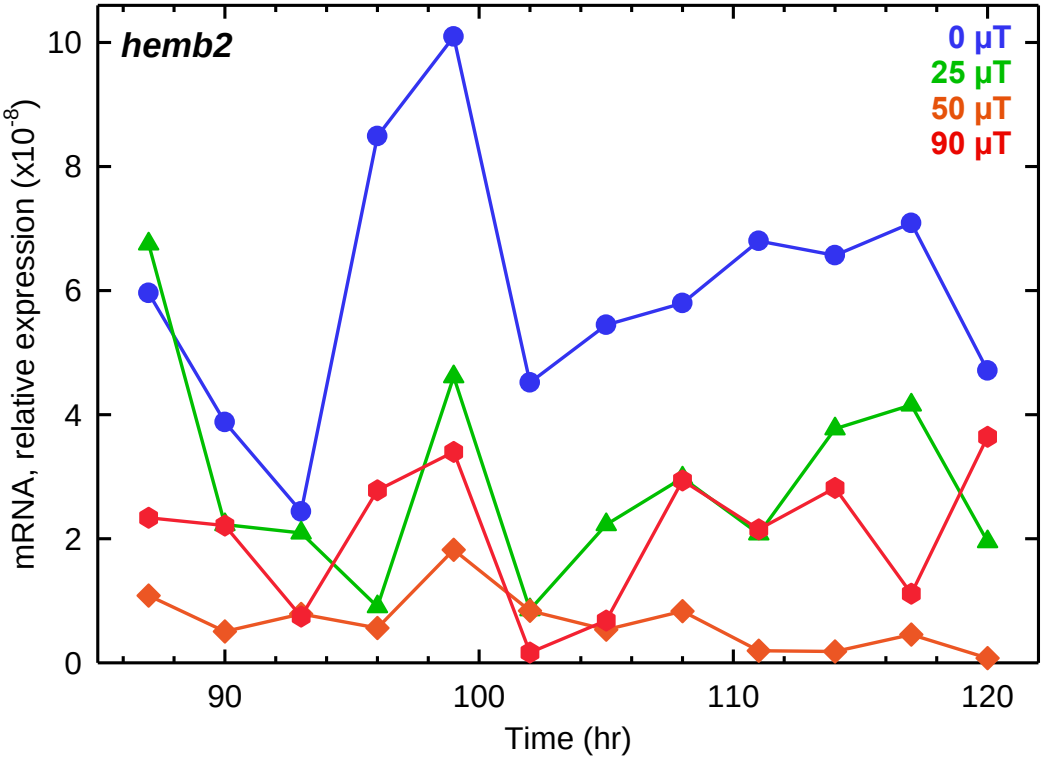

Fig 3.8: Kinetics of the transcription of porphobilinogen synthase gene (*hemb2*) from 87 hr to 120 hr at four different magnetic flux densities (0, 25, 50 and 90 µT). All the original values of mRNA expression were multiplied by 10^8 to present in the graph.

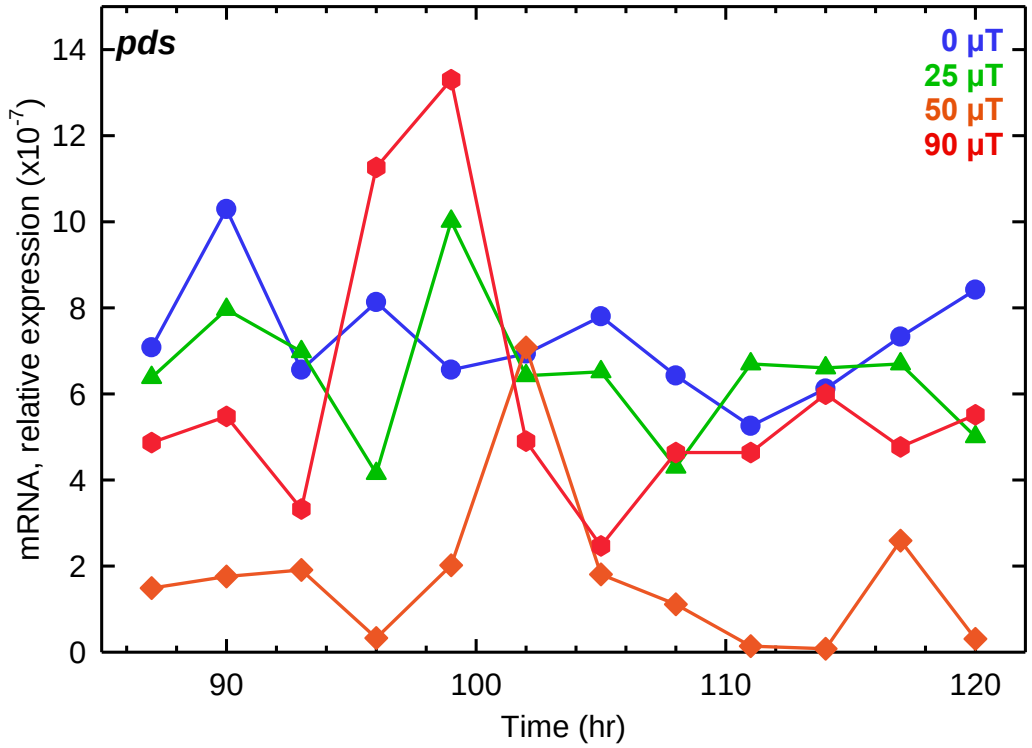

Fig 3.9: Kinetics of the transcription of phytoene dehydrogenase gene (*pds*) from 87 hr to 120 hr at four different magnetic flux densities (0, 25, 50 and 90 µT). All the original values of mRNA expression were multiplied by 10^7 to present in the graph.

3.2 Dependence of hypocotyl length on magnetic flux density

Five days old seedlings of *Ler*, *cry1cry2* double mutant and *phyAphyB* double mutant were placed on a plastic plate and photographed. Fifty seedlings were taken from each petri plate kept at a particular flux density in the Helmholtz coils. The hypocotyl length was then measured digitally using Image-J. Each of the various *Arabidopsis* strains was tested with low blue light fluence rate (3.5 W/m²) and high blue light fluence rate (22.6 W/m²). The results are shown in the following graphs.

3.2.1 Effect of magnetic fields on hypocotyl length in *Ler* seedlings

Fig. 3.10 shows the photographs of the five-days old seedlings of *Ler* placed one by one on a dark-colored plastic plate for the measurement of the hypocotyl length. Figures 3.11 and 3.12 show the results of the measure of the hypocotyl length in *Ler* seedlings in low blue light fluence rate (3.5 W/m²) and high blue light fluence rate (22.6 W/m²) respectively. Both graphs also display the data of dark grown seedlings, which have longer average length as compared to light grown seedlings. The graphs clearly indicate that magnetic flux density does not influence hypocotyl length. However in the Fig. 3.13, wherein the same data are

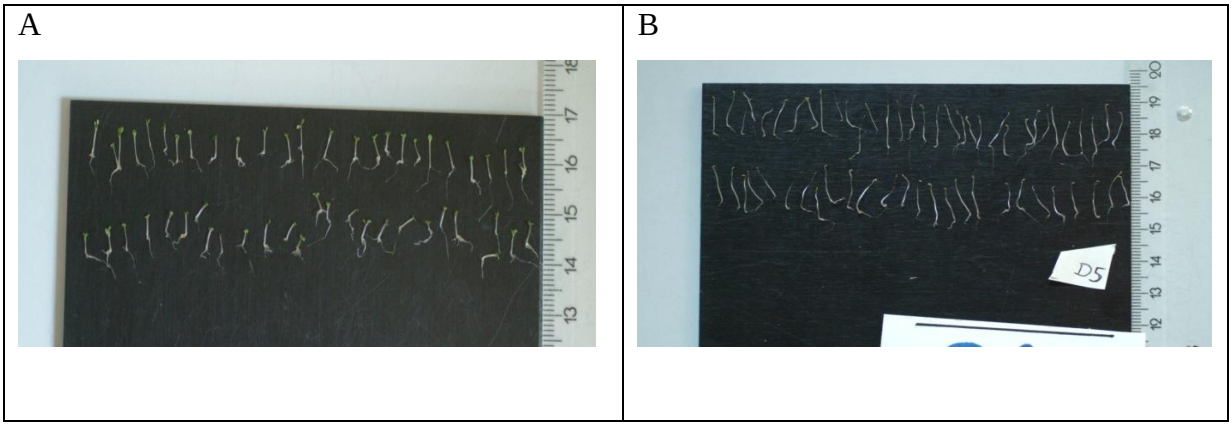

Fig 3.10: Photographs of the harvested seedlings of five days old seedlings of *Ler* placed on the dark colored plastic plate for the measurement of the hypocotyl length. **A.** *Ler* seedlings grown in blue light. **B.** *Ler* seedlings grown in darkness.

plotted as dark divided by light for both low and high blue light fluence rates, which indicates the factor by which blue light suppresses the hypocotyl length, one can easily observe some effects caused by magnetic flux density and such effects are even more visible in the plots of high fluence rate.

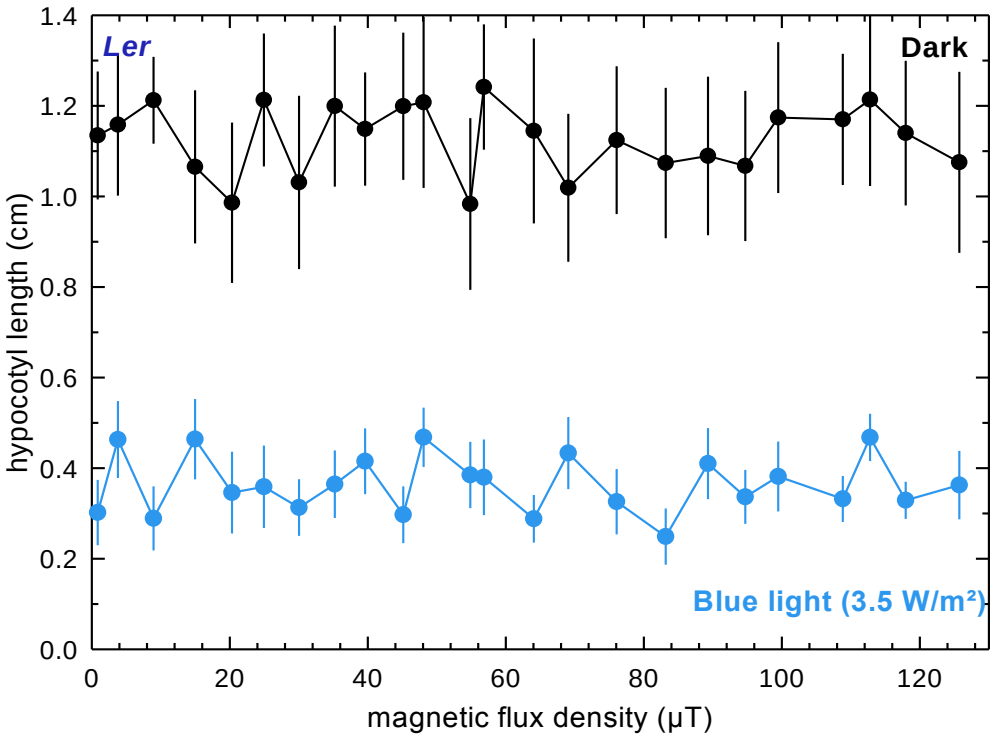

Fig 3.11: Dependence of hypocotyl length on magnetic flux density in *Ler* seedlings at low fluence rate (3.5 W/m^2) along with dark grown *Ler* seedlings. Error bars = SD (50 seedlings).

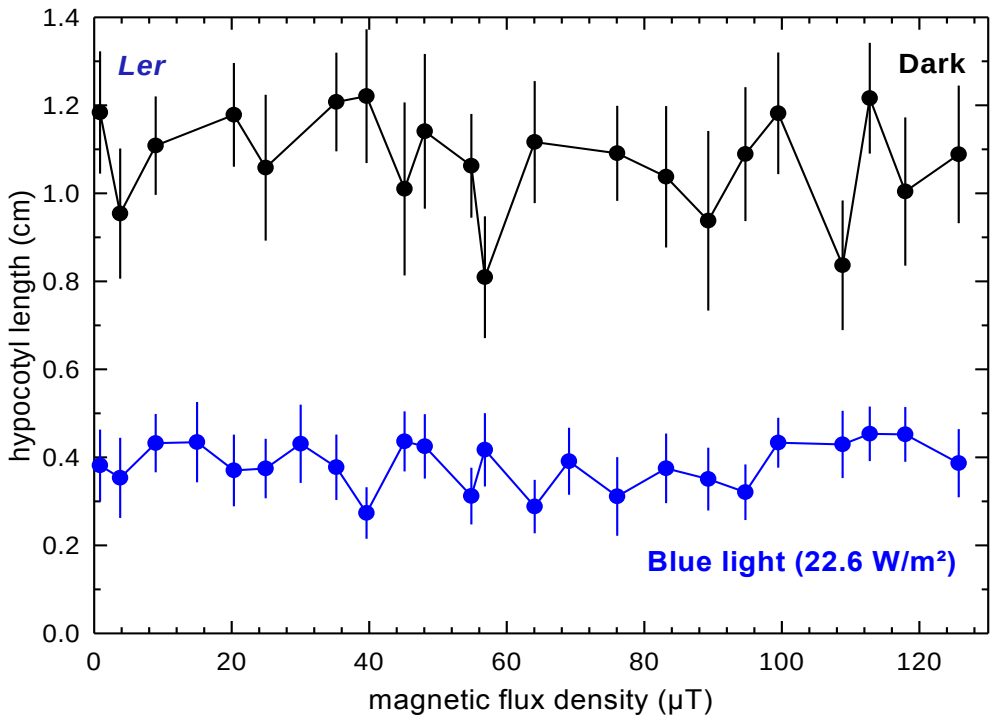

Fig 3.12: Dependence of hypocotyl length on magnetic flux density in *Ler* seedlings at high fluence rate (22.6 W/m^2) along with dark grown *Ler* seedlings. Error bars = SD (50 seedlings).

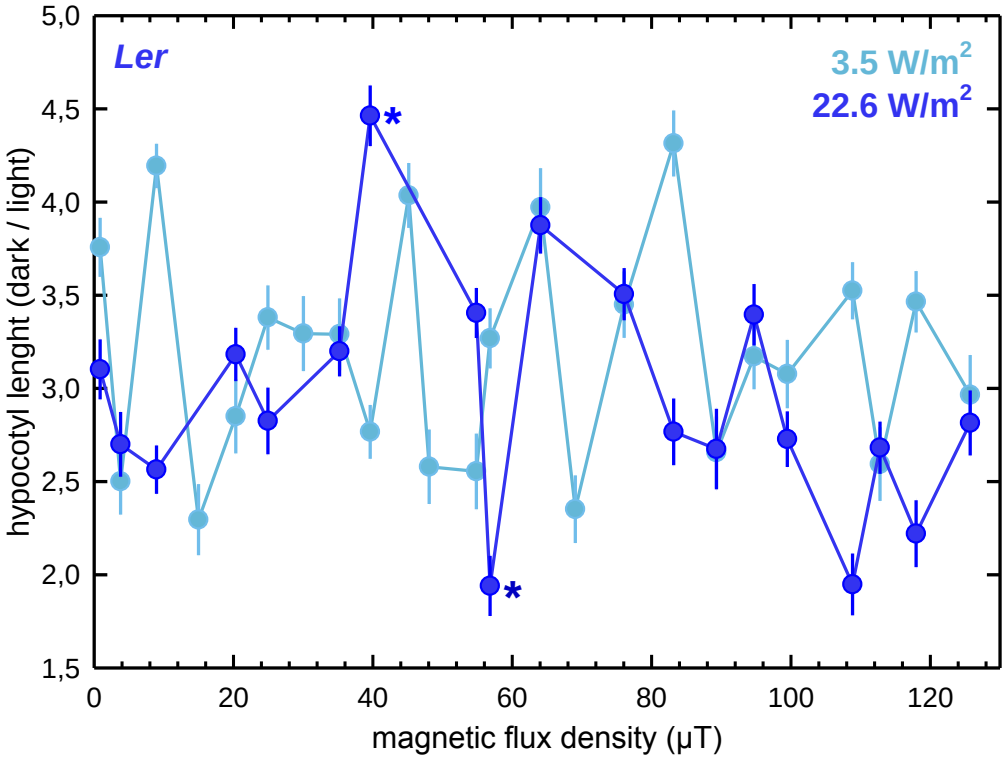

Fig 3.13: Dependence of blue-light induced hypocotyl shortening on the magnetic flux density in *Ler* seedlings at low (3.5 W/m²) and high blue light fluence rates (22.6 W/m²). The response is expressed as the ratio dark/light. Error bars = SD (50 seedlings). The difference in the mean values of the two groups marked by '*' is greater than would be expected by chance; there is a statistically significant difference between the input groups (P = <0.001; t-test). The data points marked with asterix '*' in this figure and the following figures were used for performing the t-test to find out the statistical significance of the difference between them.

3.2.2 Effect of magnetic fields on hypocotyl length in *cry1cry2* double mutant seedlings

Similar experiments with regard to hypocotyl length were repeated using *cry1cry2* double mutants. The observations are plotted in the following graphs, Fig. 3.15 and 3.16. In these seedlings, because of the absence of two main cryptochromes i.e., cryptochrome1 and cryptochrome2, which are responsible for the suppression of the hypocotyl length in blue light, the difference between the lengths of light grown and dark grown seedlings is small (Fig. 3.14). This is in contrast to *Ler* seedlings where this difference is quite significant. On account of this fact, in the stimulus-response curve for dark, 0.5 cm was added to each of the dark values to avoid it from overlapping with the stimulus-response curve for light. As it was noticed in *Ler* seedlings, apparently we fail to find any effect of magnetic flux density on the hypocotyl length. Nevertheless, as we looked for the factor of suppression of hypocotyl length by blue light, i.e., dark divided by light, the effects of magnetic flux density on hypocotyl length became more visible in the form of multiple maxima and minima in the plots. Again such an effect was more pronounced when seedlings were irradiated at higher fluence rate (22.6 W/m²) as compared to low fluence rate (3.5 W/m²).

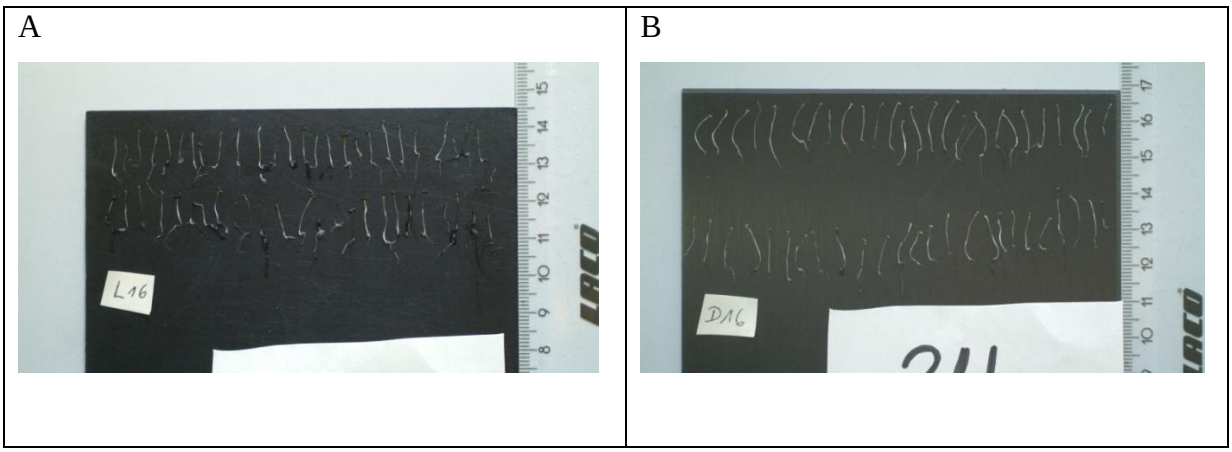

Fig 3.14: Photographs of the harvested seedlings of five days old *cry1cry2* double mutants placed on the dark colored plastic plate for the measurement of the hypocotyl length. **A.** *cry1cry2* seedlings grown in blue light. **B.** *cry1cry2* seedlings grown in darkness.

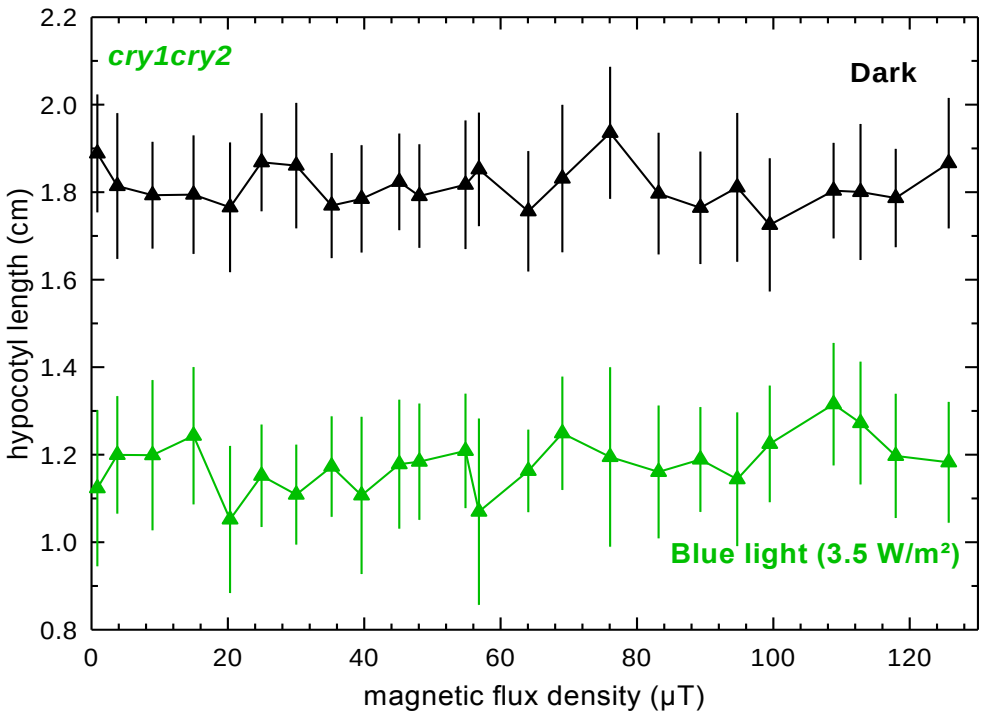

Fig 3.15: Dependence of hypocotyl length on magnetic flux density in *cry1cry2* double mutant seedlings at low fluence rate of blue light (3.5 W/m^2), plotted along with dark grown seedlings. In the stimulus-response curve for dark, 0.5 cm was added to each of the dark values to show it distinctively from the blue light plot. Error bars = SD (50 seedlings).

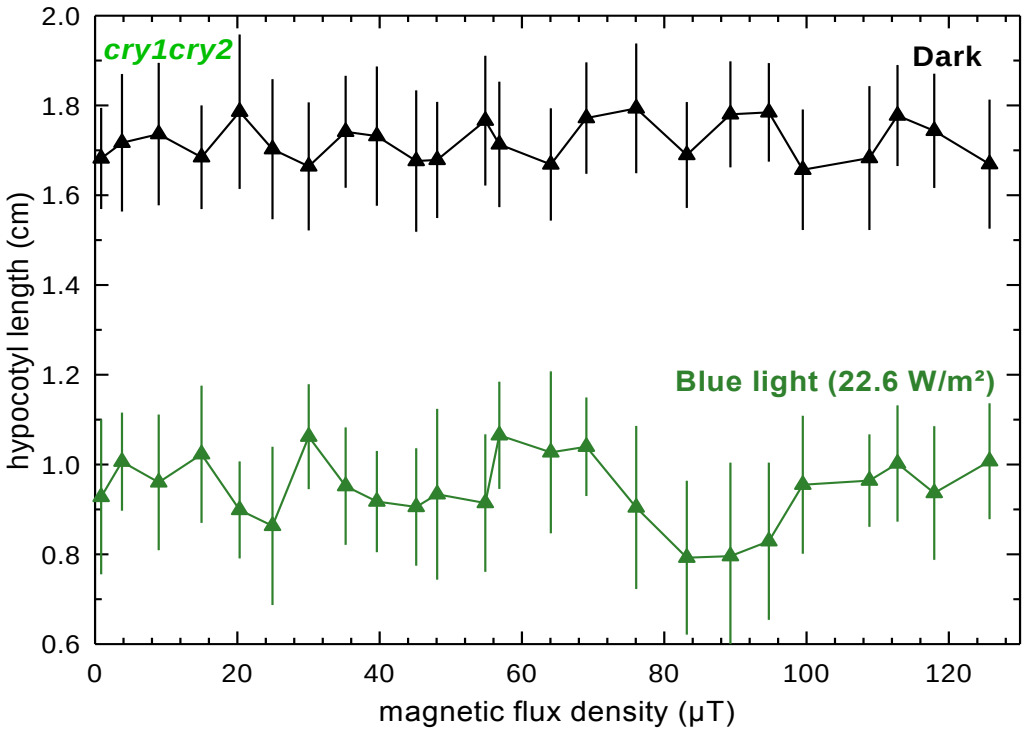

Fig 3.16: Dependence of hypocotyl length on magnetic flux density in *cry1cry2* double mutant seedlings at high fluence rate of blue light (22.6 W/m^2), plotted along with dark grown seedlings. In the dark plot, 0.5 cm was added to each of the dark values to show it distinctively from the light plot. Error bars = SD (50 seedlings).

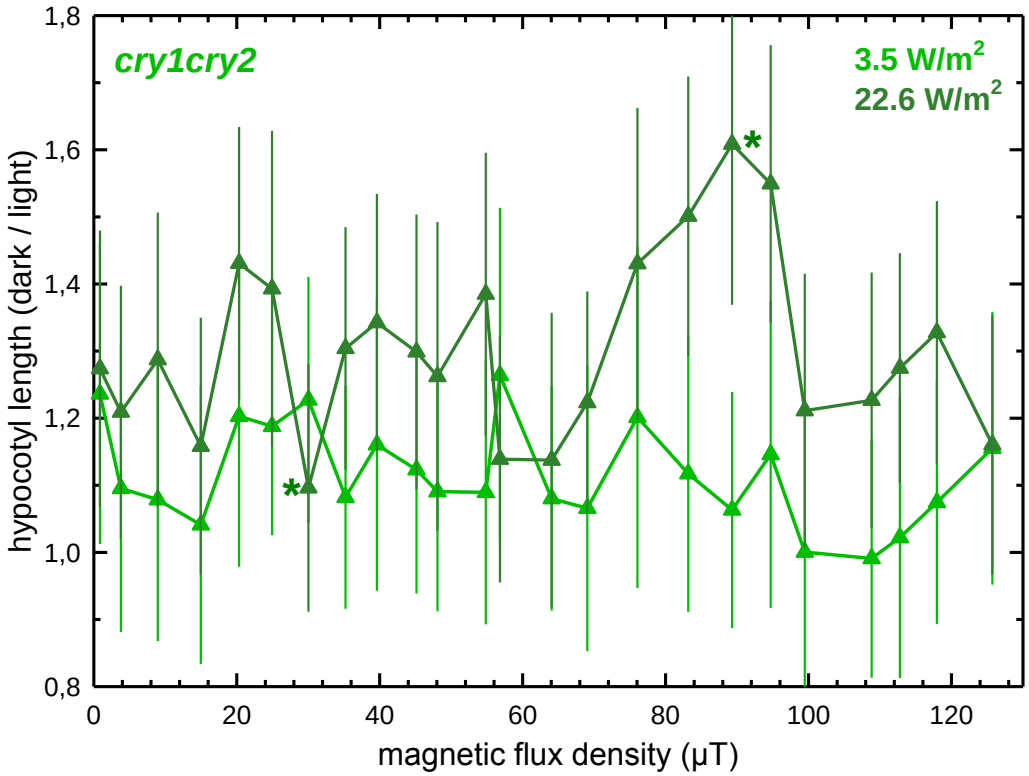

Fig 3.17: Dependence of blue light induced hypocotyl shortening on the magnetic flux density in *cry1cry2* double mutant seedlings at low (3.5 W/m²) and high blue light fluence rates (22.6 W/m²). The response is expressed as the ratio dark/light. Error bars = SD (50 seedlings). The difference in the mean values of the two groups marked by '*' is greater than would be expected by chance; there is a statistically significant difference between the input groups (P = <0.001; t-test).

3.2.3 Effects of magnetic fields on hypocotyl length in *phyAphyB* double mutant seedlings

The influence of magnetic fields was also tested on *phyAphyB* double mutants. The results of these experiments are shown in the following figures (Fig. 3.19 and 3.20). Photographs of light and dark grown *phyAphyB* double mutant seedlings are shown in Fig. 3.18. As observed earlier, no distinct effects could be made out in hypocotyl length, but as the values were plotted for the suppression of hypocotyl length, obvious effects in the form of multiple maxima and minima in the stimulus-response curves became discernible not only at high fluence rate but also at low fluence rate of blue light (Fig. 3.21). Such effects were less prominent in case of *Ler* and *cry1cry2* double mutant seedlings.

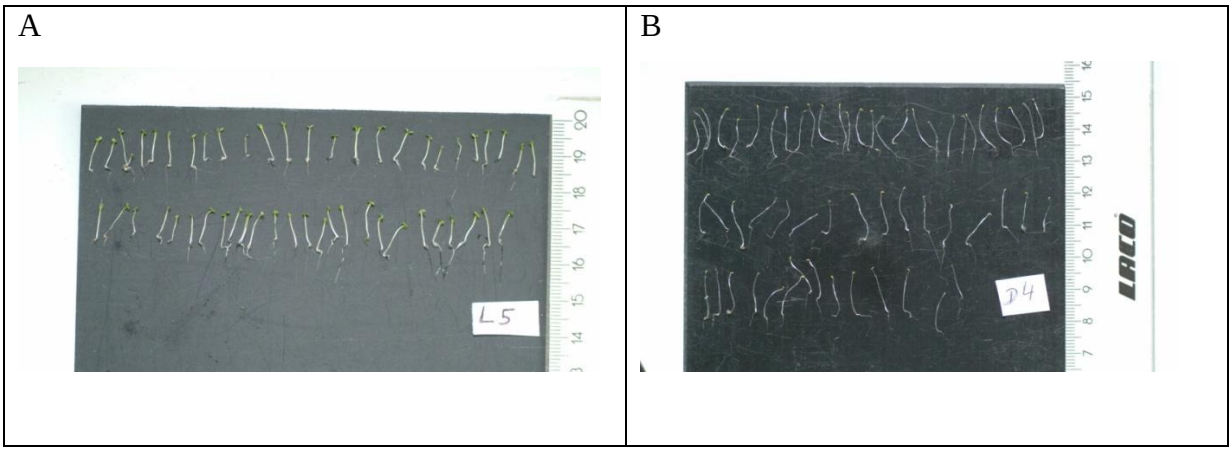

Fig 3.18: Photographs of harvested seedlings of five days old *phyAphyB double mutants* placed on the dark colored plastic plate for the measurement of the hypocotyl length. **A.** *phyAphyB* seedlings grown in blue light. **B.** *phyAphyB* seedlings grown in darkness.

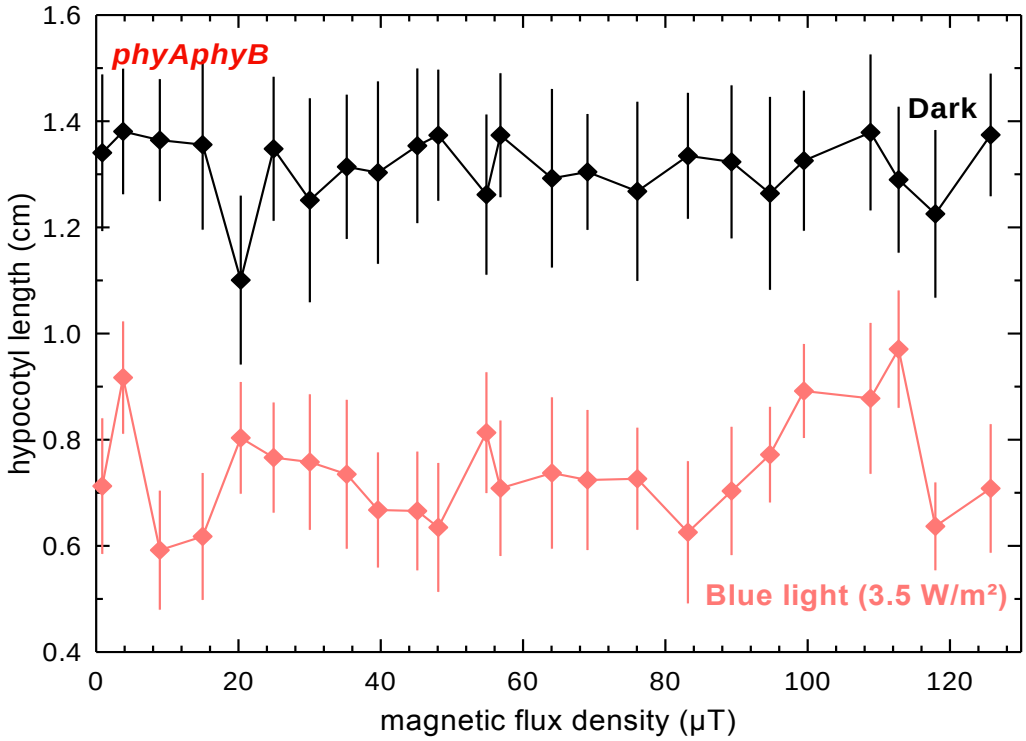

Fig 3.19: Dependence of hypocotyl length on magnetic flux density in *phyAphyB* double mutant seedlings at low blue light fluence rate (3.5 W/m^2), plotted along with dark grown seedlings. Error bars = SD (50 seedlings).

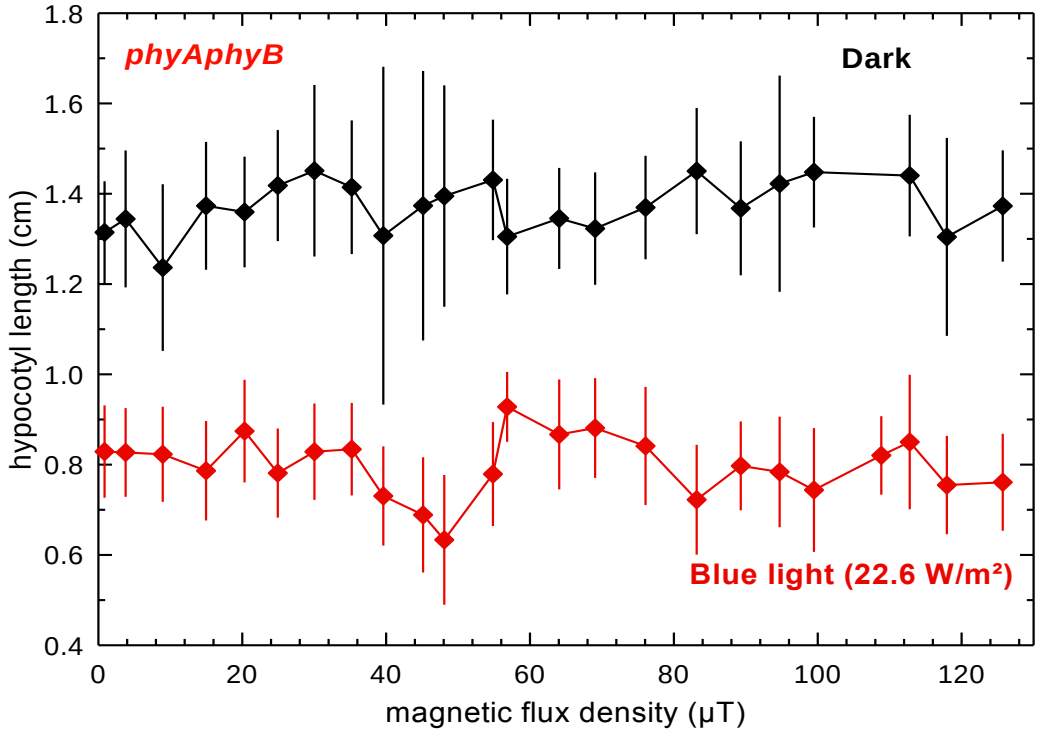

Fig 3.20: Dependence of hypocotyl length on magnetic flux density in *phyAphyB* double mutant seedlings at high blue light fluence rate (22.6 W/m^2), plotted along with dark grown seedlings Error bars = SD (50 seedlings).

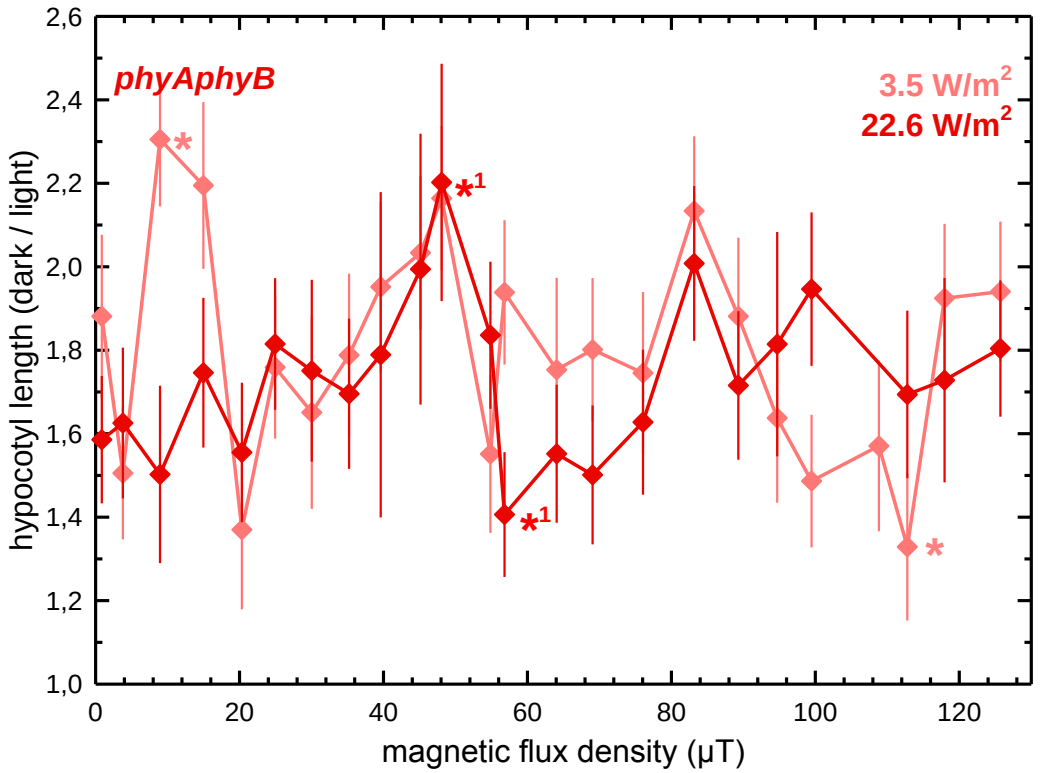

Fig 3.21: Dependence of the blue-light induced hypocotyl shortening on the magnetic flux density in *phyAphyB* double mutants seedlings at low (3.5 W/m²) and high blue light fluence rate (22.6 W/m²). The response is expressed as the ratio dark/light. Error bars = SD (50 seedlings). The difference in the mean values of the two groups marked by '*' in the low fluence rate plot (3.5 W/m²) is greater than would be expected by chance; there is a statistically significant difference between the input groups (P = <0.001; t-test). Similarly in case of high blue light fluence rate plot (22.6 W/m²) the difference in the mean values of the two groups marked by '*^{1}' is greater than would be expected by chance; there is a statistically significant difference between the input groups (P = <0.001; t-test).

3.2.4 Comparison of effects of magnetic flux density on hypocotyl length in *Ler*, *cry1cry2* and *phyAphyB* double mutant seedlings

When the stimulus-response curves of all three strains of *Arabidopsis* were compared for the effects of magnetic flux density on hypocotyl length at low and high blue light fluence rate, a very clear picture emerged. At low blue light fluence rate, the hypocotyl length seems to remain unaffected, as shown in Fig. 3.22. In contrast at higher fluence rate of blue light the hypocotyl length gets affected as a function of magnetic flux density. And this effect appears to be similar in all the three strains of *Arabidopsis*, as the position of maxima and minima in the stimulus-response curves seem to be coinciding, as seen in Fig. 3.23 and such a coincidence is more visible in case of both the double mutants (Fig. 3.24).

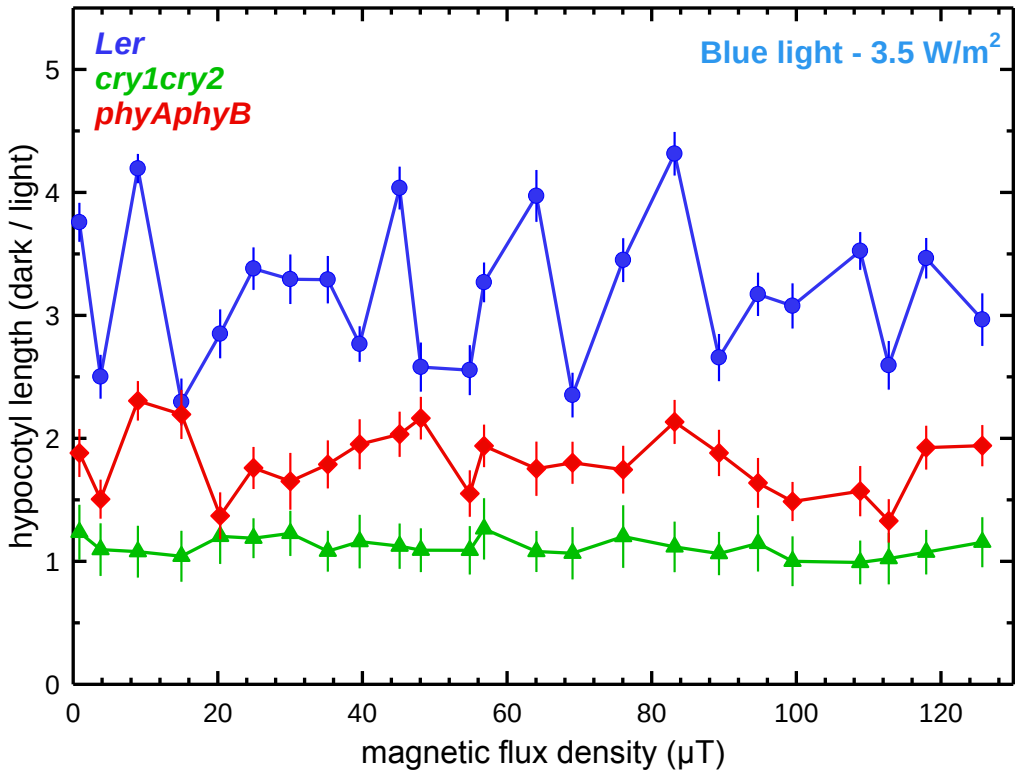

Fig 3.22: Comparison of blue-light induced shortening of hypocotyl length, expressed as ratio of dark/light, to the magnetic flux density in *Ler*, *cry1cry2* double mutant and *phyAphyB* double mutant seedlings at low fluence rate (3.5 W/m²). Error bars = SD (50 seedlings).

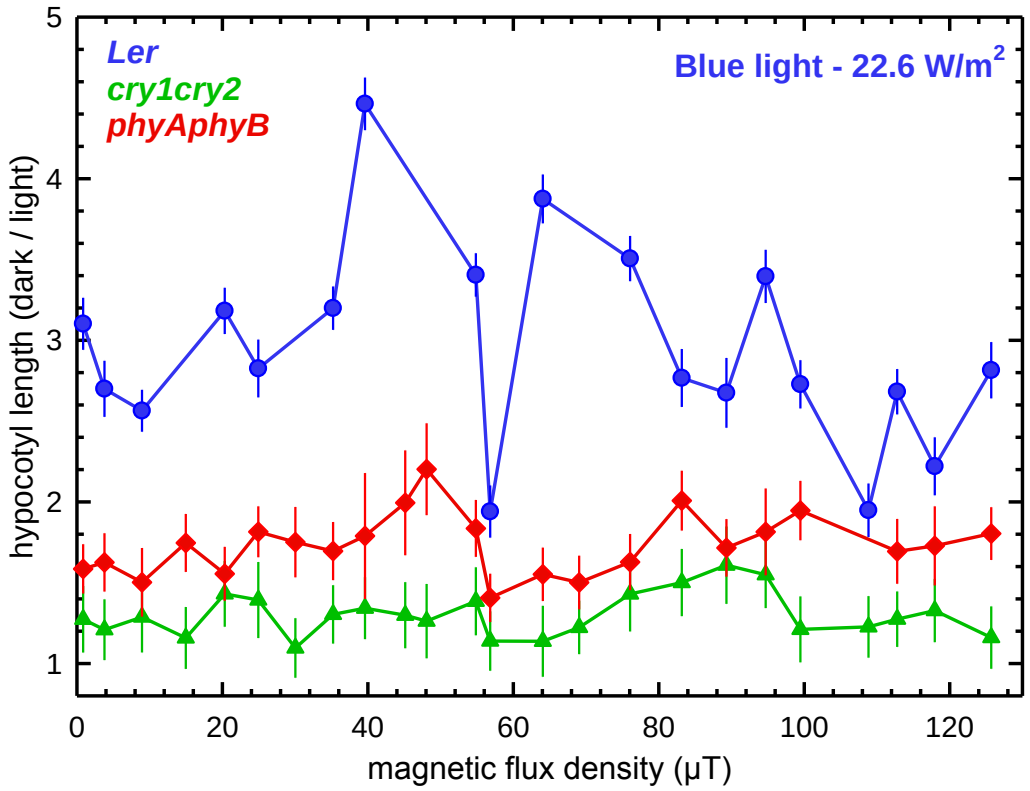

Fig 3.23: Comparison of blue-light induced shortening of hypocotyl length, expressed as ratio of dark/light, to the magnetic flux density in *Ler*, *cry1cry2* double mutant and *phyAphyB* double mutant seedlings at high fluence rate (22.6 W/m²). Error bars = SD (50 seedlings).

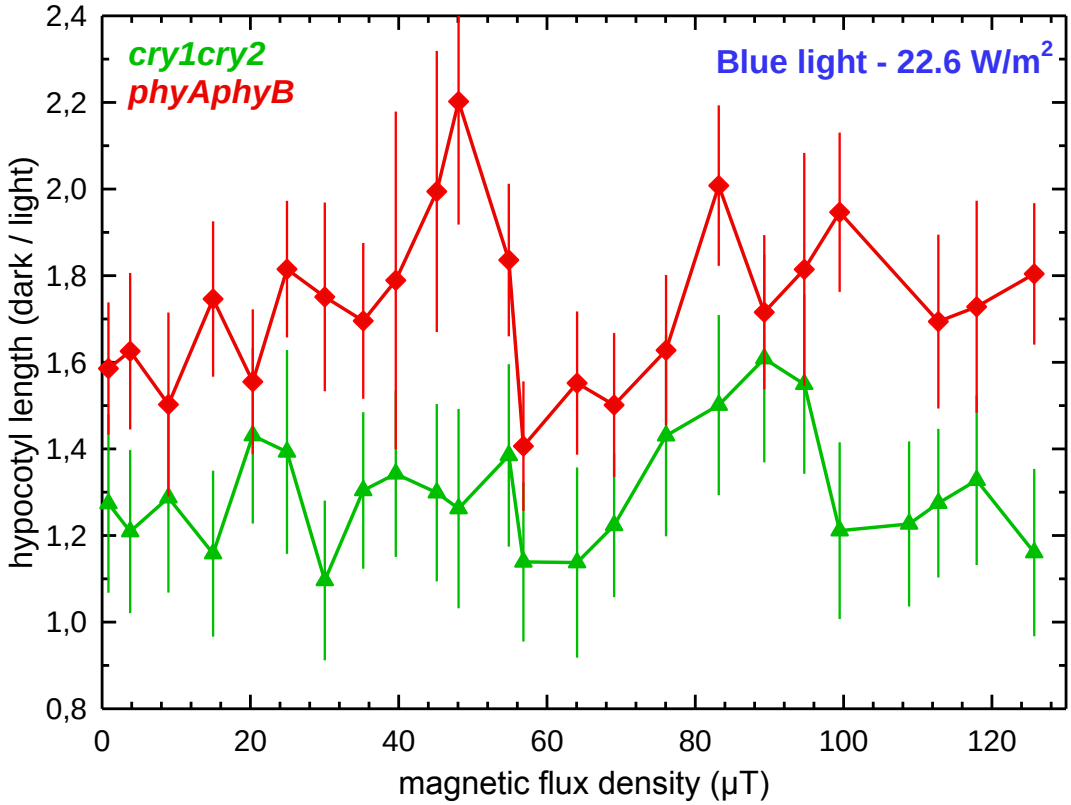

Fig 3.24: Comparison of blue-light induced shortening of hypocotyl length, expressed as ratio of dark/light, to the magnetic flux density in *cry1cry2* double mutant and *phyAphyB* double mutant seedlings at high fluence rate (22.6 W/m²). Error bars = SD (50 seedlings).

3.3 Anthocyanin accumulation

Anthocyanin production in seedlings is one of the very important blue light dependent processes. With respect to our study and the radical-pair mechanism, analysis of anthocyanin quantification was very significant. Therefore we studied it extensively. For the purpose of searching for the effects of magnetic flux density, we conducted experiments for anthocyanin quantification at three different fluence rates of blue light. These were very low (1 W/m²), low (3.5 W/m²) and high (22.6 W/m²) fluence rates. All the three strains of *Arabidopsis* (*Ler*, *cry1cry2* double mutant and *phyAphyB* double mutant) were treated by these light intensities in different experiments and five days old seedlings were harvested for anthocyanin measurement. As blue light is directly involved in anthocyanin production, experiments were done primarily with blue light; however, a few experiments were also conducted using red light. Observations for both blue light and red light experiments are shown below. Dark experiments were also conducted as control, but as negligible amounts of anthocyanin were produced in dark, the results are not shown here.

3.3.1 Effects of magnetic fields on Anthocyanin accumulation in blue light

The experiments performed for anthocyanin quantification under different blue light fluence rates were done using three strains. The following figures (Fig. 3.25 to 3.27) display the observations of these experiments. The *Ler* seedlings at very low fluence rate of blue light (1 W/m²) showed no response to variations in the magnitudes of magnetic flux densities. But at somewhat higher fluence rate (3.5 W/m²) the magnetic field was able to manifest its effects on the *Ler* seedlings. Similar effects were observed at very high fluence rates (22.6 W/m²). With these observations, it appears that magnetic fields require a certain threshold of light before they can manifest their effects on plants.

Somewhat similar observations were made with *cry1cry2* double mutants. Even *cry1cry2* double mutant displayed the influence of magnetic flux density at high fluence rate by showing multi-peaked stimulus-response curves to certain extent (Fig. 3.28). As in the case of the *Ler* seedlings, these mutants also required a certain threshold of blue light to show recognizable effects.

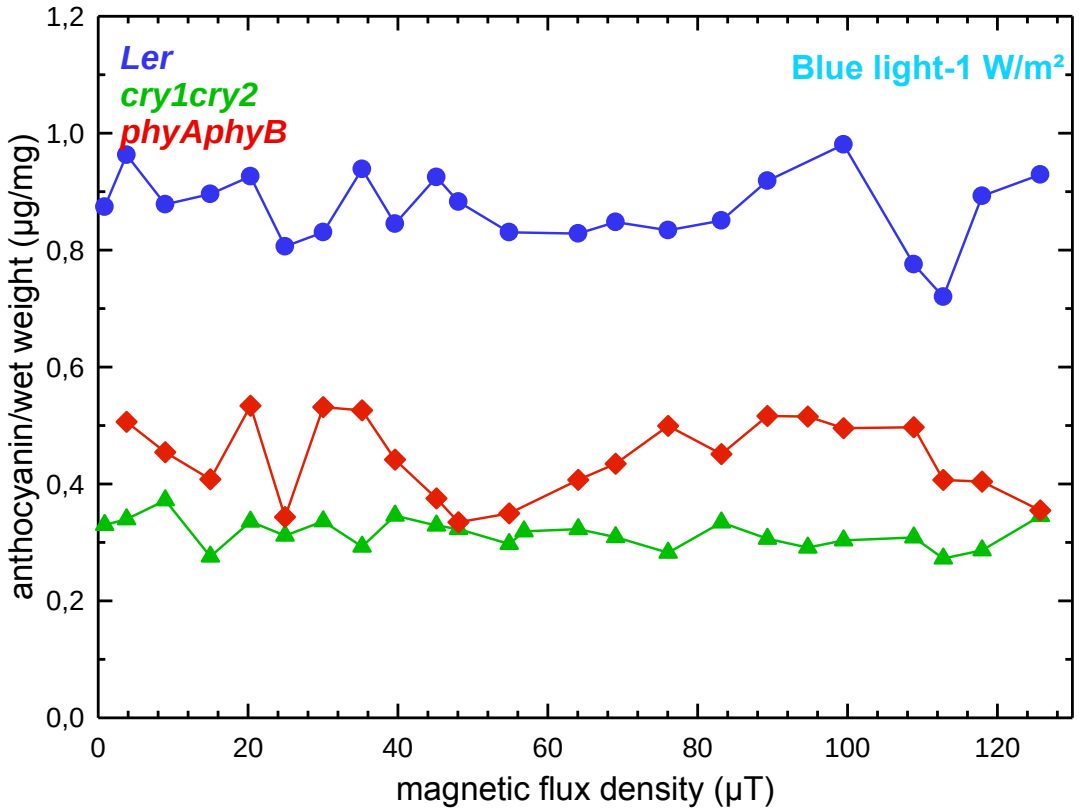

Fig 3.25: Dependence of anthocyanin accumulation on the magnetic flux density in *Ler*, *cry1cry2* double mutant and *phyAphyB* double mutant seedlings at very low blue light fluence rate (1 W/m²).

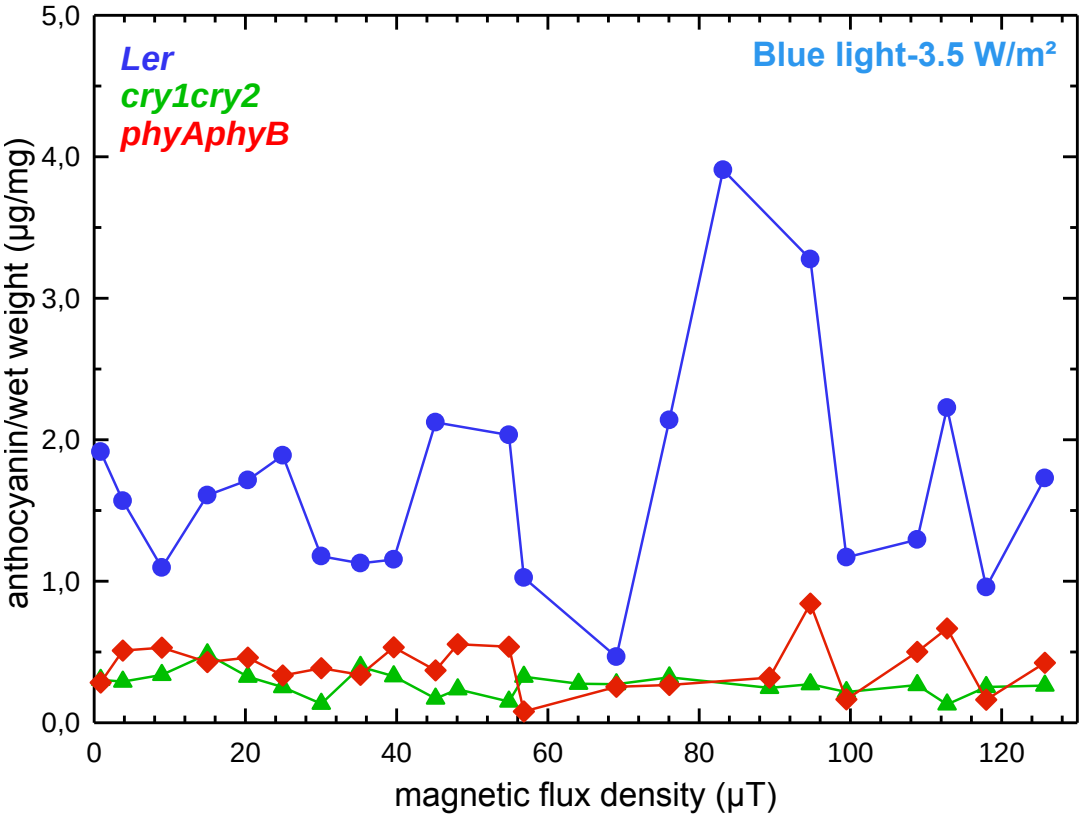

Fig 3.26: Dependence of anthocyanin accumulation on the magnetic flux density in *Ler*, *cry1cry2* double mutant and *phyAphyB* double mutant seedlings at low blue light fluence rate (3.5 W/m²).

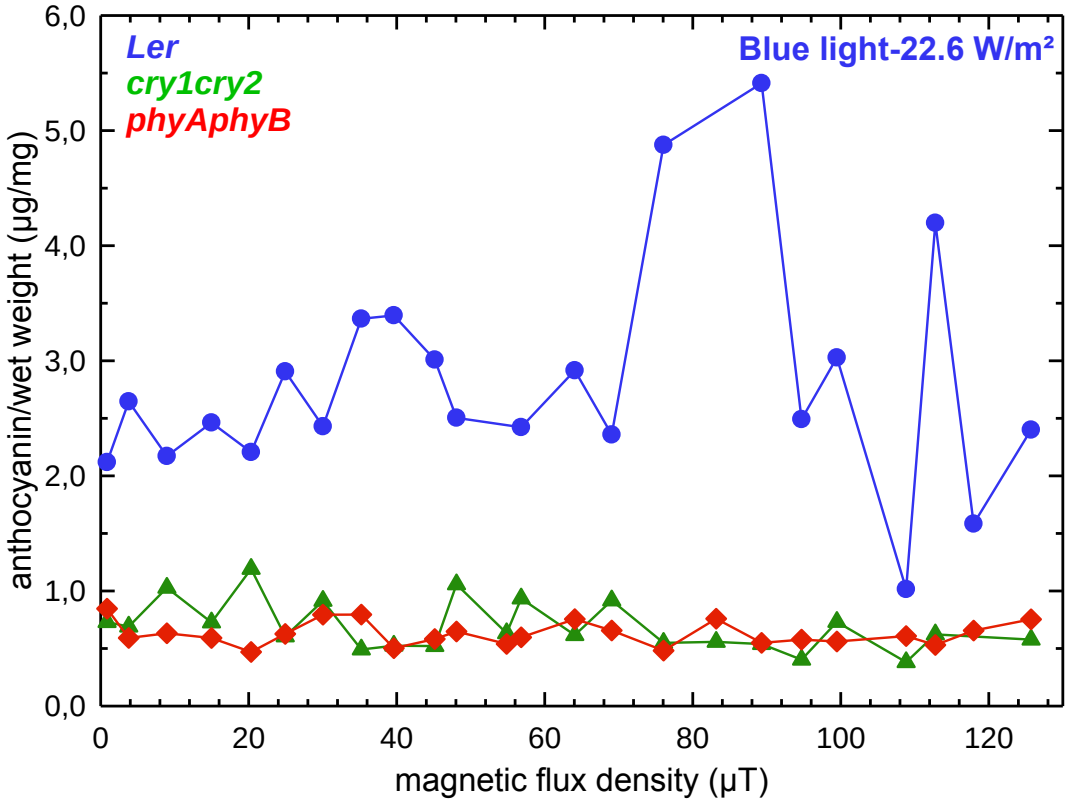

Fig 3.27: Dependence of anthocyanin accumulation on the magnetic flux density in *Ler*, *cry1cry2* double mutant and *phyAphyB* double mutant seedlings at high blue light fluence rate (22.6 W/m²).

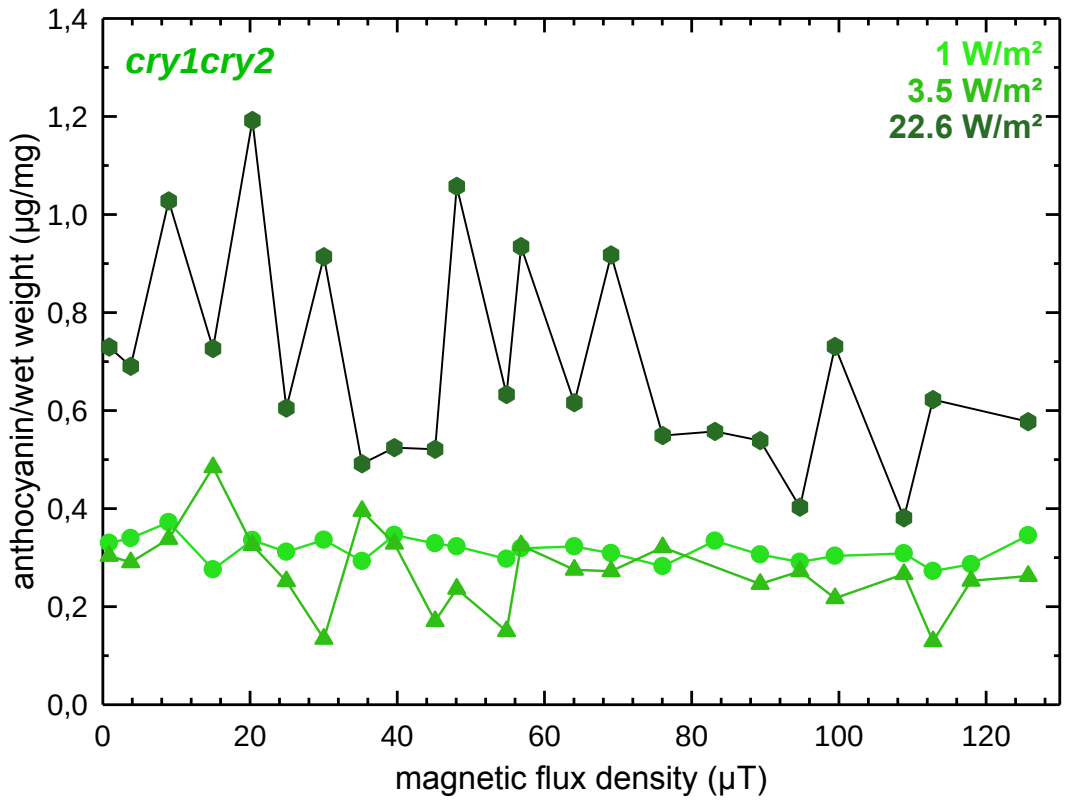

Fig 3.28: Comparison of the dependence of anthocyanin accumulation on the magnetic flux density in *cry1cry2* double mutant seedlings at very low blue light fluence rate (1 W/m²), low blue light fluence rate (3.5 W/m²) and high blue light fluence rate (22.6 W/m²).

3.3.2 Effects of magnetic fields on Anthocyanin accumulation in red light

As anthocyanin synthesis is a blue light dependent process, studying anthocyanin production under red light at a first glance appears naive. But the effects of magnetic flux density showed some puzzling results particularly in *cry1cry2* double mutants, so the idea of examining the anthocyanin quantification under red light came up as a control. Experiments were performed on all the three strains of *Arabidopsis* using 1 W/m² of red light. Fig. 3.29 displays the results of these experiments. As very low amounts of anthocyanin were produced in *phyAphyB* double mutants, the stimulus-response curve is almost a straight line, but in *Ler* and *cry1cry2* double mutant, where there was significant production of anthocyanin even in red light, the effects of magnetic fields were also visible. The stimulus-response curves of both types of seedlings show a variable anthocyanin accumulation at different flux densities.

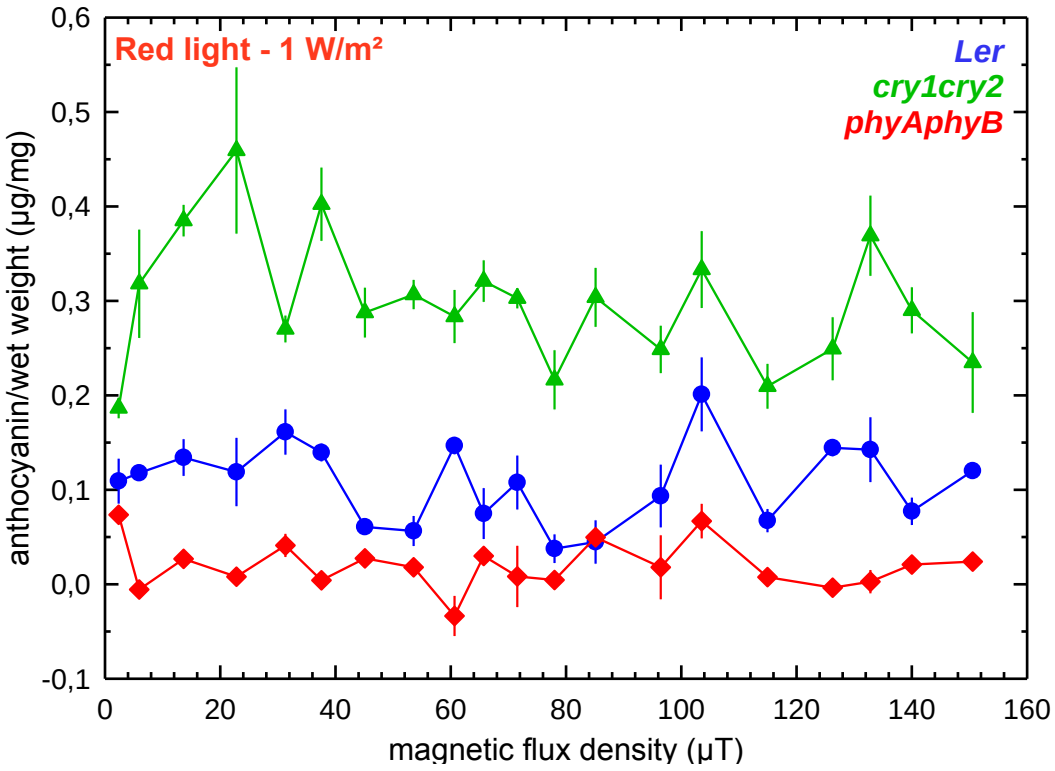

Fig 3.29: Dependence of anthocyanin accumulation on the magnetic flux density in *Ler*, *cry1cry2* double mutant and *phyAphyB* double mutant seedlings at very low red light fluence rate (1 W/m²). Error bars = SD (4 samples).

Fig. 3.30 shows the *Ler* seedlings response to magnetic flux density at 1 W/m² of red light. The two plots represent anthocyanin quantification; red plot is anthocyanin quantity per unit of plant wet weight whereas the green plot is the ratio of anthocyanin to total protein in the seedlings. Though the two plots relate anthocyanin to different factors, one relating to plant wet weight and the other to total proteins in the seedlings; still the plots match each

other perfectly. We know that the wet weight in *Arabidopsis* seedlings is closely related to their protein quantity. The measurement of wet weight is prone to errors, but measuring protein quantity is relatively more accurate. As the two plots in this figure closely follow each other, it gives an indication that the procedure used to measure wet weight has been precise.

Fig. 3.31 shows the comparison of the stimulus-response curves of *Ler* for both blue light and red light irradiated seedlings. The fluence rate in either case was 1 W/m². The results clearly indicate higher effectiveness of red light in manifesting the effects of magnetic fields.

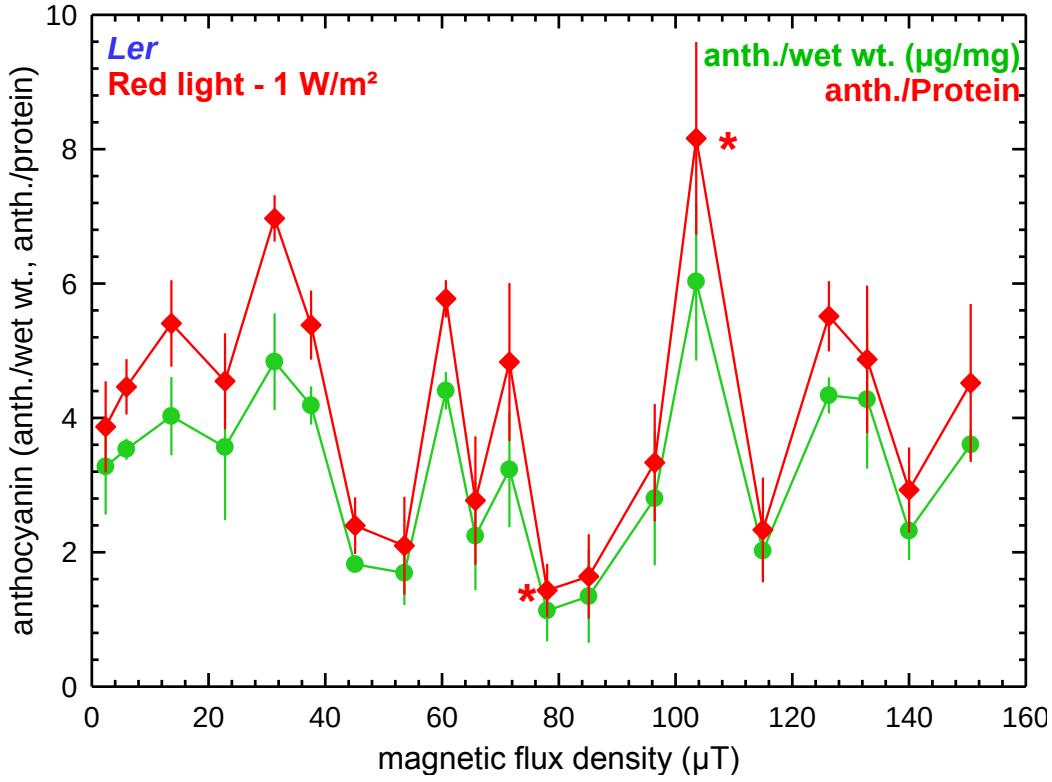

Fig 3.30: Dependence of anthocyanin accumulation on the magnetic flux density in *Ler* seedlings at very low red light fluence rate (1 W/m²). Green colored plot represents anthocyanin quantity per unit of plant weight and the original data is multiplied by a factor of 30, whereas the red plot represents the ratio of anthocyanin to total protein in the samples. In this case the original data were multiplied by a factor of 10^5. Error bars = SD (4 samples). The difference in the mean values of the two groups marked by **'*'** is greater than would be expected by chance; there is a statistically significant difference between the input groups (P = <0.001; t-test).

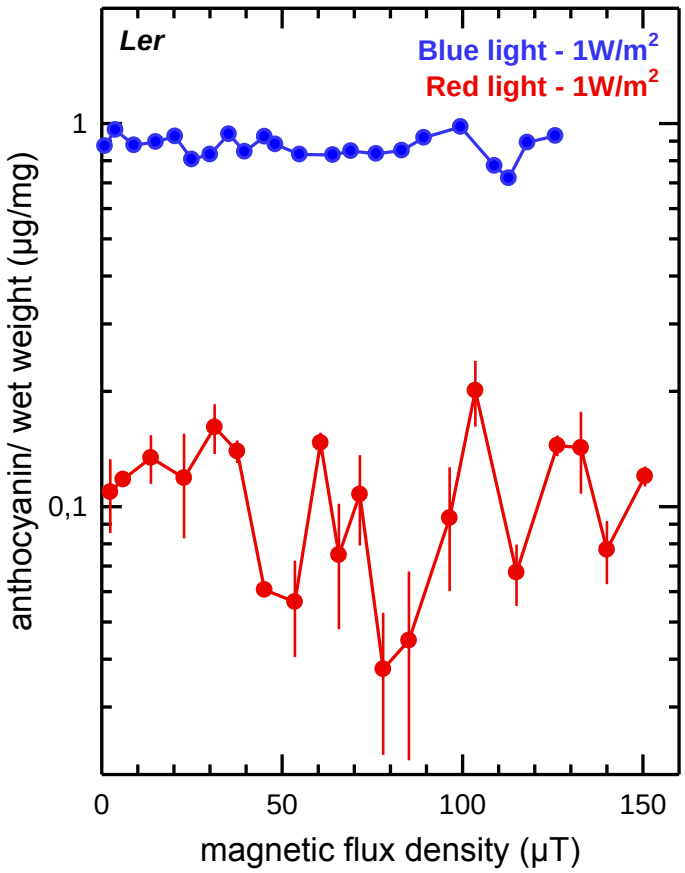

Fig 3.31: Comparison of the effects of blue light and red light on the effects of magnetic flux density on *Ler*. Stimulus-response curves for *Ler* under the fluence rate of 1 W/m² of blue light is a straight line compared to the stimulus-response curve, when the seedlings of *Ler* were irradiated with red light having the fluence rate of 1 W/m². Error bars = SD (4 samples).

3.4 Chlorophyll accumulation

One of the very important parameters in plant studies is the amount of chlorophyll produced by the plant under given conditions. Therefore we also quantified the total chlorophyll a and chlorophyll b, to examine, if there is any influence of magnetic flux density on this attribute. Similar to the studies done on hypocotyl length measurement and anthocyanin quantification, we performed experiments at low (3.5 W/m²) and high blue light (22.6 W/m²) fluence rates for chlorophyll quantification. All the three strains of *Arabidopsis* were used for the study. Fig. 3.32 and Fig. 3.33 show the results of these experiments. With respect to chlorophyll quantification, one can easily observe, particularly in case of *Ler* seedlings, that the effects of magnetic flux density were discernible only at higher fluence rates of blue light. The *phyAphyB* double mutant showed a similar pattern of chlorophyll quantity along the magnetic flux density gradient as shown by *Ler* at higher fluence rate, though the peaks are not as sharp as shown by *Ler* seedlings.

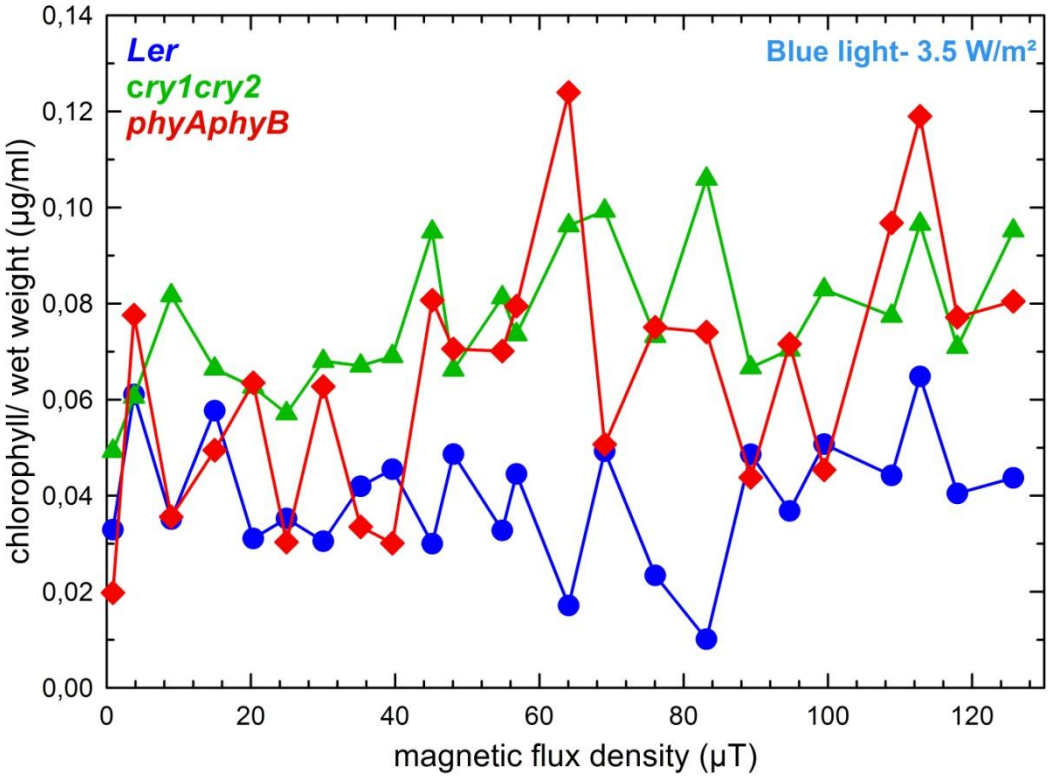

Fig 3.32: Dependence of chlorophyll amount on the magnetic flux density in *Ler*, *cry1cry2* double mutant and *phyAphyB* double mutant seedlings at low blue light fluence rate (3.5 W/m²).

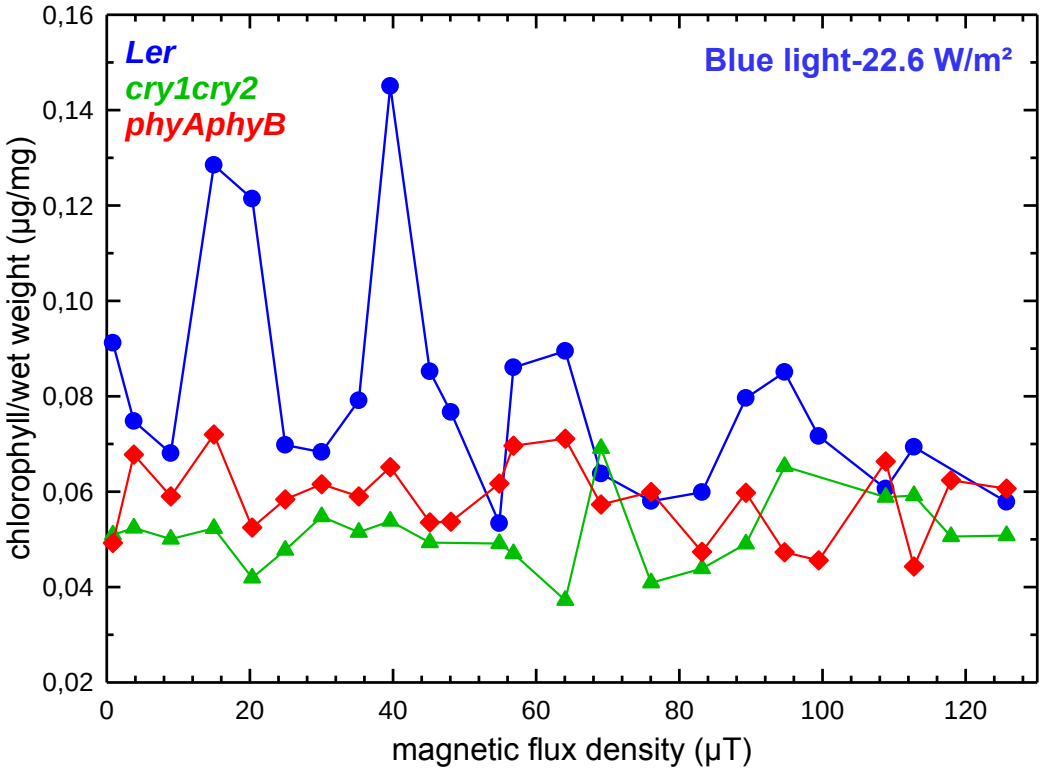

Fig 3.33: Dependence of chlorophyll amount on the magnetic flux density in *Ler*, *cry1cry2* double mutant and *phyAphyB* double mutant seedlings at high blue light fluence rate (22.6 W/m²).

3.5 Studies on Gene Expression

The observations on hypocotyl length and anthocyanin production raised the question whether magnetic flux density also influences the gene expression or not? To answer the question we performed experiments similar to the previous ones and tested the gene expression by real-time PCR. The light used in these experiments was 10 W/m² of blue light as previous experiments with *Ler* seedlings suggested it to be optimal for showing the effects (Fig. 3.34). Five days old seedlings were harvested and flash frozen in liquid nitrogen to preserve the physiological state of the seedlings. Total RNA was extracted from these seedlings and the relative amount of mRNA for various genes was determined.

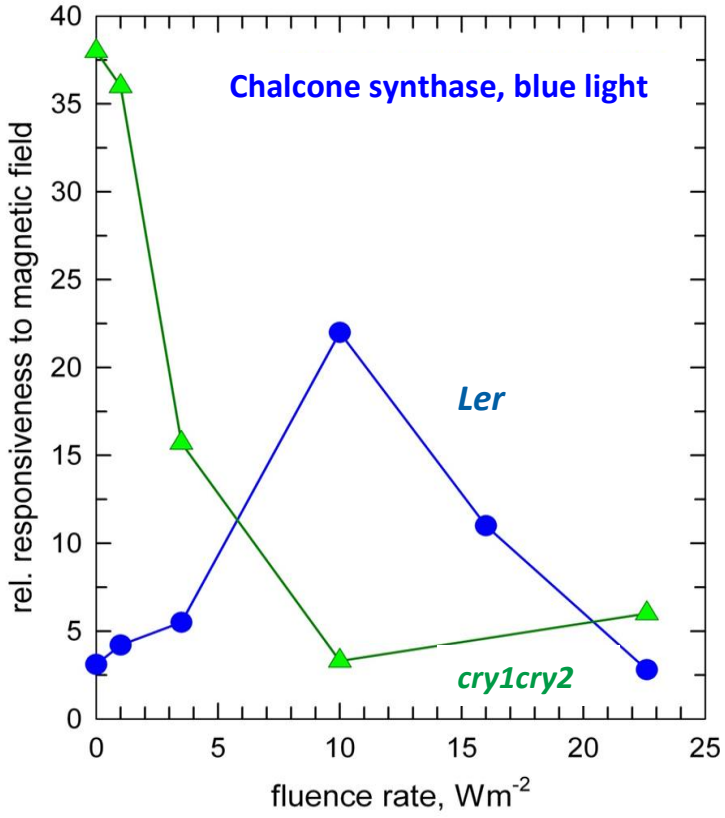

Fig 3.34: Dependence of the responsiveness of the gene expression of chalcone synthase gene (*chs*) to the fluence rate of blue light in *Ler* and *cry1cry2* seedlings. The figure shows the responsiveness of the gene to six different fluence rates of blue light, viz., 0, 1, 3.5, 10, 15 and 22.6 W/m². Note that *Ler* seedlings show maximum response at 10W/m² fluence rate of blue light that formed the basis of our selection of this quantum of blue light for all our future experiments.

3.5.1 Studies on gene expression in blue light and dark

To begin with, *Ler* seedlings were subjected to variable magnetic fields in the Helmholtz coils under blue light and in darkness. Eight genes were analyzed for their expression at different magnetic flux densities. Out of them the results of four are shown here. They are the genes for large subunit of RuBisCO (*rbcl*), chlorophyll a/b binding protein-4

(*cab4*), lycopene cyclase (*lyc*) and porphobilinogen synthase (*hemb2*). Following figures (Fig. 3.35 to 3.38) display the expression of these genes at different magnetic flux densities in 10 W/m² of blue light and in dark.

A very interesting picture emerges from these figures. Most interesting, the magnetic flux density down-regulates and up-regulates the genes expression in a wave like pattern along its increasing gradient. So the stimulus-response curves for the effects of magnetic flux density are completely different from the usually sigmoidal stimulus-response curves encountered in physiology.

Large subunit of RuBisCO gene (*rbcl*) shows three maximas under blue light, in the ranges of 0-20 µT, 35-50 µT and 100-130 µT (Fig. 3.35). This gene remains unaffected in dark as displayed by a straight line in the graph. The gene *Cab4* displays similar peaks, but here the first peak (0-20 µT range) is absent (Fig. 3.36). The other two peaks (35-50 µT and 100-130 µT ranges) are clearly visible. An additional peak within the range of 150-165 µT is displayed in *cab4*. In dark *cab4* gene remains unaffected, however, there is some tendency of up-regulation of this gene as depicted by little peaks at the corresponding positions to those observed in the blue light plot. The results of expression of *lyc* make the things more interesting as the up-regulation and down-regulation of the gene are not only occurring under blue light but also are quite prominent in darkness (Fig. 3.37). The three peak positions of *lyc* are similar to those of *cab4* under both light and dark experimental conditions. Almost similar results are shown by the porphobilinogen synthase gene (*hemb2*). It is to be noted here that this gene has higher expression levels in dark as compared to its expression under blue light (Fig. 3.38). Thus, the results of both *lyc* and *hemb2* strongly suggest that magnetic fields can manifest their effects even in darkness.

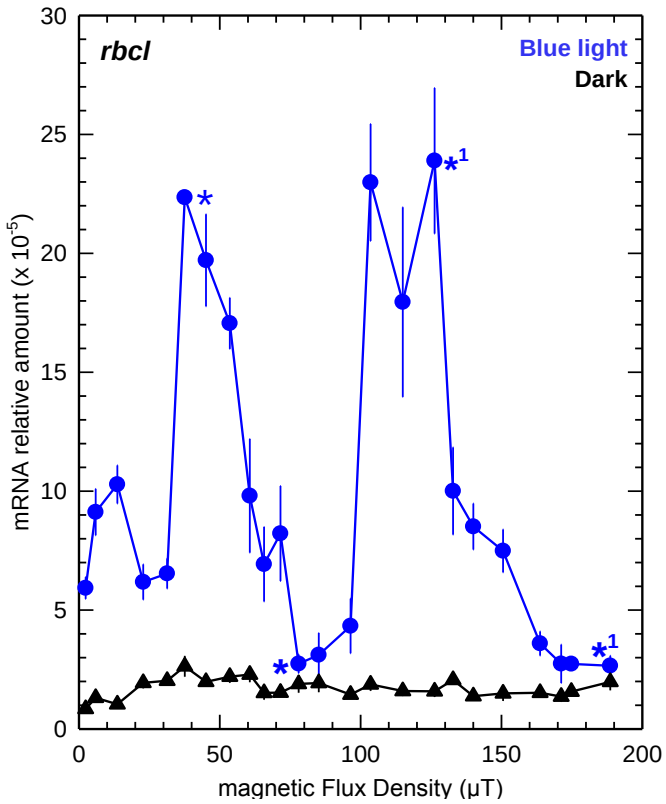

Fig 3.35: Dependence of mRNA levels of large subunit of RuBisCO gene (*rbcl*) on the magnetic flux density in *Ler* seedlings in blue light (fluence rate-10 W/m²). Dark grown seedlings were also analyzed and the result is expressed as black plot. Error bars = SE (4 samples). The difference in the mean values of the two groups marked by '*' is greater than would be expected by chance; there is a statistically significant difference between the input groups (P = <0.001). Similarly the difference in the mean values of the two groups marked by '*1' is greater than would be expected by chance; there is a statistically significant difference between the input groups (P = 0.001; t-test).

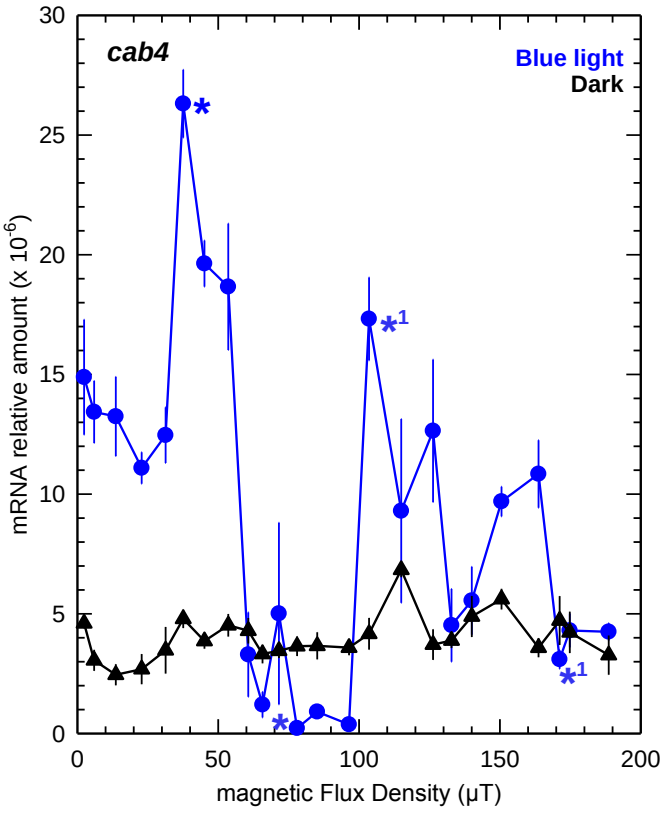

Fig 3.36: Dependence of mRNA levels of chlorophyll a/b binding protein-4 gene (*cab4*) on the magnetic flux density in *Ler* seedlings in blue light (fluence rate-10 W/m²). Dark grown seedlings were also analyzed and the result is expressed as black plot. Error bars = SE (4 samples). The difference in the mean values of the two groups marked by '*' is greater than would be expected by chance; there is a statistically significant difference between the input groups (P = <0.001). Similarly the difference in the mean values of the two groups marked by '*1' is greater than would be expected by chance; there is a statistically significant difference between the input groups (P = 0.002; t-test).

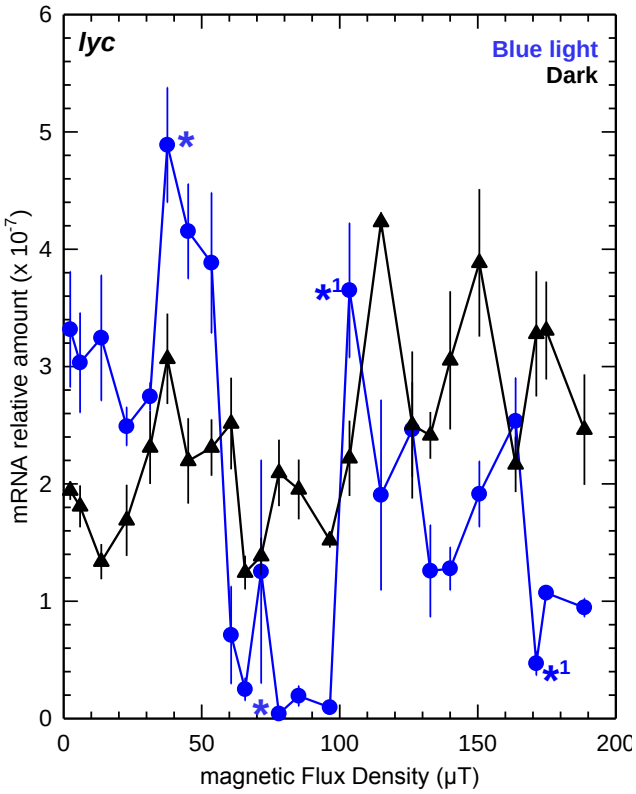

Fig 3.37: Dependence of mRNA levels of lycopene cyclase gene (*lyc*) on the magnetic flux density in *Ler* seedlings in blue light (fluence rate-10 W/m²). Dark grown seedlings were also analyzed and the result is expressed as black plot. Error bars = SE (4 samples). The difference in the mean values of the two groups marked by '*' is greater than would be expected by chance; there is a statistically significant difference between the input groups (P = <0.001). Similarly the difference in the mean values of the two groups marked by '*1' is greater than would be expected by chance; there is a statistically significant difference between the input groups (P = 0.003; t-test).

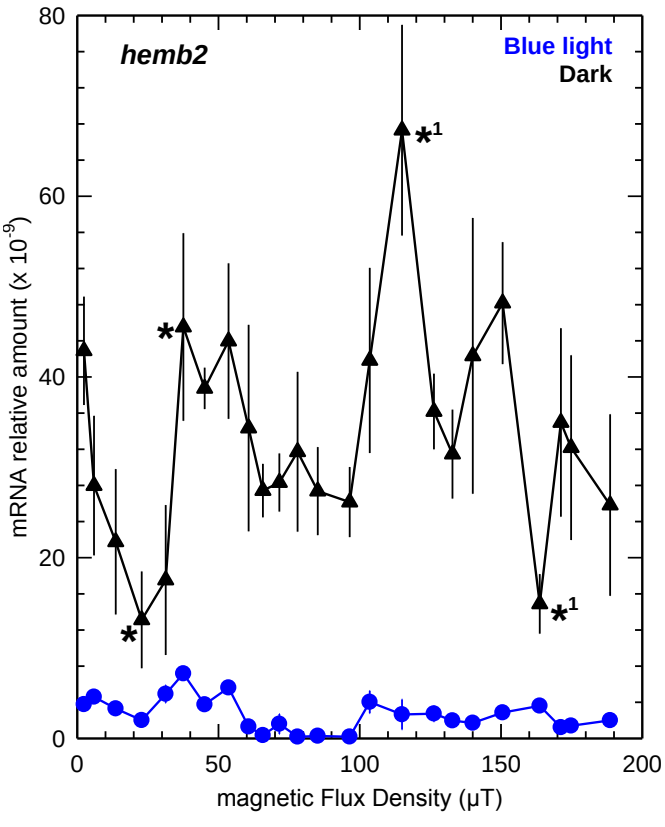

Fig 3.38: Dependence of mRNA levels of porphobilinogen synthase gene (*hemb2*) on the magnetic flux density in *Ler* seedlings in blue light (fluence rate-10 W/m²). Dark grown seedlings were also analyzed and the result is expressed as black plot. Error bars = SE (4 samples). The difference in the mean values of the two groups marked by '*' is not great enough to reject the possibility that the difference is due to random sampling variability. There is not a statistically significant difference between the input groups (P = 0.053). However the difference in the mean values of the two groups marked by '*1' is greater than would be expected by chance; there is a statistically significant difference between the input groups (P = 0,002). The difference in the mean values of the two groups, one marked by '*' at 22.5 µT and the other marked by '*1' at 115 µT is greater than would be expected by chance; there is a statistically significant difference between the input groups (P = <0.001; t-test).

3.5.2 Comparison of gene expression in *Ler* and *cry1cry2* double mutant in blue light and in darkness

The prerequisite for the occurrence of cryptochrome-based radical-pair mechanism is the presence of cryptochrome which absorbs blue light. Therefore we used cryptochrome mutants in our experiments to look for the effects on gene expression at variable magnetic flux densities. *Cry1cry2* double mutant was exposed to the same magnetic flux densities (0-190 µT) in both blue light (10 W/m²) and in darkness, as it has been done for *Ler* seedlings. The dark experiments with *cry1cry2* double mutant were done only in the range of 0 – 135 µT.

Eight genes were studied and the results were compared with the results of *Ler* seedlings. The results for the large subunit of RuBisCO (*rbcl*), chlorophyll a/b binding protein-4 (*cab4*), lycopene cyclase (*lyc*), porphobilinogen synthase (*hemb2*), chalcone synthase (*chs*), phenylalanine ammonia lyase (*pal4*), nitric oxide synthase (*nos1*), and elongation factor-1 (*ef1*) are shown in Fig. 3.39 to 3.46 in comparison to *Ler* seedlings.

In Fig. 3.39 (B), the gene *rbcl* in the *cry1cry2* double mutant in light grown seedlings shows a similar behaviour as found in *Ler* (Fig. 3.39A), with three maxima at the corresponding positions. In darkness the first peak (0-20 µT) was absent but the other two peaks appeared at the positions similar to those of the light grown seedlings.

Fig. 3.40 (B) shows the stimulus-response curve for expression of the *cab4* gene. In the *cry1cry2* double mutant its expression remains more or less uninfluenced by the magnetic fields, except that there is a down-regulation in the range of 75-100 µT which is similar to light grown *Ler* seedlings (Fig. 3.40 A).

.

A

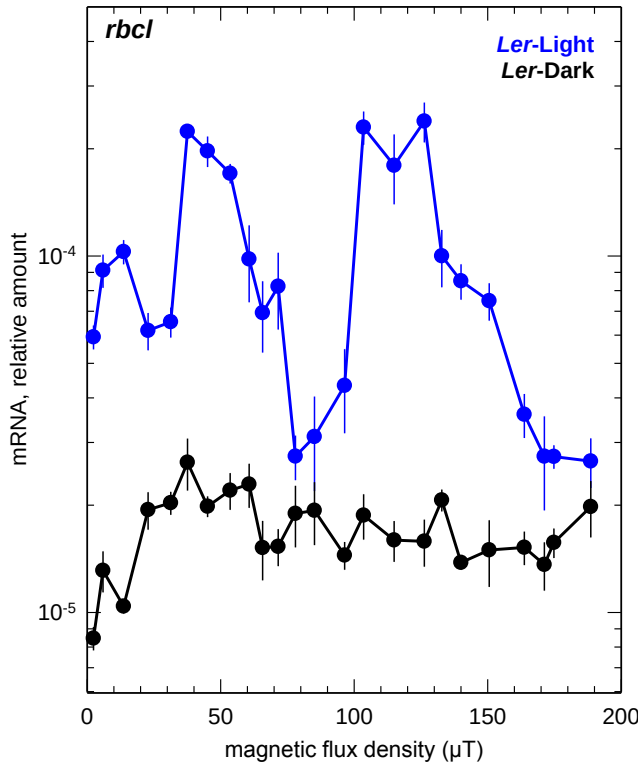

Fig 3.39 (A): Comparison of mRNA levels of large subunit of RuBisCO gene (*rbcl*) of *Ler* seedlings grown under blue light (fluence rate-10 W/m²) and in dark and their comparison to the mRNA levels in *cry1cry2* double mutant seedlings (Fig. 3.39 B) along the magnetic flux density gradient under similar light conditions. Error bars = SE (4 samples)

B

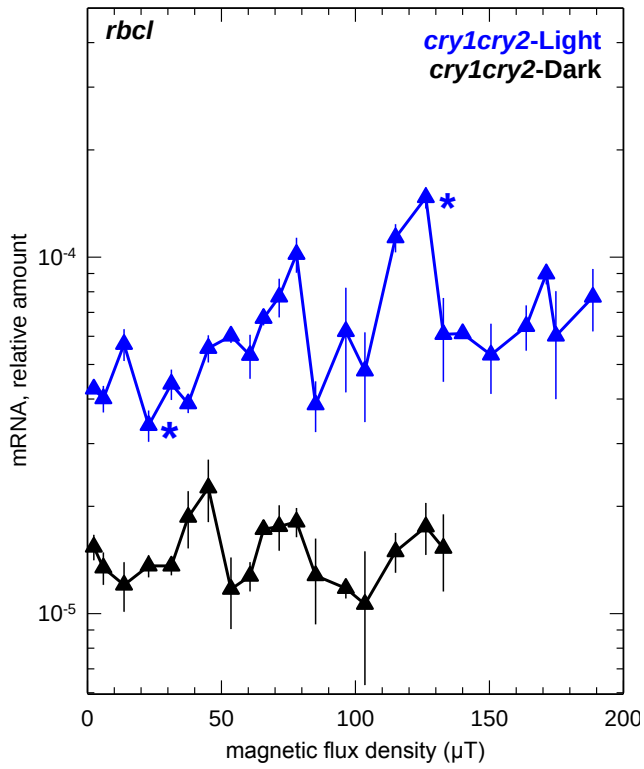

Fig 3.39 (B): Comparison of mRNA levels of large subunit of RuBisCO gene (*rbcl*) in *cry1cry2* double mutant seedlings in blue light (fluence rate-10 W/m²) and in dark. Error bars = SE (4 samples). The difference in the mean values of the two groups marked by **'*'** is greater than would be expected by chance; there is a statistically significant difference between the input groups (P = <0.001; t-test).

Stimulus-response curves of lycopene cyclase gene (*lyc*) as presented in Fig. 3.41 (B) showed a comparable pattern of differential expression along the magnetic flux density gradient. The peaks at 35-50 µT range and at 100-130 µT range are clearly visible in both light as well as in dark grown seedlings of the *cry1cry2* double mutants.

Stimulus-response curves for porphobilinogen synthase gene (*hemb2*) in Fig. 3.42 (B), also show the peak in the range of 35-50 µT, but the other peak (100-130 µT) is absent in both light and dark grown seedlings of *cry1cry2* double mutants.

In Figs. 3.43, 3.44, 3.45 and 3.46, a comparison of the stimulus-response curves of expression profiles of the genes chalcone synthase (*chs*), phenylalanine ammonia lyase (*pal4*), nitric oxide synthase (*nos1*) and elongation factor-1 (*ef1*) respectively is displayed in *cry1cry2* double mutants. All these genes prominently show the two peaks. One is in the range of 35-50 µT and the other in the range of 100-130 µT, with minor variations.

A

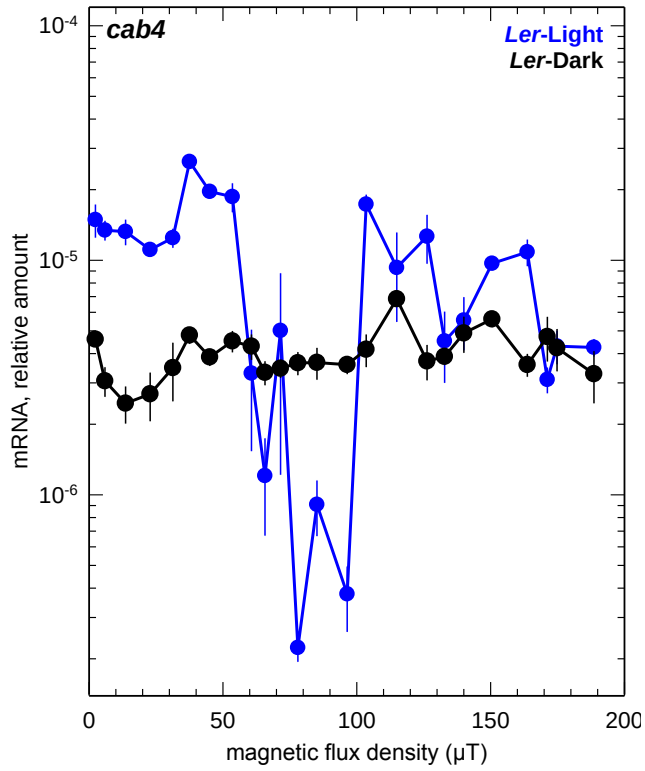

Fig 3.40 (A): Comparison of mRNA levels of chlorophyll a/b binding protein-4 gene (*cab4*) of *Ler* seedlings grown under blue light (fluence rate-10 W/m²) and in dark and their comparison to the mRNA levels in *cry1cry2* double mutant seedlings (Fig. 3.40 B) along the magnetic flux density gradient under similar light conditions. Error bars = SE (4 samples).

B

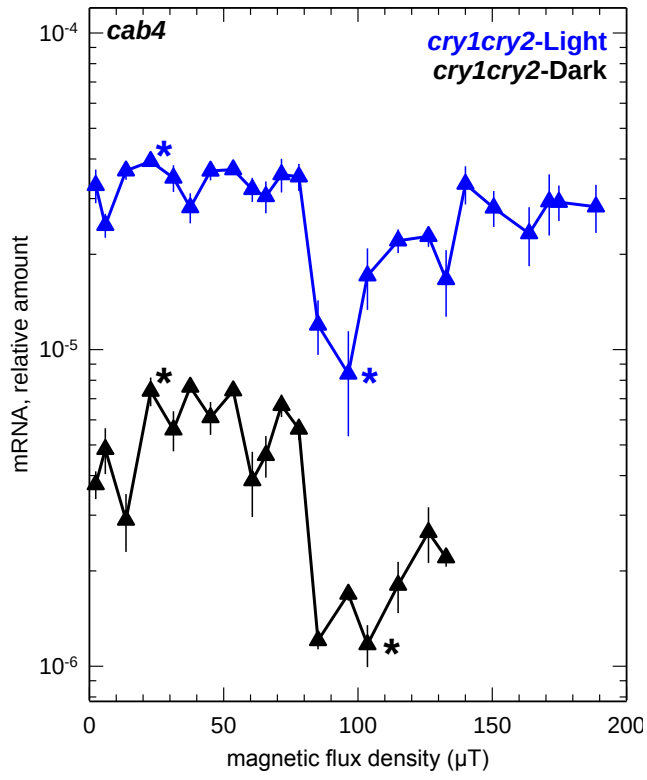

Fig 3.40 (B): Comparison of mRNA levels of chlorophyll a/b binding protein-4 gene (*cab4*) in *cry1cry2* double mutant seedlings in blue light (fluence rate-10 W/m²) and in dark. Error bars = SE (4 samples). The difference in the mean values of the two groups marked by '*' (blue) is greater than would be expected by chance; there is a statistically significant difference between the input groups (P = <0.001; t-test). Similarly in case of dark plot, the difference in the mean values of the two groups marked by '*' (black) is greater than would be expected by chance; there is a statistically significant difference between the input groups (P = <0,001; t-test).

A

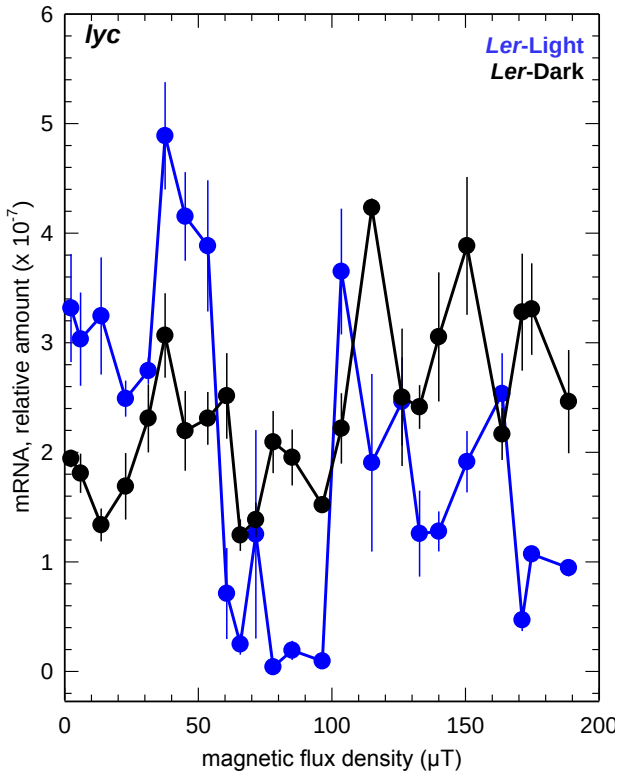

Fig 3.41(A): Comparison of mRNA levels of lycopene cyclase gene (*lyc*) of *Ler* seedlings grown under blue light (fluence rate-10 W/m²) and in dark, and their comparison to the mRNA levels in *cry1cry2* double mutant seedlings (Fig. 3.41 B) along the magnetic flux density gradient under similar light conditions. Error bars = SE (4 samples).

B

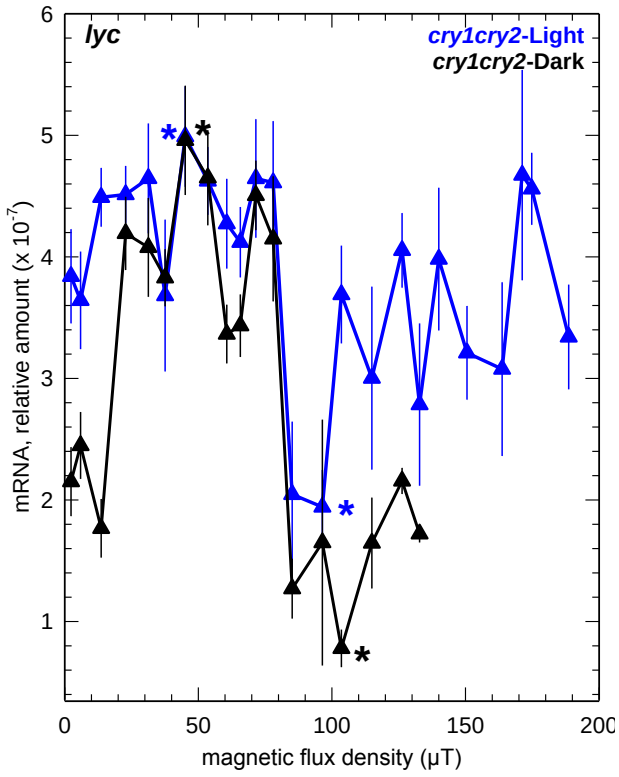

Fig 3.41 (B): Comparison of mRNA levels of lycopene cyclase gene (*lyc*) in *cry1cry2* double mutant seedlings in blue light (fluence rate-10 W/m²) and in dark. Error bars = SE (4 samples). The difference in the mean values of the two groups marked by **'*'** (blue) is statistically significant (P = 0.002; t-test). In case of dark plot also the difference in the mean values of the two groups marked by **'*'** (black) is greater than would be expected by chance; there is a statistically significant difference between the input groups (P = <0.001; t-test).

A

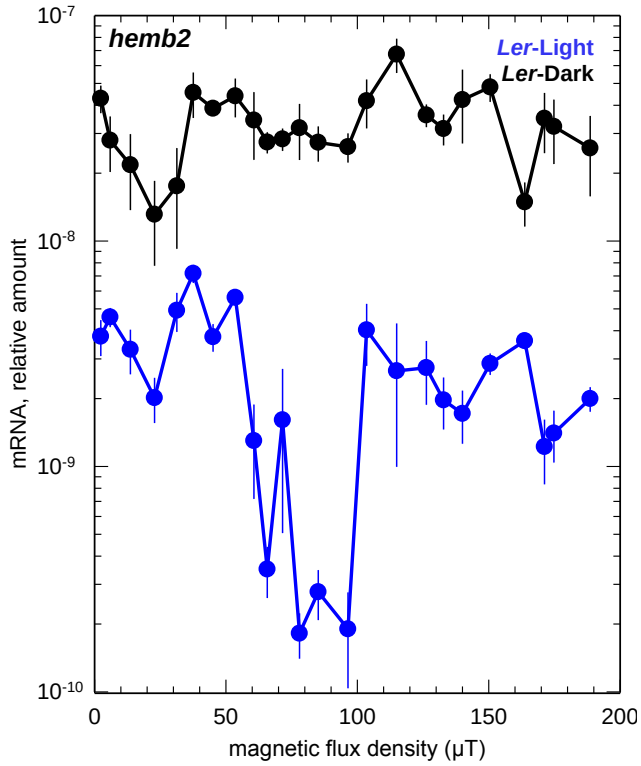

Fig 3.42 (A): Comparison of mRNA levels of porphobilinogen synthase gene (*hemb2*) of *Ler* seedlings grown under blue light (fluence rate-10 W/m²) and in dark and their comparison to the mRNA levels in *cry1cry2* double mutant seedlings (Fig. 3.42 B) along the magnetic flux density gradient under similar light conditions. Error bars = SE (4 samples).

B

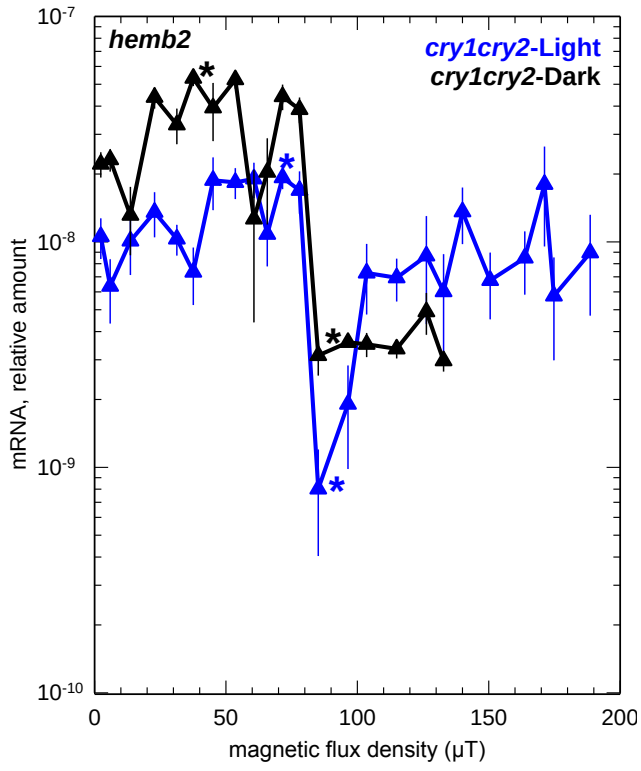

Fig 3.42 (B): Comparison of mRNA levels of porphobilinogen synthase gene (*hemb2*) in *cry1cry2* double mutant seedlings in blue light (fluence rate-10 W/m²) and in dark. Error bars = SE (4 samples). The difference in the mean values of the two groups marked by '*' (blue) is greater than would be expected by chance; there is a statistically significant difference between the input groups (P = <0.001; t-test). Similarly in case of dark plot, the difference in the mean values of the two groups marked by '*' (black) is greater than would be expected by chance; there is a statistically significant difference between the input groups (P = <0.001; t-test).

A

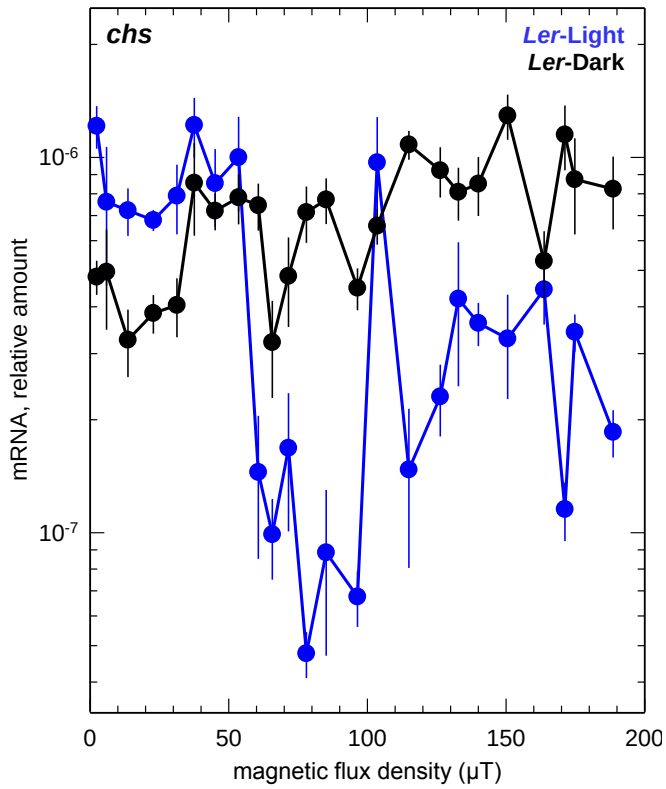

Fig 3.43 (A): Comparison of mRNA levels of chalcone synthase gene (*chs*) in *Ler* seedlings under blue light (fluence rate-10 W/m²) and in dark and their comparison to the mRNA levels in *cry1cry2* double mutant seedlings (Fig. 3.43 B) along the magnetic flux density gradient under similar light conditions. Error bars = SE (4 samples).

B

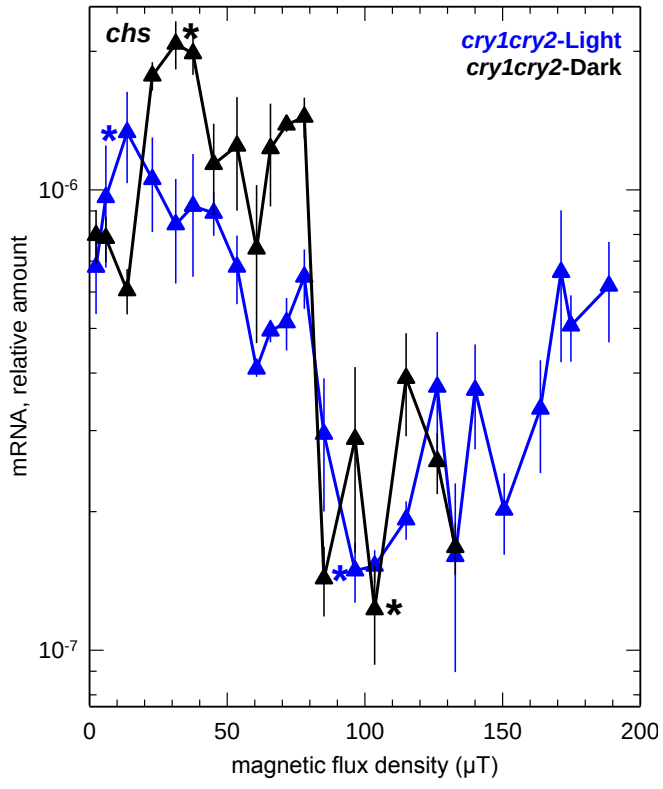

Fig 3.43 (B): Comparison of mRNA levels of chalcone synthase gene (*chs*) in *cry1cry2* double mutant seedlings in blue light (fluence rate-10 W/m²) and in dark. Error bars = SE (4 samples). The difference in the mean values of the two groups marked by '*' (blue) is greater than would be expected by chance; there is a statistically significant difference between the input groups (P = 0.014; t-test). Similarly in case of dark plot, the difference in the mean values of the two groups marked by '*' (black) is greater than would be expected by chance; there is a statistically significant difference between the input groups (P = <0.001; t-test).

A

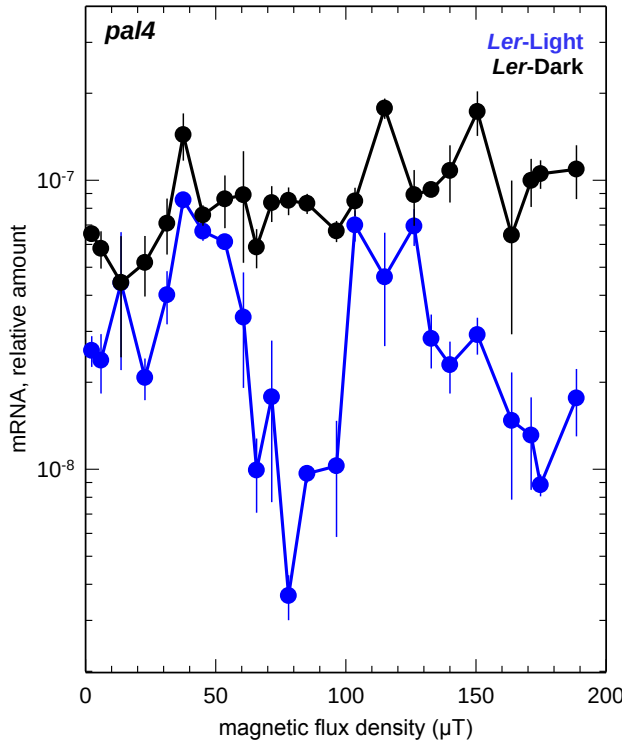

Fig 3.44 (A): Comparison of mRNA levels of phenylalanine ammonia lyase-4 gene (*pal4*) in *Ler* seedlings under blue light (fluence rate-10 W/m²) and in dark and their comparison to the mRNA levels in *cry1cry2* double mutant seedlings (Fig. 3.44 B) along the magnetic flux density gradient under similar light conditions. Error bars = SE (4 samples).

B

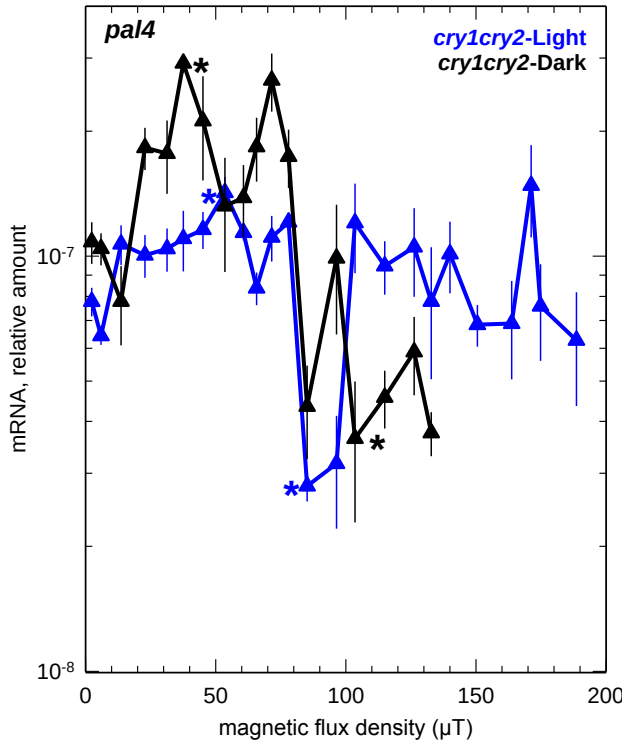

Fig 3.44 (B): Comparison of mRNA levels of phenylalanine ammonia lyase-4 gene (*pal4*) in *cry1cry2* double mutant seedlings in blue light (fluence rate-10 W/m²) and in dark. Error bars = SE (4 samples). The difference in the mean values of the two groups marked by **'*'** (blue) is greater than would be expected by chance; there is a statistically significant difference between the input groups (P = <0.001; t-test). Similarly in the dark plot, the difference in the mean values of the two groups marked by **'*'** (black) is greater than would be expected by chance; there is a statistically significant difference between the input groups (P = <0.001; t-test).

A

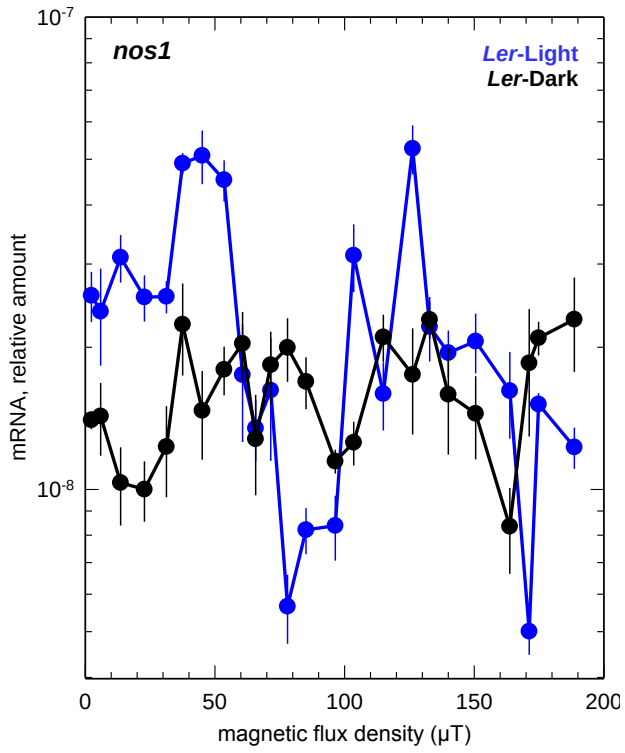

Fig 3.45 (A): Comparison of mRNA levels of nitric oxide synthase gene (*nos1*) in *Ler* seedlings under blue light (fluence rate-10 W/m²) and in dark and their comparison to the mRNA levels in *cry1cry2* double mutant seedlings (Fig. 3.45 B) along the magnetic flux density gradient under similar light conditions. Error bars = SE (4 samples).

B

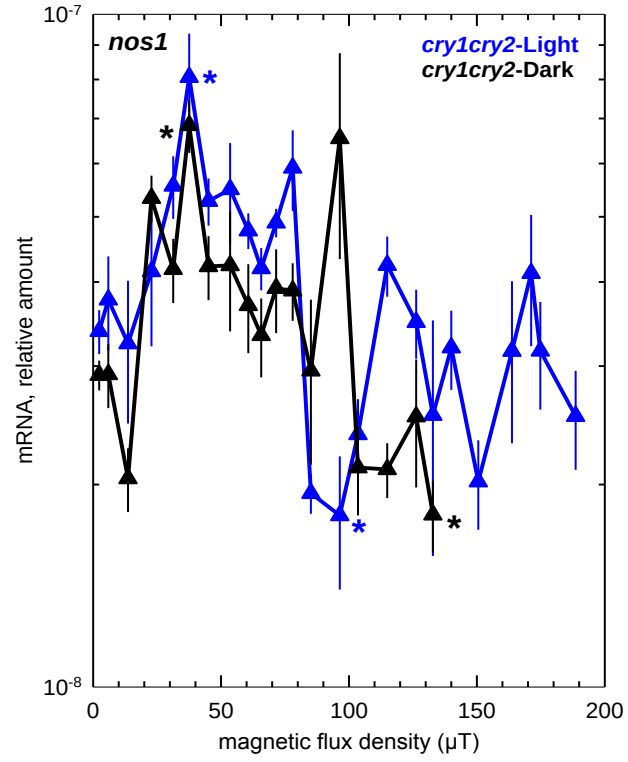

Fig 3.45 (B): Comparison of mRNA levels of nitric oxide synthase gene (*nos1*) in *cry1cry2* double mutant seedlings in blue light (fluence rate-10 W/m²) and in dark. Error bars = SE (4 samples). The difference in the mean values of the two groups marked by **'*'** (blue) is greater than would be expected by chance; there is a statistically significant difference between the input groups (P = 0.012; t-test). Similarly in case of dark plot, the difference in the mean values of the two groups marked by **'*'** (black) is greater than would be expected by chance; there is a statistically significant difference between the input groups (P = <0.001; t-test).

A

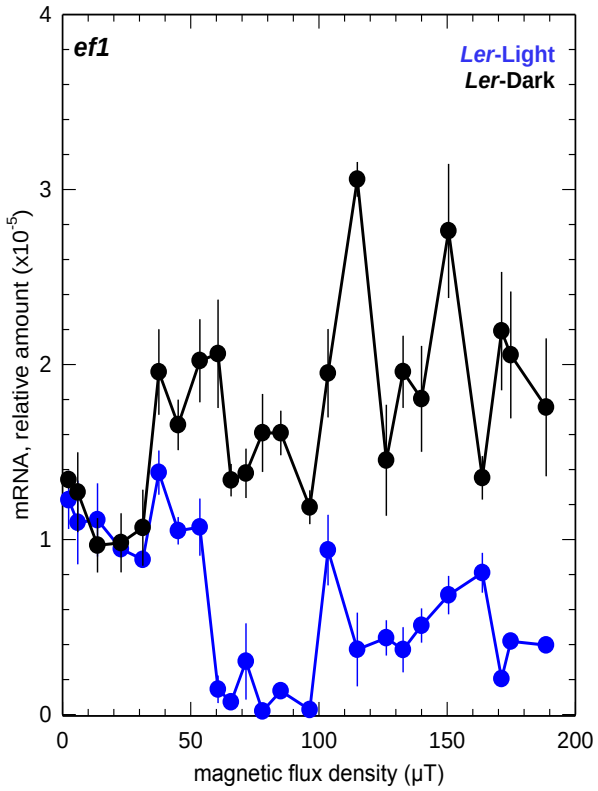

Fig 3.46 (A): Comparison of mRNA levels of elongation factor-1 gene (*ef1*) in *Ler* seedlings under blue light (fluence rate-10 W/m²) and in dark and their comparison to the mRNA levels in *cry1cry2* double mutant seedlings (Fig. 3.46 B) along the magnetic flux density gradient under similar light conditions. Error bars = SE (4 samples).

B

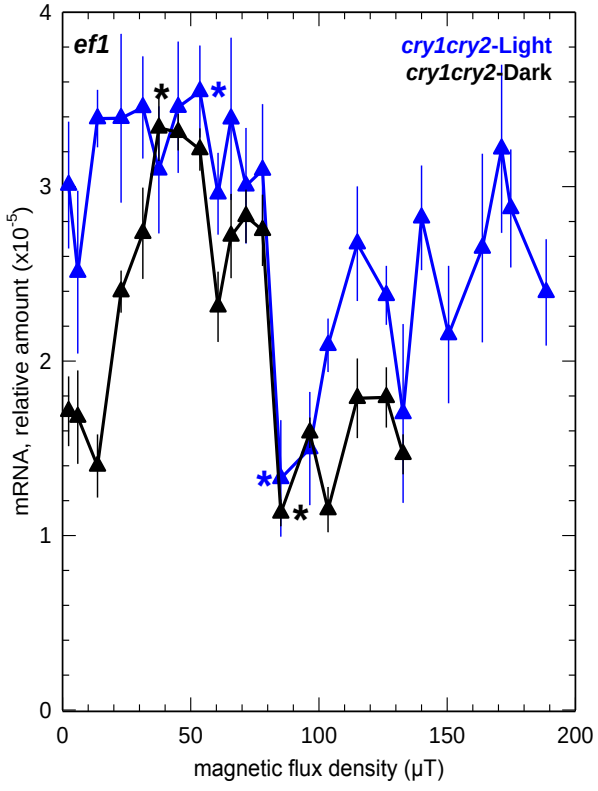

Fig 3.46 (B): Comparison of mRNA levels of elongation factor-1 gene (*ef1*) in *cry1cry2* double mutant seedlings in blue light (fluence rate-10 W/m²) and in dark. Error bars = SE (4 samples). The difference in the mean values of the two groups marked by **'*'** (blue) is greater than would be expected by chance; there is a statistically significant difference between the input groups (P = 0.004; t-test). Similarly in case of dark plot, the difference in the mean values of the two groups marked by **'*'** (black) is greater than would be expected by chance; there is a statistically significant difference between the input groups (P = <0.001; t-test).

3.5.3 Comparison of gene expressions in blue and red light in *Ler* and *phyAphyB* double mutants

It is obvious from the stimulus-response curves of the expression profiles of various genes, that the magnetic field is able to affect the gene expression even in the *cry1cry2* double mutants. In order to check the effect of light quality, we studied the effects of magnetic flux density on gene expression of *Arabidopsis*, after illumination by red light instead of blue light. Keeping all other conditions the same as in our previous experiments we only changed the LED arrays from blue to red and performed our experiments under 7.26 W/m² of red light which has the same fluence rate as that of 10 W/m² of blue light. We examined the response of genes in *Ler* seedlings and in *phyAphyB* double mutant seedlings. The range of magnetic flux density selected was 0-80 µT, which includes the range of geomagnetic field. The results of both of these experiments are presented in the following figures (Fig. 3.47 to 3.54) along with the expression of the corresponding genes in *Ler* seedlings as well as in *cry1cry2* double mutant seedlings.

The stimulus-response curves for the large subunit of RuBisCO gene (*rbcl*) present a very clear picture of the effects of magnetic fields on gene expression in red light. Fig. 3.47 shows the comparison of the gene expression of *rbcl* in *Ler* seedlings under blue light with that under red light. In both cases there is a very prominent peak in the range of 35-50 µT, although little shifted in case of the stimulus-response curve for red light. The same peak is also clearly visible in the stimulus-response curve for *phyAphyB* double mutant when exposed to red light. The same peak was also presented by *cry1cry2* double mutants.

In case of the *cab4* gene (Fig. 3.48), *Ler* and *phyAphyB* double mutant seedlings under red light, also show the rise of mRNA levels in the range of 35-50 µT as shown by the *Ler* seedlings under blue light. However, these peaks are not as clearly marked as in the case of *rbcl* gene.

Lycopene cyclase gene (*lyc*) definitely shows a very prominent increase in its mRNA levels between 35-50 µT in both *Ler* and in *phyAphyB* double mutants under red light (Fig. 3.49). The gene porphobilinogen synthase (*hemb2*) also has some tendency to show up regulation within 35-50 µT range in both *Ler* and *phyAphyB* double mutant seedlings (Fig. 3.50) but less conspicuous than the *cab4* gene.

Chalcone synthase (*chs*) also shows up-regulation near the 35-50 µT range; however, there is a shift in the position of the peak (Fig. 3.51). In this case the peak falls beyond the

range of 35-50 µT, and is present between 50-65 µT. The gene phenylalanine ammonia lyase-4 (*pal4*) under red light in *Ler* seedlings also displays increase in the levels of its mRNA, corresponding to the position of the peak of blue light exposed seedlings. In *phyAphyB* seedlings, this gene also shows some up-regulation, but not as striking as shown by *Ler* seedlings (Fig. 3.52). Similarly, the stimulus-response curves of the gene nitric oxide synthase (*nos1*) show a clear tendency of up-regulation in the range 35-50 µT (Fig. 3.53). Elongation factor-1 gene (*ef1*) seems to remain more or less unaffected in the range of 35-50 µT in *Ler* seedlings grown under red light, but its rise in the same range in *Ler* seedlings grown under blue light is also not that spectacular as shown by other genes (Fig. 3.54).

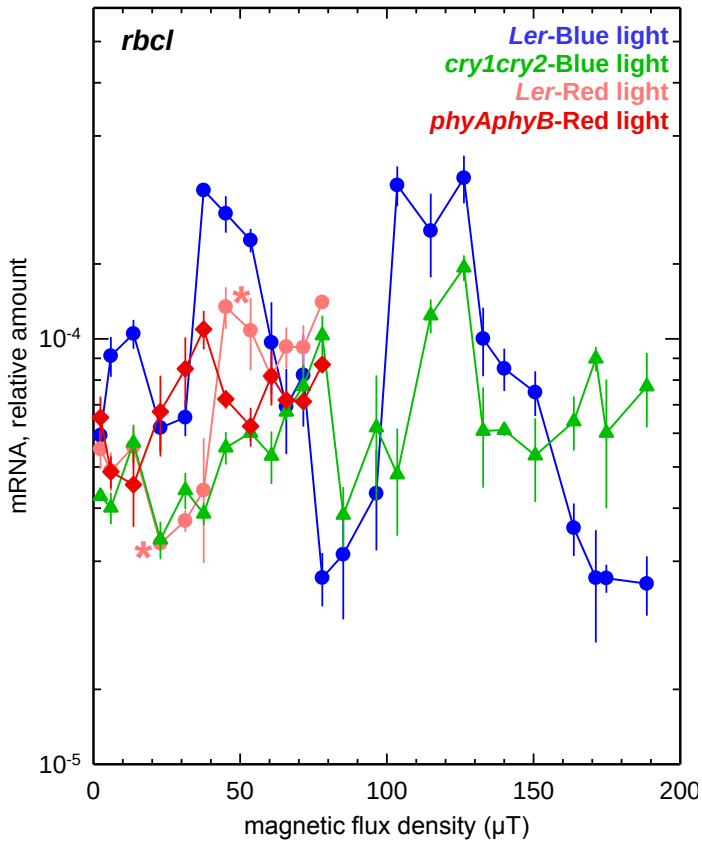

Fig 3.47: Comparison of mRNA levels of large subunit of RuBisCO gene (*rbcl*) in *Ler* seedlings when illuminated with blue (10 W/m²) and red light (7.26 W/m²). Also presented are the mRNA levels of the same gene in *phyAphyB* double mutants illuminated by red light (7.26 W/m²) and the expression in *cry1cry2* double mutant seedlings illuminated by blue light (10 W/m²). Error bars = SE (4 samples). The difference in the mean values of the two groups marked by '*' is greater than would be expected by chance; there is a statistically significant difference between the input groups (P = 0.021; t-test).

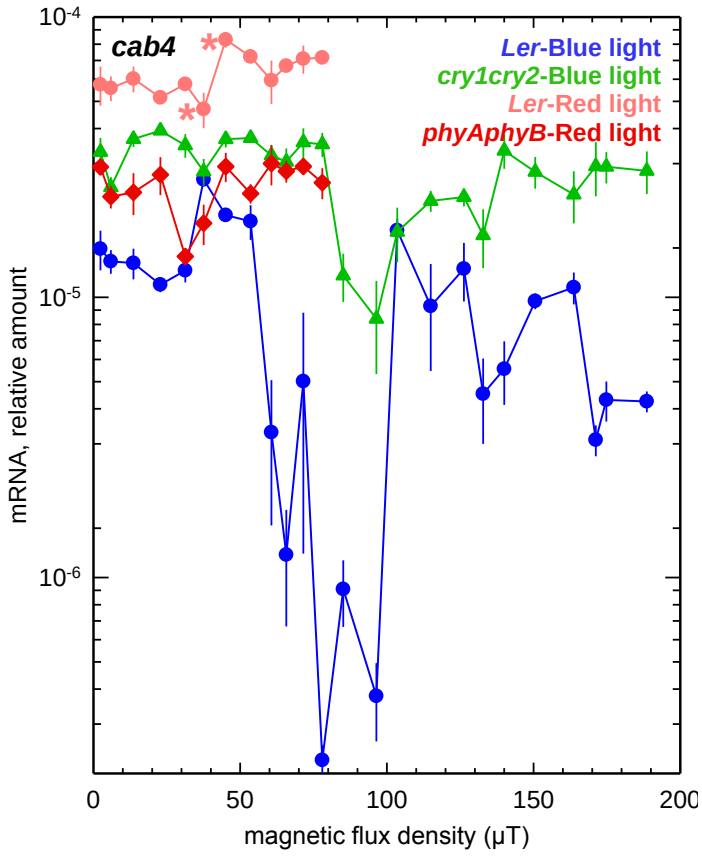

Fig 3.48: Comparison of mRNA levels of chlorophyll a/b binding protein-4 gene (*cab4*) in *Ler* seedlings when illuminated with blue (10 W/m²) and red light (7.26 W/m²). Also presented are the mRNA levels of the same gene in *phyAphyB* double mutants illuminated by red light (7.26 W/m²) and the expression in *cry1cry2* double mutant seedlings illuminated by blue light (10 W/m²). Error bars = SE (4 samples). The difference in the mean values of the two groups marked by '*' is greater than would be expected by chance; there is a statistically significant difference between the input groups (P = 0.011; t-test).

.

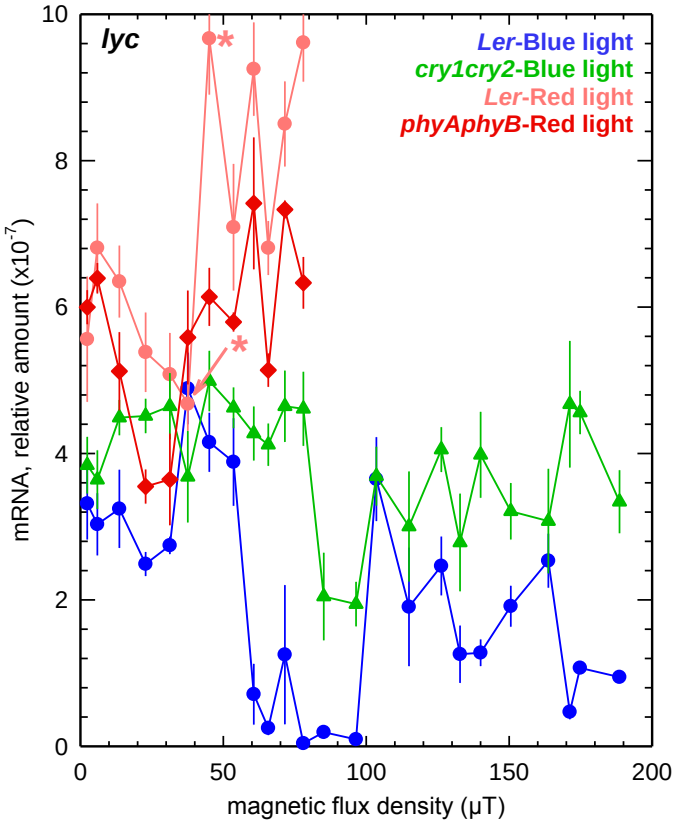

Fig 3.49: Comparison of mRNA levels of lycopene cyclase gene (*lyc*) in *Ler* seedlings when illuminated with blue (10 W/m²) and red light (7.26 W/m²). Also presented are the mRNA levels of the same gene in *phyAphyB* double mutants illuminated by red light (7.26 W/m²) and the expression in *cry1cry2* double mutant seedlings illuminated by blue light (10 W/m²). Error bars = SE (4 samples). The difference in the mean values of the two groups marked by '*' is greater than would be expected by chance; there is a statistically significant difference between the input groups (P = 0.002; t-test).

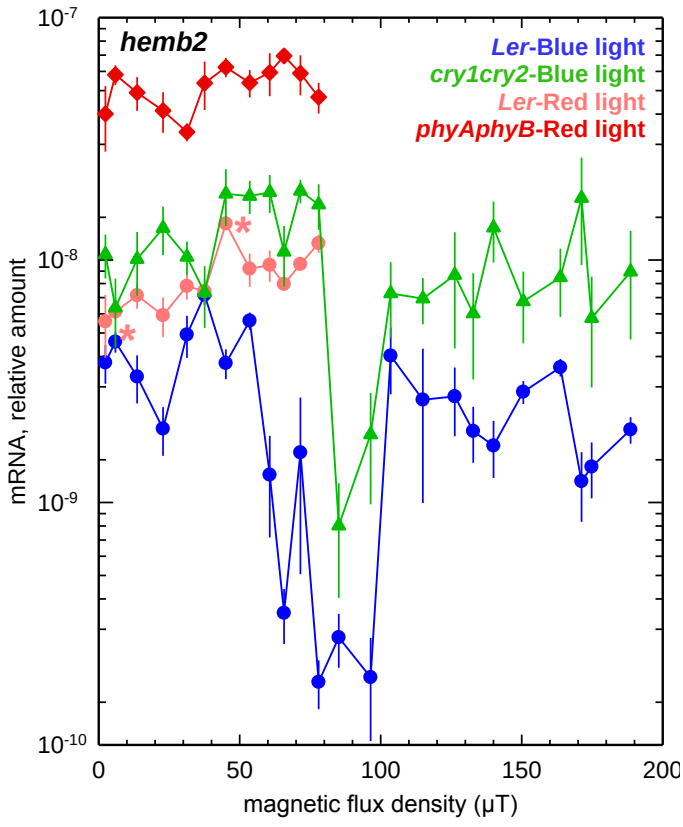

Fig 3.50: Comparison of mRNA levels of porphobilinogen synthase gene (*hemb2*) in *Ler* seedlings when illuminated with blue (10 W/m²) and red light (7.26 W/m²). Also presented are the mRNA levels of the same gene in *phyAphyB* double mutants illuminated by red light (7.26 W/m²) and the expression in *cry1cry2* double mutant seedlings illuminated by blue light (10 W/m²). Error bars = SE (4 samples). The difference in the mean values of the two groups marked by '*' is greater than would be expected by chance; there is a statistically significant difference between the input groups (P = 0.005; t-test).

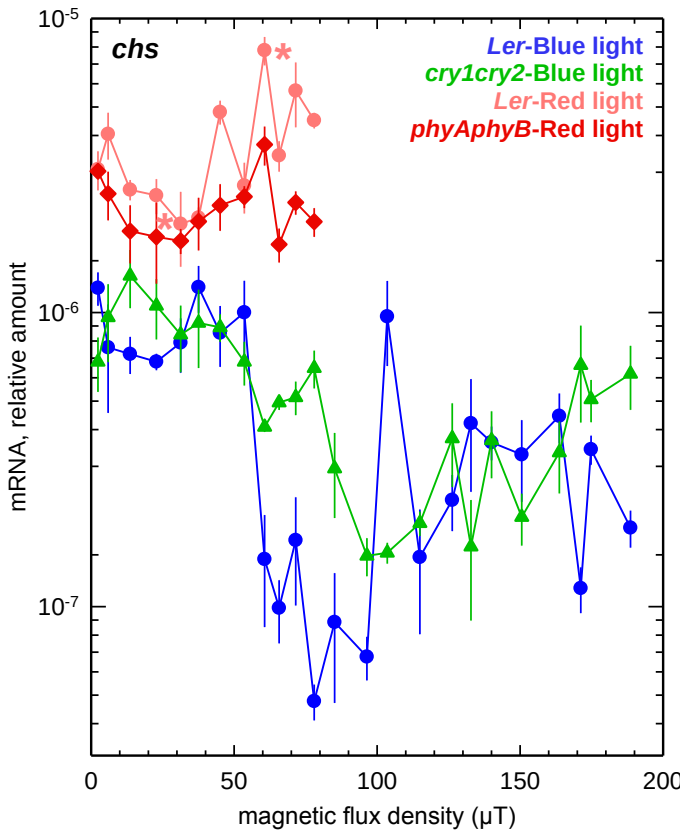

Fig 3.51: Comparison of mRNA levels of chalcone synthase gene (*chs*) in *Ler* seedlings when illuminated with blue (10 W/m²) and red light (7.26 W/m²). Also presented are the mRNA levels of the same gene in *phyAphyB* double mutants illuminated by red light (7.26 W/m²) and the expression in *cry1cry2* double mutant seedlings illuminated by blue light (10 W/m²). Error bars = SE (4 samples). The difference in the mean values of the two groups marked by '*' is greater than would be expected by chance; there is a statistically significant difference between the input groups (P = 0.003; t-test).

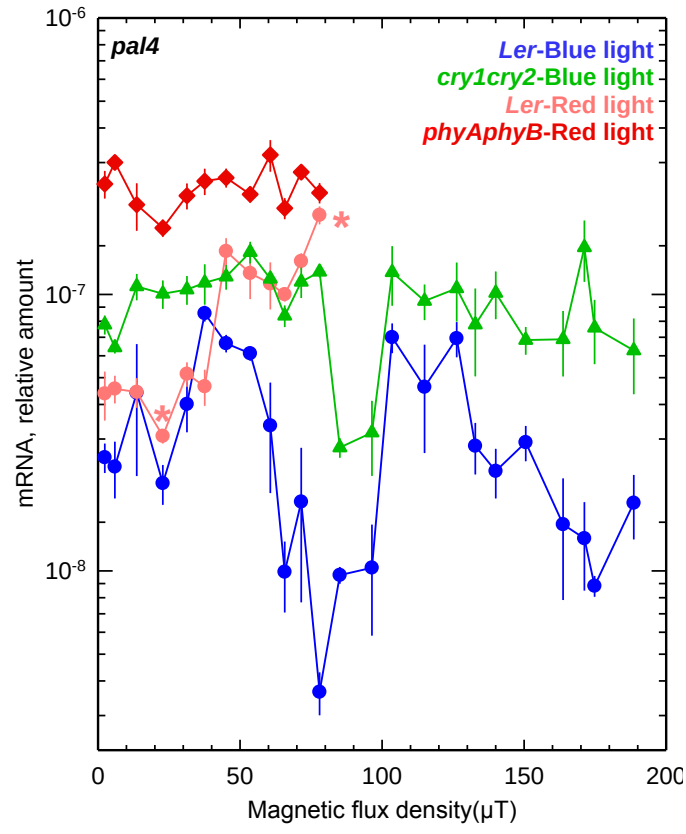

Fig 3.52: Comparison of mRNA levels of Phenylalanine ammonia lyase-4 gene (*pal4*) in *Ler* seedlings when illuminated with blue (10 W/m²) and red light (7.26 W/m²). Also presented are the mRNA levels of the same gene in *phyAphyB* double mutants illuminated by red light (7.26 W/m²) and the expression in *cry1cry2* double mutant seedlings illuminated by blue light (10 W/m²). Error bars = SE (4 samples). The difference in the mean values of the two groups marked by '*' is greater than would be expected by chance; there is a statistically significant difference between the input groups (P = 0.003; t-test).

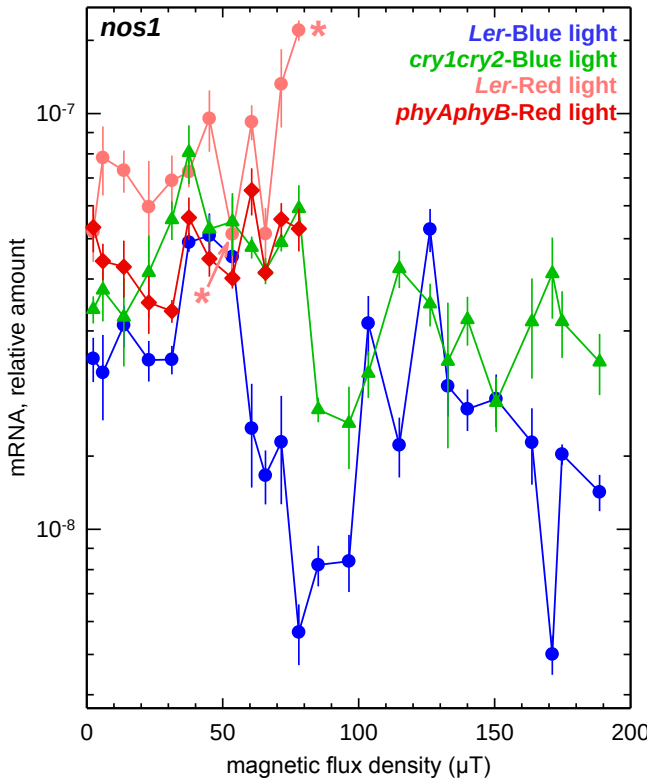

Fig 3.53: Comparison of mRNA levels of nitric oxide synthase gene (*nos1*) in *Ler* seedlings when illuminated with blue (10 W/m²) and red light (7.26 W/m²). Also presented are the mRNA levels of the same gene in *phyAphyB* double mutants illuminated by red light (7.26 W/m²) and the expression in *cry1cry2* double mutant seedlings illuminated by blue light (10 W/m²). Error bars = SE (4 samples). The difference in the mean values of the two groups marked by '*' is greater than would be expected by chance; there is a statistically significant difference between the input groups (P = <0.001; t-test).

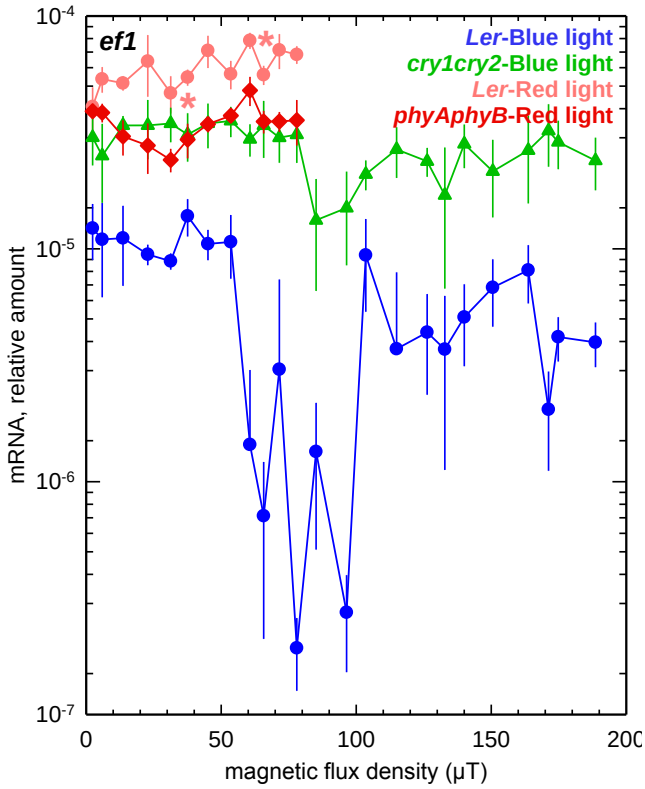

Fig 3.54: Comparison of mRNA levels of elongation factot-1gene (*ef1*) in *Ler* seedlings when illuminated with blue (10 W/m²) and red light (7.26 W/m²). Also presented are the mRNA levels of the same gene in *phyAphyB* double mutants illuminated by red light (7.26 W/m²) and the expression in *cry1cry2* double mutant seedlings illuminated by blue light (10 W/m²). Error bars = SE (4 samples). The difference in the mean values of the two groups marked by '*' is greater than would be expected by chance; there is a statistically significant difference between the input groups (P = 0,002; t-test).

3.6 Effects of magnetic fields on protein quantity

The results of the experiments on effects of magnetic flux density on gene expression posed another question to us. What happens at the process of translation to these differential quantities of mRNA at different flux densities? Are these effects perpetuated at the level of translation or not? To answer these questions we tested two proteins with the help of western blotting. These were chlorophyll a/b binding protein-4 (CAB4) and large subunit of RuBisCO (RBCL). Similar experiments were done as those done for the gene expressions and seedlings were harvested for protein analysis. Total proteins were extracted by the TCA-acetone extraction method and separated by PAGE. Proteins transferred on membranes were tested for the presence of our target proteins using western methodology. The developed PvDF membranes were photographed and proteins bands of interest were analyzed using image-J program.

3.6.1 Western blotting performed on CAB4

Different experiments were done using *Ler*, *cry1cry2* double mutant and *phyAphyB* double mutant seedlings to quantify the protein chlorophyll a/b binding protein-4 (CAB4) at different magnetic flux densities. The resu
lts of these experiments are presented in Fig. 3.55. The peak that represents protein increase in the range of 35-50 µT was presented by all plant types. The second peak (100-130 µT range) presented by the stimulus-response curves of many genes could also be seen in both the mutants, though little shifted from its position. This peak, however, was absent in *Ler* seedlings. Fig 3.56 shows the western blots for CAB4 in *Ler*.

The data for CAB4 protein estimation were also compared with the gene expression data; the results are depicted in Fig. 3.57. The comparison makes it very clear that the peak of gene expression at 35-50 µT is reproduced in the CAB4 western analysis. However, the other increase in expression in the range of 100-130 µT was absent at the protein level. These data suggest that the effects due to magnetic fields are also translated, though partially, at the protein level.

Similarly Fig. 3.58 shows the comparison of gene and protein expressions of CAB4 in *cry1cry2* double mutants. Although the picture is little more complex here, the peak at 35-50 µT is present at both the gene expression and the protein expression. The second peak at 100-130 µT seems to shift towards the range of 120-150 µT in case of protein.

In Fig. 3.59 the relative quantification of mRNA and the relative quantification of protein of CAB4 in *phyAphyB* double mutant are compared. Data for gene expression were obtained only for the range from 0 µT to 80 µT. Within this range, the stimulus-response curve for the CAB4 protein shows a clear peak in the 35-50 µT range. In case of gene expression plot, there appears a valley in the same range. But as we go beyond this valley, there is a peak that denotes the up-regulation of the *cab4* gene.

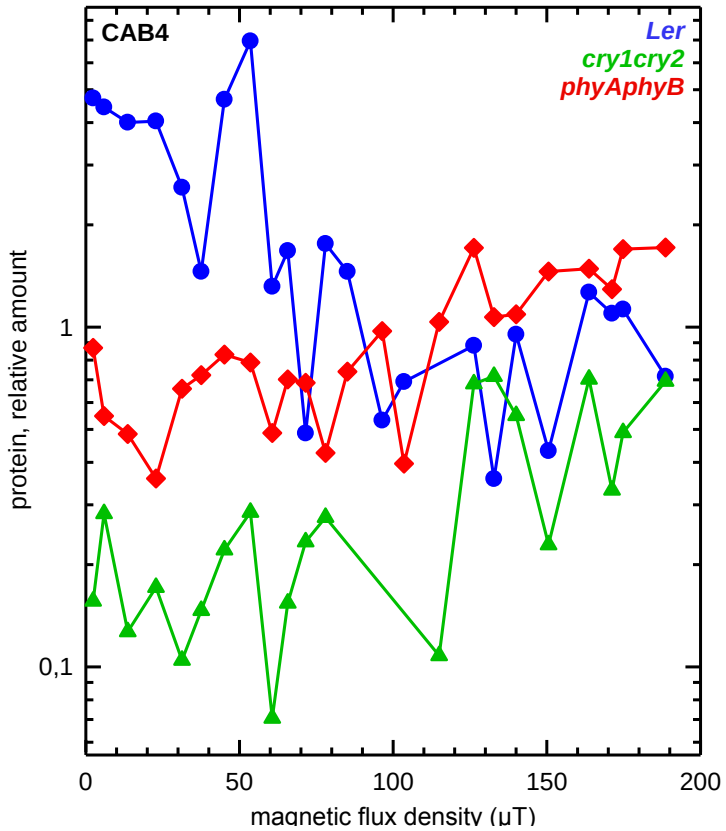

Fig 3.55: Comparison of relative quantification of chlorophyll a/b binding protein (CAB4) at different magnetic flux densities in *Ler*, *cry1cry2* double mutants and *phyAphyB* double mutant seedlings of *Arabidopsis*.

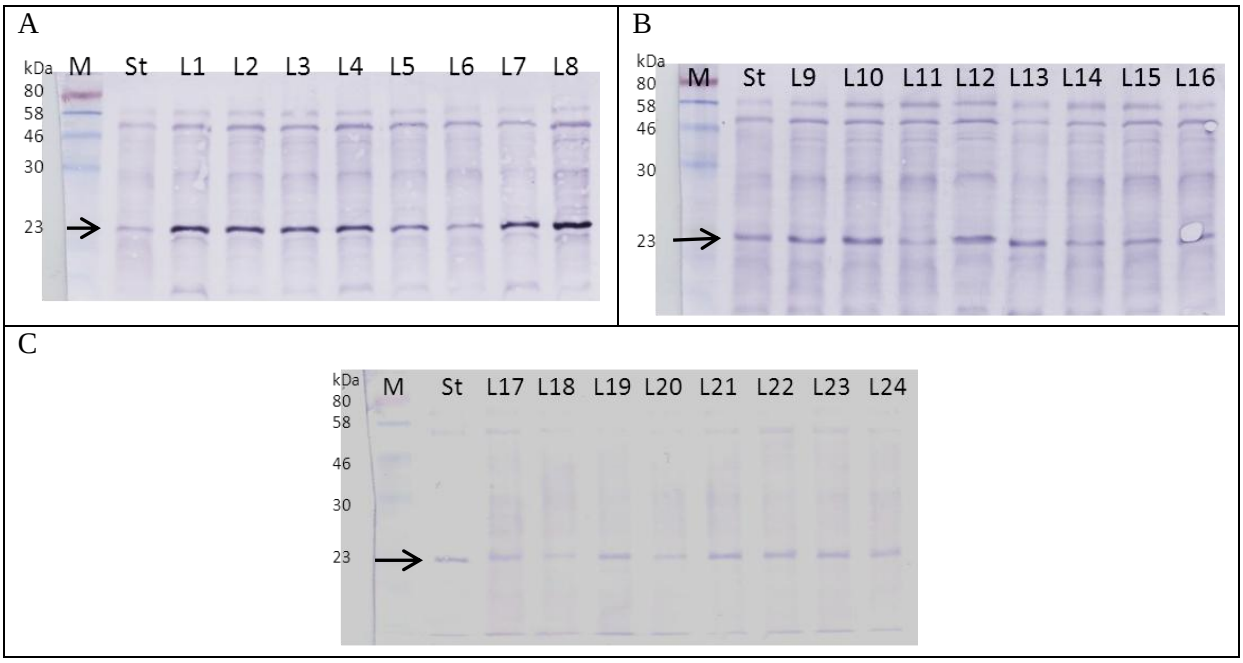

Fig 3.56: Western blots of the CAB4 protein in *Ler* seedlings. The three sheets, A, B and C present the samples of one experiment with 24 different magnetic flux densities (L1 to L24). The first lane 'M' in each sheet refers to the protein marker. The CAB4 protein has a molecular weight of 22 kDa and the respective protein band has been marked by arrow. The second lane 'St' refers to a common standard sample that was used in all the western blotting experiments uniformly as a reference for comparing the results of different experiments.

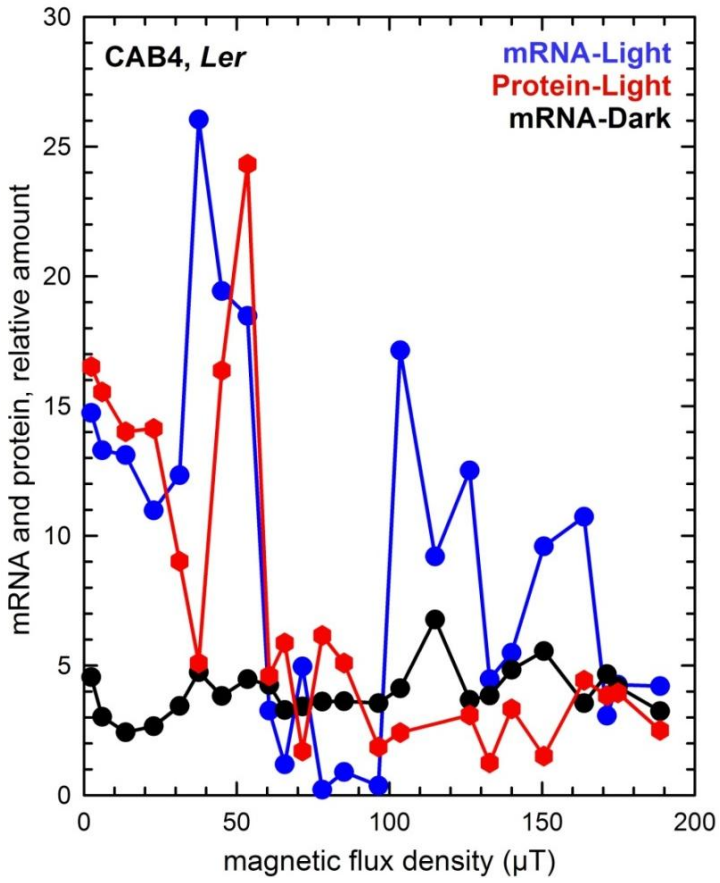

Fig 3.57: Comparison of mRNA and protein amounts of chlorophyll a/b binding protein (CAB4) at different magnetic flux densities in *Ler* seedlings. The original data for both light and dark gene expression has been multiplied by 10^6 to depict in this figure and the original protein data were multiplied by a factor of 3.5 to show the overlaps in the peak positions.

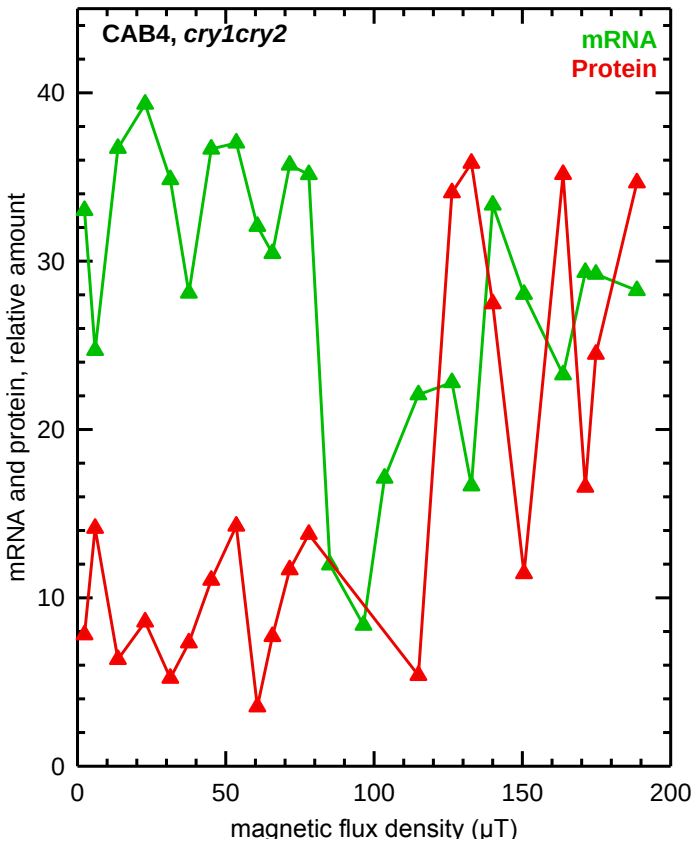

Fig 3.58: Comparison of mRNA and protein amounts of chlorophyll a/b binding protein-4 (CAB4) at different magnetic flux densities in *cry1cry2* double mutant seedlings. The original data for gene expression has been multiplied by 10^6 to depict in this figure and the original protein data is shown without any changes.

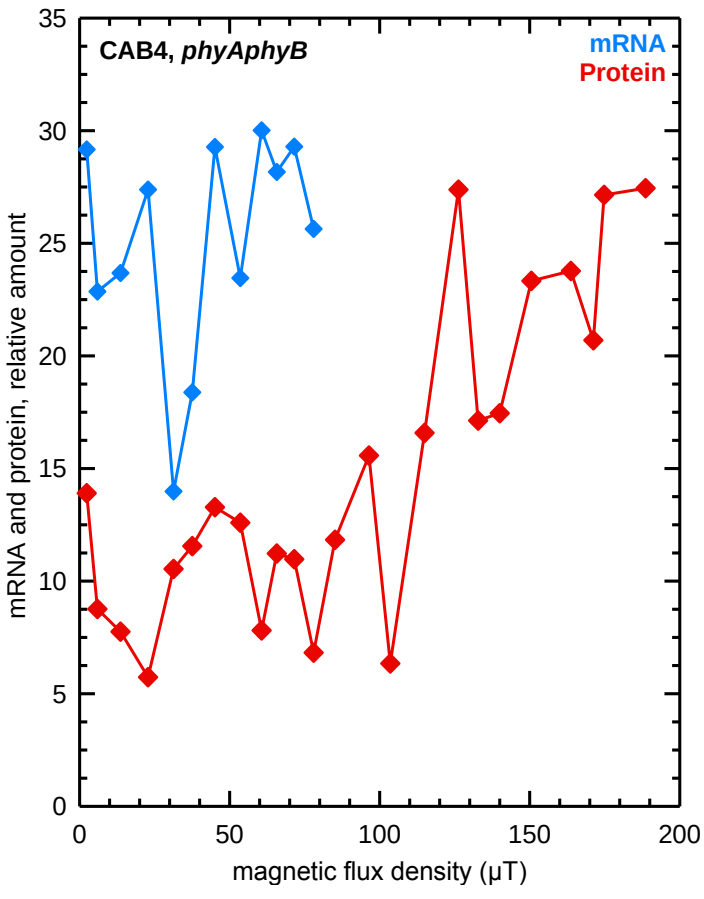

Fig 3.59: Comparison of mRNA and protein amounts of chlorophyll a/b binding protein-4 (CAB4) at different magnetic flux densities in *phyAphyB* double mutant seedlings. The original data for gene expression has been multiplied by 10^6 to depict in this figure whereas the original protein data has been multiplied by a factor of 16 to show the comparison.

3.6.2 Western blotting performed on large subunit of RuBisCO (RBCL)

Samples that were used to determine the amount of CAB4 protein were also used for the second protein, the large subunit of RuBisCO (RBCL). The results of the western blots for all the three strains used are shown in Fig. 3.60. In all the strains, no effect was observed between 0 to 30 µT, but there is a prominent peak beyond 30 µT, representing higher protein quantity in both the double mutants, which is followed by a valley beyond 50 µT. However in *Ler* seedlings, there is just opposite picture. There is a prominent valley between 35-50 µT and a prominent peak beyond 50 µT. There appears a minute peak in the range of 70-85 µT in all three strains. Beyond 85 µT, in *Ler* seedlings and in *phyAphyB* double mutant seedlings, there appears no apparent effect on RBCL protein, but in *cry1cry2* mutants, there is a prominent valley reaching to 120 µT. Beyond this point the protein shows a prominent rise in its quantity, which is also shown by *Ler* seedlings beyond 150 µT. Fig 3.61, shows the western blots for RBCL in *Ler*.

In Fig. 3.62 and Fig. 3.63 the amounts of mRNA and protein of the large subunit of RuBisCO, measured at different magnetic flux densities in *Ler* seedlings are compared. Fig. 3.62 shows relative mRNA and relative protein quantity both in light and dark, whereas Fig. 3.63 represents the same data in the form of light minus dark effect. This resulted in a very clear picture of the effects of magnetic fields on seedlings both at the transcriptional and further at the translational level which were in proper match with each other. The multi-peaked pattern of these stimulus-response curves is very well demonstrated and also reproducible at the protein level. The three peaks in the wave-like pattern i.e. in the range of 0-20 µT, 35-50 µT and 100-130 µT are prominently visible in the figure.

Fig. 3.64 displays relative mRNA and protein amounts of large subunit of RuBisCO at different flux densities in *cry1cry2* double mutants. The picture presented by this mutant is very complex. The first peak at 0-20 µT range is present in the gene expression data but not reflected in the protein abundance. The second peak usually found in the range from 35-50 µT, appears to be shifted to the range from 65-90 µT for both mRNA and protein. The third peak at 100-130 µT range is clearly shown by gene expression data, whereas the rise in protein amount starts even beyond 130µT.

Fig. 3.65 displays the relative mRNA and protein amounts of large subunit of RuBisCO at different flux densities in *phyAphyB* double mutants. Again the multi-peaked appearance of the stimulus-response curve is apparent at both the gene expression and protein level. The first

peak at 0-20 µT range is absent in both the gene and protein plots, the second peak in the 35-50 µT range appears prominently in both the plots. Another peak at 65-90 µT range is displayed in *cry1cry2* mutants. The third peak at 100-130 µT range is absent in both the plots.

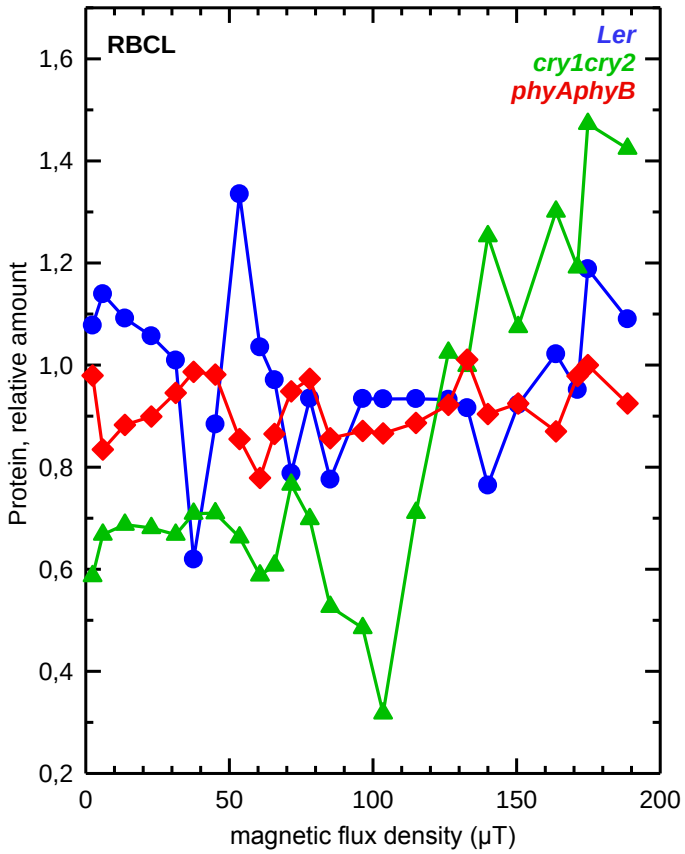

Fig 3.60: Comparison of relative quantification of large subunit of RuBisCO (RBCL) at different magnetic flux densities in *Ler*, *cry1cry2* double mutants and *phyAphyB* double mutant seedlings of *Arabidopsis.*

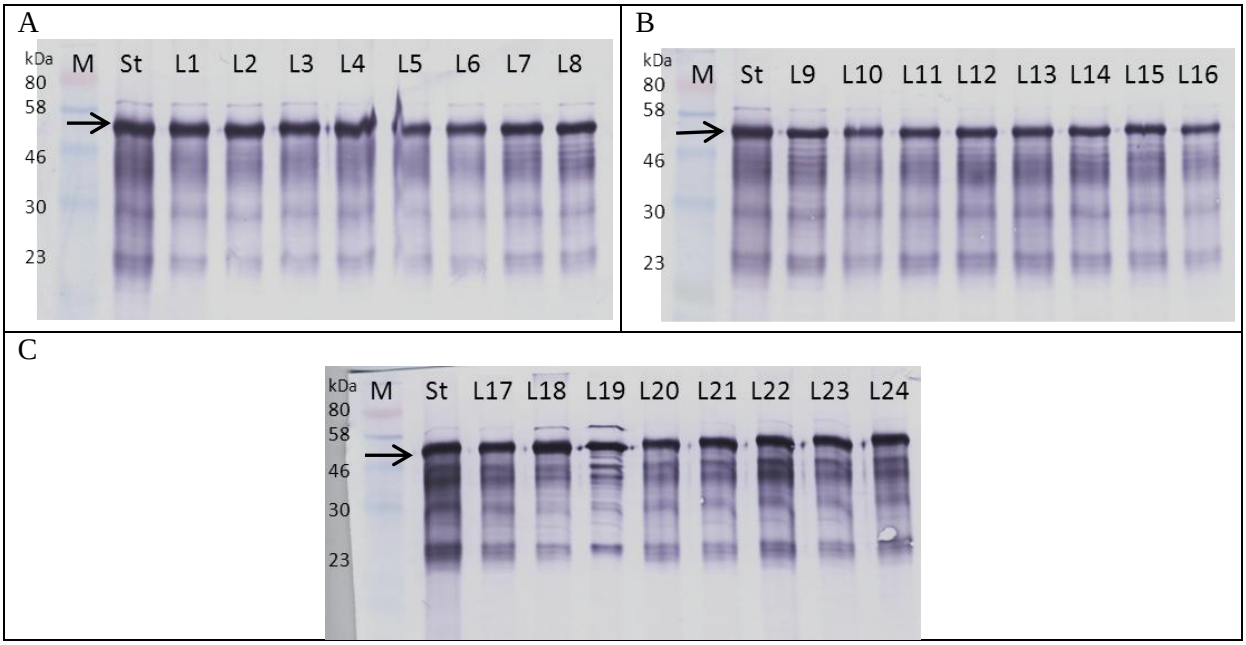

Fig 3.61: Western blots of the RBCL protein in *Ler* seedlings. The three sheets, A, B and C present the samples of one experiment with 24 different magnetic flux densities (L1 to L24). The first lane 'M' in each sheet refers to the protein marker. The RBCL protein has a molecular weight of 52.7 kDa and the respective protein band has been marked by arrow. The second lane 'St' refers to a common standard sample that was used in all the western blotting experiments uniformly as a reference for comparing the results of different experiments.

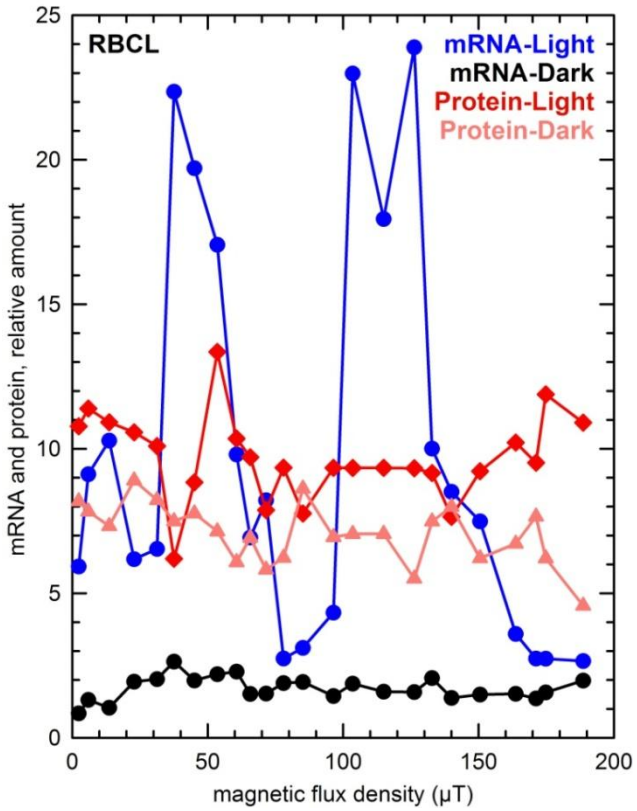

Fig 3.62: Comparison of mRNA and protein amounts of large subunit of RuBisCO (RBCL) at different magnetic flux densities in *Ler* seedlings. The original data for both light and dark gene expression has been multiplied by a factor of 10^5 to depict in this figure and the original protein data for both light and dark experiments has been multiplied by a factor of 10 to show the overlaps in the peak positions more clearly.

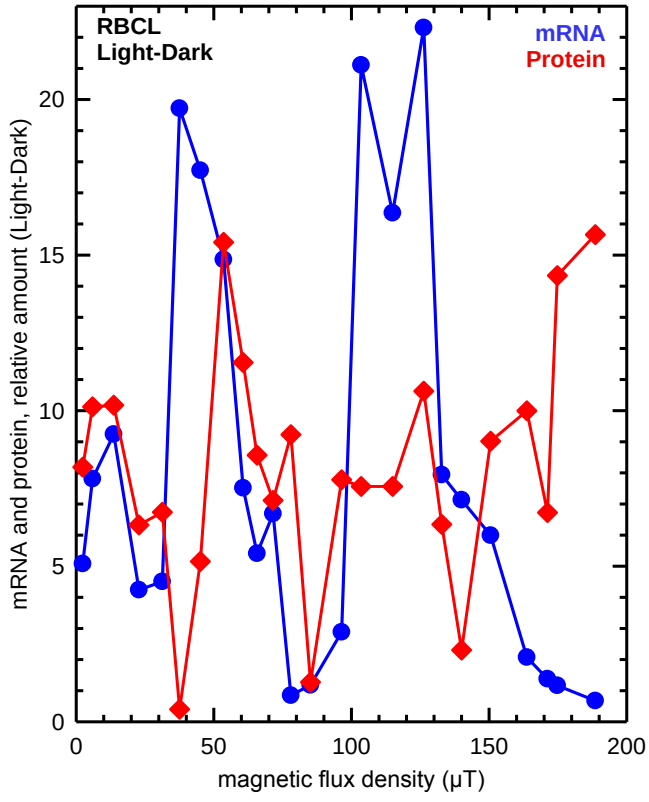

Fig 3.63: Comparison of mRNA and protein amounts (Light – Dark) of large subunit of RuBisCO (RBCL) at different magnetic flux densities in *Ler* seedlings. This figure is prepared using the same data as shown in Fig. 3.62. The original data for both light and dark gene expression has been multiplied by a factor of 10^5 to depict in this figure and the original protein data for both light and dark experiments has been multiplied by a factor of 10 to show the overlaps in the peak positions as shown in Fig. 3.62. Thereafter the values of dark were subtracted from value of light for each data point and the resulting values were used to plot the graph.

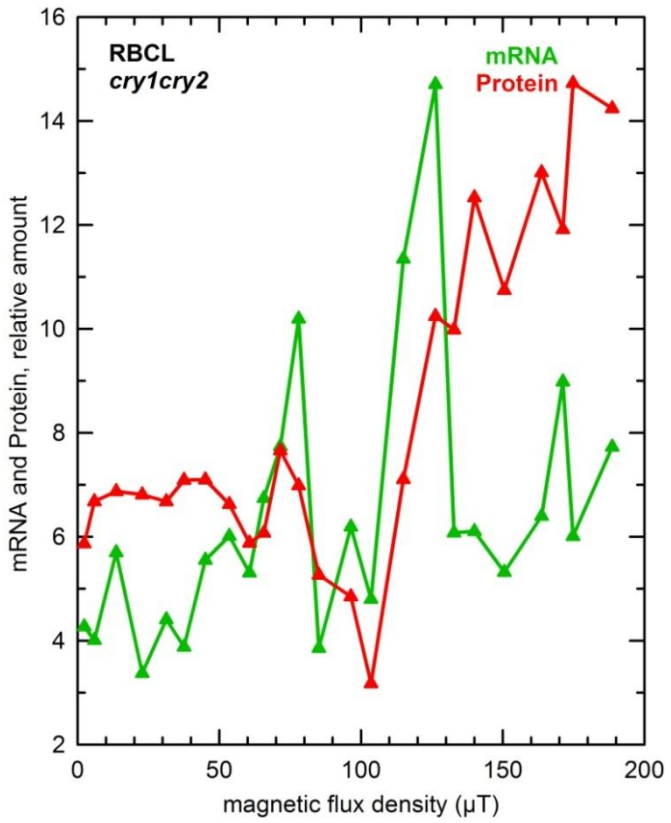

Fig 3.64: Comparison of mRNA and protein amounts of large subunit of RuBisCO (RBCL) at different magnetic flux densities in *cry1cry2* double mutant seedlings. The original data for gene expression has been multiplied by 10^5 to depict in this figure and the original protein data is shown without any changes

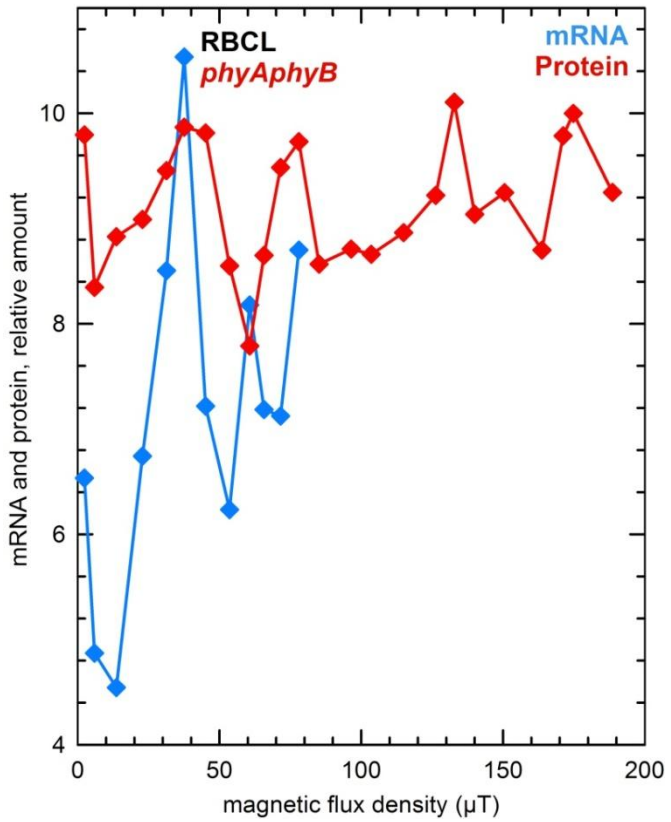

Fig 3.65: Comparison of mRNA and protein amounts of large subunit of RuBisCO (RBCL) at different magnetic flux densities in *phyAphyB* double mutant seedlings. The original data for gene expression has been multiplied by 10^5 to depict in this figure whereas the original protein data has been multiplied by a factor of 10 to show the comparison.

4 Discussion

The present work was undertaken to look for the answers of the questions put forward by Galland and Pazur, 2005:

1. Do plants perceive the geomagnetic field?
2. If yes, which biological molecule act as the magnetoreceptor and what is its mode of action?
3. Is the geomagnetic field necessary for the existence of plants?

With these questions in mind, the experiments were planned to generate stimulus-response curves with regard to magnetic flux density to test the responsiveness of the *Arabidopsis* seedlings. Following responses were assessed:

1. Hypocotyl length
2. Light induced anthocyanin accumulation
3. Chlorophyll accumulation
4. Gene expression (transcription)
5. Protein expression (translation)

4.1 Stimulus-response curves

Stimulus-response curves are very basic to understand any response in plant physiology and the studies on the effects of magnetic flux density on plants at isolated flux densities don't provide a clear picture of the underlying process. Therefore, generating these curves was essential for getting insight in the phenomenon.

4.1.1 Hypocotyl length

The stimulus-response curves for hypocotyl length show that the length of the hypocotyl remains similar with negligible changes all along the range of magnetic field under low as well as high fluence rates of blue light and this holds true for the three strains examined (*Ler*, Fig. 3.11 and 3.12; *cry1cry2* double mutants, Fig. 3.15 and 3.16; *phyAphyB* double mutants, Fig. 3.19 and 3.20). These figures clearly demonstrate that the magnetic fields are not able to influence the seedling growth of *Arabidopsis*. On the other hand, examining the factor by which the blue light suppresses the hypocotyl growth, by plotting the same data as the ratio dark/light, there appears a structure in the stimulus-response curves. This structure is in the form of a multi-peaked pattern with many maximas and minimas. In

Ler seedlings (Fig. 3.13), the highest response at 40 µT is almost more than twice as compared to the lowest response shown at 55 µT, which is quite significant (P = <0.001; t-test) with the sample size of 50 seedlings. For *cry1cry2* double mutants (Fig. 3.17) and *phyAphyB* double mutants (Fig. 3.21) similar responses were observed.

A comparison of the stimulus-response curves of all the strains together at low and high fluence rates of blue light (Fig. 3.22 and 3.23), brings out two very significant points: first that the magnetic fields require certain quantum of light for exhibiting their effects, and second that such an effect at higher fluence rates of blue light, through whichever mechanism, appears quite precise, as the pattern of the effects are very similar in all the three strains with the peak positions lying in the range of 5-20 µT, 35-50 µT and 75-90 µT. Such a similarity is even more pronounced in the two double mutants (Fig. 3.24). In case of *phyAphyB* double mutants, the response was found to be similar in low and high fluence rates which could be an indication that the phytochromes may be diminishing the magnetic effects caused by cryptochromes.

4.1.2 Anthocyanin accumulation

The stimulus-response curves at 1 W/m² of blue light in all the three strains didn't show any noticeable change in anthocyanin quantity in *Arabidopsis* seedlings (Fig. 3.25). A similar observation was made at 3.5 W/m² of blue light in both *cry1cry2* and *phyAphyB* double mutants (Fig. 3.26). The *Ler* seedlings, however, exhibited a response that was similar to what we noticed in case of suppression of hypocotyl length by high fluence rate of blue light. There were three well defined peaks in the stimulus-response curve in the ranges, 0-20 µT, 35-50 µT, and 75-90 µT. The highest anthocyanin accumulation at 82 µT was about eight times higher than the lowest at 69 µT.

The stimulus-response curve at higher fluence rate (22.6 W/m², Fig. 3.27) for *Ler* seedlings show a similar multi-peaked structure. On the other hand, at the same fluence rate, the two mutants remained unresponsive. The response of *cry1cry2* double mutant at different fluence rates of blue light as depicted in Fig. 3.28 brought out few interesting observations: It appears that magnetic flux density requires a much higher threshold of blue light to show its effects in this mutant, as there is hardly any change in the anthocyanin accumulation at 1 and 3.5 W/m² of blue light. It is only at 22.6 W/m² one observes any change in the anthocyanin quantity. Secondly, there are some changes in the peak positions as compared to *Ler*

seedlings, which suggest that cryptochromes form an important part of the magnetosensory mechanism.

At 1 W/m² of red light, the *Ler* seedlings revealed the similar multiple-peaked pattern of anthocyanin accumulation whereas in both the mutants such a response appears to be absent (Fig. 3.29). The low fluence rate of light could be the factor responsible for magnetic insensitivity of these mutants. Fig. 3.30 shows the data for *Ler* seedlings more clearly. Again the multiple peak patterns are displayed. The significance of this graph also lies in the fact that-although the two plots (green and red) showing anthocyanin synthesis are plotted with reference to plant weight and total protein, the resulting pattern is very similar. Additionally the differences in the anthocyanin accumulation response of the *Arabidopsis* seedling to variable magnetic flux density seem to be significant.

Fig. 3.31 shows the comparison of the influence of both blue and red light on the effects of magnetic flux density. With the fluence rates of both qualities of light being the same (1 W/m^2), the efficiency of red light in causing the effects of magnetic fields is clearly very high. This is a very significant observation with respect to the cryptochrome based radical-pair mechanism which is currently the most accepted modal for explaining the effects of magnetic fields on biological systems. Obviously this observation cannot be explained within the limits of radical-pair model.

4.1.3 Chlorophyll synthesis

In stimulus-response curves for chlorophyll quantification, *Ler* seedlings did not show much dependence of chlorophyll synthesis on magnetic field in low light (Fig. 3.32), whereas under higher fluence rate of blue light, we find the same characteristic multi-peaked pattern (Fig. 3.33). The first two peaks in the range of 0-20 µT and 35-50 µT, which were found in case of hypocotyl length and anthocyanin accumulation, were also displayed here. The third peak (75-90 µT), however, was found missing. Similar to what we found in case of red light experiment for anthocyanin accumulation, nearly flat third peak region was flanked by peaks on either side i.e. in the range of 55-70 µT and 85-110 µT. Although the two new peaks are placed similar to what we have observed in red light anthocyanin accumulation, it is very difficult to draw any conclusion, because both experiments differ in many respects.

The chlorophyll synthesis in *cry1cry2* and *phyAphyB* double mutants appears to remain uninfluenced by magnetic flux density at low and high fluence rates of blue light (Fig. 3.32 and 3.33).

4.1.4 Gene expression

The stimulus-response curves for the relative mRNA levels of large subunit of RuBisCO (*rbcl*) show that this gene remains unaffected in darkness. In blue light, however, we got spectacular effects of magnetic fields (Fig. 3.35). The highest stimulation at 130 µT is about 10 fold more than the lowest at 78 µT. Moreover, the multi-peaked pattern in the stimulus-response curves reappeared again. Within this curve three maxima are resolved and the peak positions fall in the range of 0-20 µT, 35-60 µT and 100-130 µT. Similarly in the stimulus-response curve of chlorophyll a/b binding protein-4 gene (*cab4*) we also observed three peaks (Fig. 3.36). .The first peak (0-20 µT) seems to be unclear, although there is relatively higher transcription in this range. The second peak is prominently present at its position in the range of 35-60 µT and the third peak is also positioned in the same range as that of *rbcl*. In addition, another peak makes its appearance in the range of 140-170 µT.

Another very significant observation was made in the stimulus-response curves of genes encoding lycopene cyclase (*lyc*) and porphobilinogen synthase (*hemb2*). Both genes responded to variable magnetic flux density even in darkness. The lycopene cyclase gene (*lyc*, Fig. 3.37) displayed the multiple-peaked pattern in its stimulus-response curves in both light and darkness. Though the relative stimulation by the magnetic fields in light certainly is higher, the dark stimulus-response curve strongly suggests the effects of magnetic fields in darkness. Such a testimony is further strengthened by the observations made in the stimulus-response curves of the gene coding for porphobilinogen synthase (*hemb2*, Fig. 3.31).

In *cry1cry2* double mutants the expression of large subunit of RuBisCO (*rbcl*) gets affected by variable magnetic flux densities and here too the effect is essentially similar to that observed in the *Ler* seedlings (Fig. 3.39A and B). The stimulus-response curve of this mutant shows a similar multi-peaked pattern although there appear some shifts in the peak positions. The stimulus-response curve of the gene *rbcl* in the same plant in darkness also depicts the similar peculiar pattern of effects, although the relative stimulation in darkness is considerably less than in light. A similar response was shown by other genes (Fig. 3.40 to Fig 3.46). All these response curves document the influence of magnetic fields on gene expression in the *cry1cry2* double mutant. We observe a structure in these curves that is similar to that of *Ler* seedlings grown in blue light and in darkness. Such a correlation of responses between *Ler* seedlings and the *Arabidopsis* seedlings which are devoid of the two cryptochromes CRY1 and CRY2 suggest a mechanism of action of magnetic fields on plants independent of cryptochromes.

Effects of magnetic fields on gene expression in red light were also studied. Figure 3.47 shows a stimulus-response curve for large subunit of RuBisCO (*rbcl*), which shows the same multi-peaked pattern as observed in *Ler* seedlings and *cry1cry2* double mutant seedlings, suggesting a similar mechanism by which magnetic flux density exerts its influence on gene expression even in red light. Stimulus-response curves, showing similar effects of magnetic fields on other genes under red light (Fig. 3.48 to 3.54), further support the existence of a common mechanism of action of magnetic fields in blue and red light.

The results of kinetics experiments also support the differential expression of genes at different flux densities. For example the mRNA levels of the *cab4* gene in Fig. 3.4 at different flux densities remain at different levels, even though they follow the usual circadian rhythm. The lowest transcription at 50 µT follows our stimulus-response curves as it is this point at which our second peak (35-50 µT range) ends, and there is a sudden dip not only in the stimulus-response curves of gene expression but also in the response curves of the blue light suppression of hypocotyl length and anthocyanin accumulation. In the kinetics done at 0 µT, the levels of gene transcripts are highest, which is not the case in the stimulus-response curves, however, even in these curves the majority of the genes show relatively higher transcription. The higher transcription at 0 µT is also predicted by ion-interference mechanism (Binhi et al. 2001). The kinetics of transcription of large subunit of RuBisCO (*rbcl*) also illustrates the differential effects of variable magnetic flux densities (Fig. 3.5). The observed levels of mRNA for a particular flux density remain roughly at same level but these levels differ at different flux densities, supporting the differential influence of magnetic fields of variable magnitudes on the transcription of genes. Kinetic data of other genes studied further supports this fact (rubisco activase gene, Fig. 3.6; chalcone synthase gene, Fig. 3.7; porphobilinogen synthase gene, Fig. 3.8; phytoene dehydrogenase gene, Fig. 3.9).

4.1.5 Proteins

Comparison of the stimulus-response curves of CAB4 for mRNA transcripts and its protein (Fig. 3.57) in *Ler* seedlings reveals a great deal of parallelism of response of transcription and translation at least in the range of 0-100 µT. The rise of the response from 0 µT to 25 µT and the prominent presence of the second peak (35-50 µT) in both curves show that the increased transcripts of *cab4* gene are being transported to cytoplasm and translated there. Such a parallelism is difficult to draw in case of *cry1cry2* (Fig. 3.58) and *phyAphyB* (Fig. 3.59) double mutants.

Also in the case of *Ler* seedlings, the stimulus-response curves showing gene expression and protein expression data of RBCL in Fig. 3.63 are very significant. The stimulus-response curves for gene and protein expression show very good correlation. The multi-peaked pattern of the curves with all the three peaks in the ranges, 0-20 µT, 35-50 µT and 100-130 µT are clearly visible. This suggests that the differential quantity of mRNAs due to effects of magnetic fields leads to differential quantity of proteins as well and the effects of magnetic fields are reproducibly detectable even at the level of translation in the cell.

4.2 Common characteristics of various stimulus-response curves

An overview of the effects of magnetic fields on various responses in the form of stimulus-response curves show a characteristic multi-peaked response pattern along the increasing gradient of magnetic flux density. Such a response also depends upon the fluence rate of the overhead light, being higher at higher fluence rates of light. In certain cases, particularly in case of anthocyanin accumulation (Fig. 3.25 and 3.26) it appears that the effects of magnetic fields require a certain threshold of light to show its effects. But when we look at gene expression in darkness, there are clear indications that the magnetic fields are also able to manifest their effects without light (Fig. 3.37 and 3.38). So the idea of requirement of a threshold of quantum of light for showing the effects by magnetic field is doubtful. But certainly light magnifies the magnetic effects as we get higher amplitudes of the maximas when we increase the fluence rate of light.

Multi-peaked stimulus-response curves as described here are unique because usually stimulus-response curves in biology show a pattern of rising exponential functions, with a plateau finally. The multiple-peaked stimulus-response curves for magnetoresponses are thus in obvious contrast to the response pattern typically found in physiology.

4.3 Radical-pair mechanism

The radical-pair mechanism provides one possible explanation for the mode of action of the magnetic fields on the biological system. As we have seen there are certain preconditions for the applicability of the modal. These prerequisites are:

1. The response should be observed only in near UV and blue light.
2. There should be no response when plants are exposed to red light.
3. No response should be observed in darkness.
4. The responses should be absent in cryptochrome mutants.
5. A single optimum should be displayed by the stimulus response curves similar to the stimulus response curves for the radical yield in dependence of the magnetic flux density.

Our stimulus-response curves are difficult to explain on the basis of these criteria. First of all, the presence of blue light is essential for the functioning of cryptochrome-based radical-pair mechanism. Contrary to this we have observed the effects even in darkness. There are certain genes (e.g. *lyc*, Fig. 3.37 and *hemb2*, Fig. 3.38) which are showing the effects of magnetic fields even in darkness, at the time when the cryptochromes are inactive. Moreover, according to the radical-pair mechanism, there should be no effect on seedlings in red light, but our results show otherwise. Our experiments reveal a response of the *Arabidopsis* seedlings to magnetic fields even under a fluence rate of 1 W/m² of red light. As the radical-pair model is based on formation of photo-induced radical pairs in cryptochromes, the presence of cryptochrome is an integral and essential part of the model. But our experiments with *cry1cry2* double mutants reveal contradictory results: Even these mutants are getting affected by the variable magnetic fields and show the responses, which are similar to *Ler* seedlings. Finally, the radical-pair mechanism predicts only a single maximum in the stimulus-response curve, a prediction which has been consistently negated by our multiple-peaked stimulus-response curves.

It is obvious that our stimulus-response curves cannot be comprehended in the framework of the radical-pair model. The observations that *Arabidopsis thaliana* demonstrates magnetoresponsiveness regardless of light conditions and the fact that they are also responsive in red light are all in conflict with cryptochrome-mediated mechanism of magnetoreception. Even *cry1cry2* double mutants retained magnetoresponsiveness. Such contradictions strongly call for a mechanism that is independent of cryptochrome.

4.4 Ion-interference mechanism

The mechanism of action of magnetic fields on living systems that is cryptochrome-independent was originally proposed by Belyaev (Belyaev et al. 1994), and afterwards by Belyaev and Binhi (Binhi et al. 2001). It is known as ion-interference mechanism. These investigators were looking for the effects of weak static magnetic fields on *E. coli* in the range of 0 – 110 μT. The effects were measured with the reference of the parameter known as "anomalous viscosity time dependence" (AVTD). The AVTD method is based on radial movement of large DNA-protein conglomerates in the high-gradient hydrodynamic field of a rotary viscometer (Kryuchkov et al. 1995) and measures the physical state of DNA-RNA-protein complexes that strongly depends on the conformational state of the genome (Binhi et al. 2001). As those *E. coli* cells were used in the experiments that have no DNA replication activity, the measured AVTD was assumed to reflect overall transcriptional activity (Binhi et al. 2001). Authors made a comparison of the obtained experimental results with the theoretical predictions based on the ion interference mechanism. The logic behind this comparison is based upon the fact that the confirmation of chromatin strongly depends on the concentration of different ions. For instance, Mg^{2+} results in condensation of chromatin and Na^{+} ions lead to relaxation of chromatin from V-79 cells (Heussen et al. 1987). The effects of magnetic fields were found to be inhibited in the presence of EGTA, the specific Ca^{2+} chelator (Belyaev et al. 1999). Interestingly their stimulus-response curves displayed a multi-peaked structure, with several maxima and minima, much like the stimulus-response curves obtained by us. One such comparison between one of our results showing anthocyanin accumulation and Binhi's graphs has been depicted in Fig. 4.1. A direct measurement of transcriptional activity of the gene of chalcone synthase, a key enzyme in anthocyanin production, at variable magnetic fields and its comparison with Binhi's data in Fig. 4.2 also illustrates the similarity of the transcriptional activity in *Arabidopsis* seedlings to that of *E. coli*. The transcription pattern of another gene i.e., small subunit of RuBisCO (*rbcs1a*), unrelated to anthocyanin production, and its correlation to Binhi's observations, presented in Fig. 4.3, also displays remarkable similarity with Binhi's findings.

All three figures point out a close analogy between our observations in *Arabidopsis* and the observations made by Belyaev et al. 1994 and Binhi et al. 2001 in *E. coli*, and from them it is evident that the peak patterns displayed by *E. coli* and *Arabidopsis* are surprisingly similar. The three peaks, which we obtained in *Arabidopsis* in the geomagnetic field range between 25 and 75 μT, are also recognizable in *E. coli*. It is also evident from the Fig. 4.2 and

4.3 and the data not shown, that the response in terms of gene stimulation in *Arabidopsis* varied from 10 to 40 fold for different genes. In contrast, the corresponding amplitudes for the parameter "anomalous viscosity time dependence" in *E. coli* amounted only to some 30%.

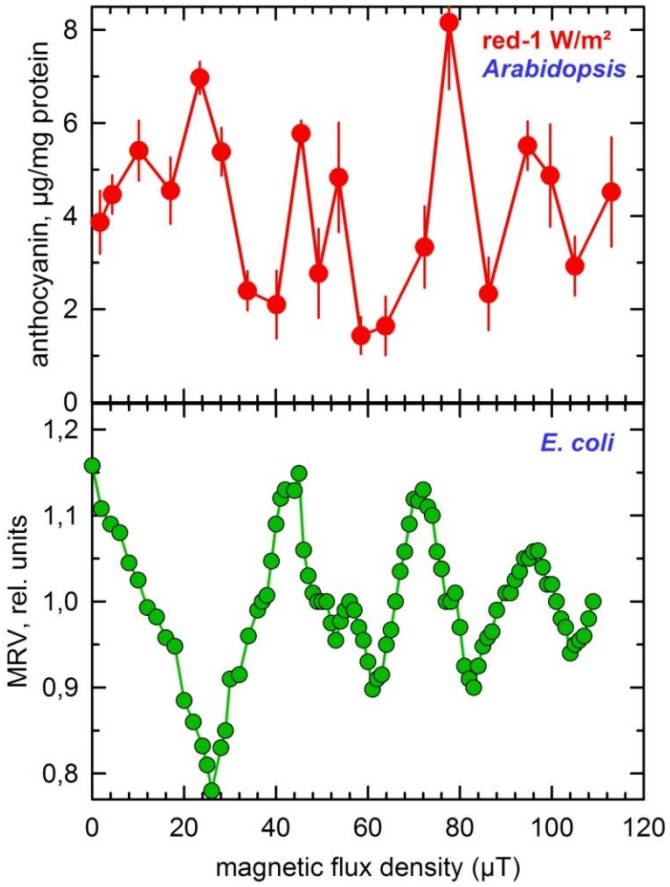

Fig 4.1: Comparison of the effects of magnetic flux density on the photoaccumulation of anthocyanin in *Arabidopsis* with the data obtained by Binhi et al. (2001) in *E. coli*. MRV = Maximum relative viscosity that denotes DNA viscosity.

Belyaev, Binhi and their coworkers elucidated their experimental results on the basis of correlation between their experimental observations and theoretical predictions derived from ion-interference mechanism. This mechanism is based on the interference of the quantum states of the ions involved and links the dissociation probability of ion-protein complexes to magnetic flux density. Ions like Ca^{2+}, Mg^{2+} are required by proteins for their function and they must be bound to proteins at certain specific cavities. Normally the probability cloud of the ion is spread all over the cavity. When such an ion bound protein is subjected to certain magnetic conditions, the probability cloud shrinks and concentrates to a smaller volume, which is comparable to "gate" size. This shrink leads to easy escape of the ion from the cavity. This occurs on account of the interference of the quantum states of the ion. The escape of ion might lead to alterations in the equilibrium of the biological reactions which finally results in the biological effects of the magnetic fields.

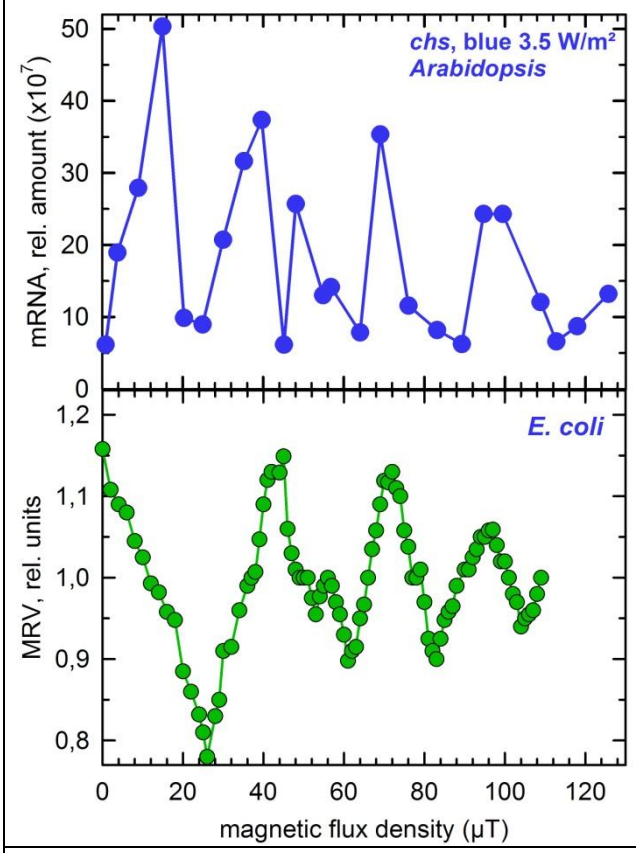

Fig 4.2: Comparison of the effects of magnetic flux density on the expression of the gene chalcone synthase (*chs*) in *Arabidopsis* with the data obtained by Binhi et al. (2001) in *E. coli*. MRV = Maximum relative viscosity that denotes DNA viscosity.

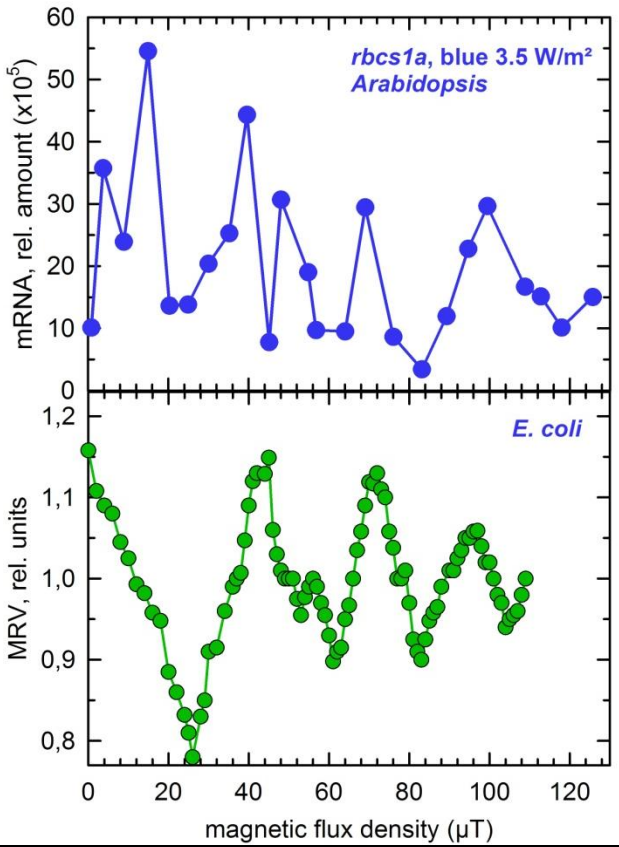

Fig 4.3: Comparison of the effects of magnetic flux density on the expression of the small subunit of RuBisCO gene (*rbcs1a*) that is not related to anthocyanin production, in *Arabidopsis* with the data obtained by Binhi et al. (2001) in *E. coli*. MRV = Maximum relative viscosity that denotes DNA viscosity.

On the basis of theoretical calculations done by Binhi, the probability of escape of the ion from the protein cavity is maximum at zero magnetic flux density. Contrary to the predictions made by the theoretical calculations, the experiments done on *E.coli* reveal multiple maximas in the biological output under the influence of static magnetic fields. The authors explain these additional extrema by assuming that the targets of the static magnetic fields i.e., ion-protein complexes are rotating at a velocity of 18 revolutions per second. Therefore, the ion interference mechanism is able to predict a wave-like dependence of effects of magnetic flux density by incorporation of the angular velocity of the ions in question. The authors propose that the carrier of these rotating ion-protein complexes is RNA polymerase complex, indicating towards the RNA-polymerase and transcription (Binhi et al. 2001).

Molecular rotations have been found to occur in *E. coli* cells. The process of transcription accompanies the relative rotation of DNA and RNA polymerase (Cook et al. 1992) which may result in periodic rotation of RNA polymerase around DNA. Enzymes like topoisomerases may also give rise to additional rotation of DNA. For example, Vacinia topoisomerase I rotates the cleaved DNA strand at a speed of 20 rps, for removing the supercoils from the DNA. On account of the close connection between transcription and supercoiling, the required speed of 18 rps can easily be reached during the transcription for the ion interference model to function. Additionally, metal ions are very significant part of the transcription complex. For example, three Mg^{2+} are required for the formation of active transcription complex (Suh et al. 1992). RNA polymerase of *E.coli* has two Zn^{2+} ions per molecule of enzyme, one in the substrate binding subunit β and the DNA binding template binding subunit β' (Miller et al. 1979).

Theoretical calculations based on the model, using different values of model parameters, were performed for many ions of biological relevance, including Li, K, Na, Mg, Ca, and Zn. Only one combination of ions, namely Ca, Mg and Zn led to a good overlap (coincidence) of peaks and valleys with the experimental data.

$$P_{sum} = P_{Ca} - P_{Mg} + P_{Zn}$$

Other combinations did not fit to the observed graph. The overlap (coincidence) was found to be good when the model parameter, angular velocity (Λ), i.e. 'the same speed of rotation' was chosen for all ion-protein complexes and the considered 'Λ' was 110/s which was equal to 18

rps. The calculated results, for individual ions and for linier superposition of the three ions, have been shown in Fig. 4.4 together with the experimental observations. The minus sign for dissociation probability of Mg^{2+} have been used as they act opposite to Ca^{2+}. Therefore involvement of Mg^{2+} in binding process might lead to opposite biological effects.

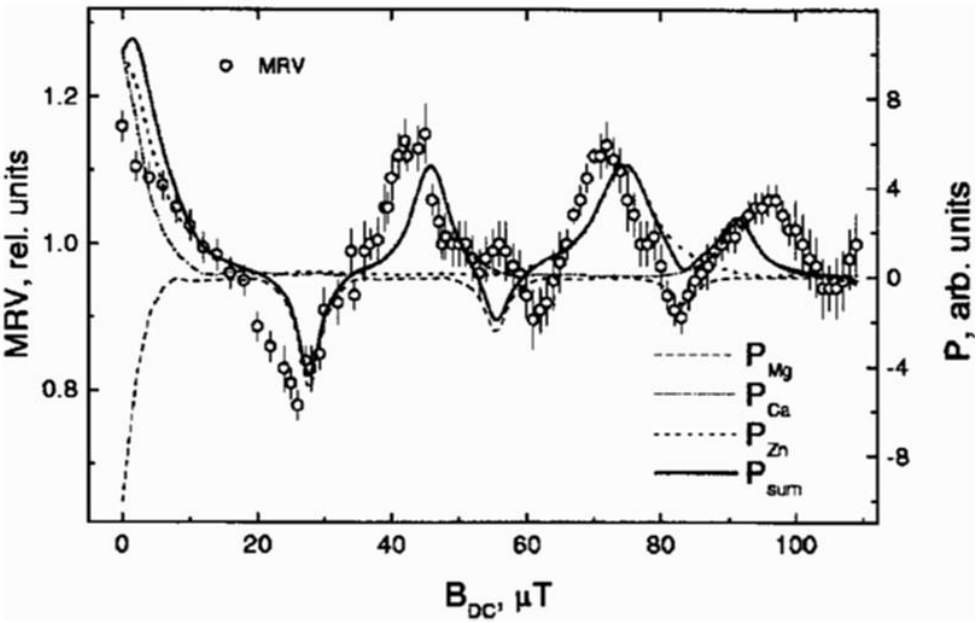

Fig 4.4: Concurrence of the experimental data with results of computer simulations. Points represent experimental observations, which is maximum relative viscosity in cell lysates after exposure of *E. coli* cells to static magnetic field. Lines indicate the magnetic part of dissociation probability of Ca, Mg, Zn and linear superposition of these probabilities (Binhi et al. 2001). MRV = maximum relative viscosity indicating the DNA viscosity, P = dissociation probability of ion-protein complexes.

From figure 4.4 it is clear that there is a good qualitative congruence of the theoretical multipeak curve and the experimental data. Such a coincidence of peak positions between calculated and measured values are the result of the assumption that natural rotations of ion-protein complexes are the prerequisite for the final effects of the magnetic fields.

4.5 Studies on the modulation of gene transcription by static and alternating magnetic fields

There have been various attempts to investigate the effects of static and particularly alternating magnetic fields on gene transcription. The few studies done to demonstrate the effects of static magnetic fields on modulation of gene transcription were done at high magnetic flux densities; they were done without any intention to investigate a stimulus-response relationship. For instance, Worczak et al. in 2007 showed that strong magnetic fields (9 T) affect the function of T7 RNA polymerase, by changing its structure on account of its diamagnetic anisotropic properties. The magnetic fields of a strength more than 15 T were

found to induce the expression of Adh/GUS transgene (alcohol dehydrogenase (*Adh*) gene promoter driving the β-glucuronidase (GUS) gene Reporter) in roots and leaves of transgenic *Arabidopsis* (Paul et al. 2005). In a whole genome microarray study done on bacterium *Shewanella*, it was found that static fields of some 14 T increased or decreased the transcription of 65 genes (Gao et al. 2005). Cultured hippocampal cells of rats exposed to a continuous static magnetic field of 100 mT showed a down-regulation of transcription of many responsive genes, including a striking decrease of mRNA of the transcription factors ALF1 and histone H3.3A (Hirai and Yoneda 2005). In contrast, at somewhat lower static magnetic fields (30 and 80 mT) bone sialoprotein (BSP), a sulfated and phosphorylated glycoprotein expressed in osteoblast-like cells, reacted to a 24 hr lasting exposure to static magnetic fields by increasing the transcript levels (Shimizu et al. 2004). The response requires a region within nucleotides −116 to −84 of the BSP promoter and the response elements FGF2 and the transcription factor-1 motif. These studies also showed that strong static magnetic fields enhanced BSP transcription through a tyrosine kinase-dependent pathway (Shimizu et al. (2004). In case of *E. coli* sigma factor (σ^s) of RNA polymerase has been shown to be required to respond to high strength magnetic fields 5.2–6.1 T (Tsuchiya et al. 1999).

A large number of studies conducted to search for the transcription factors and promoters of the magnetoresponsive genes, however, have been done using alternating magnetic fields. For instance, elevated mRNA transcription was observed, when the extracts of *E. coli* cells and nuclear extracts of *HeLa* cells were exposed to 5-7 minutes of AC fields (1.1 mT, 45Hz) (Tuinstra et al. 1997). Similar work on effects of electromagnetic fields has been done by Blank and Goodman and their co-workers, that was recently reviewed (Blank and Goodman 2008). These authors have provided a very interesting explanation for the cause of effects of AC magnetic fields. They recognized that a specific sequence in the c-myc promotor is required for the responsiveness of the genes to electric and magnetic fields (Lin et al. 1994). This specific sequence was identified to be nCTCTn and was present in multiple copies in promoters of magnetoresponsive genes. The responsiveness of the genes to magnetic fields also depends upon the number of these nCTCTn sequences (Lin et al 2001). Electrons are moving in the DNA and these authors propose that electromagnetic fields potentially accelerate the electron transfers in DNA, which displaces the electrons in hydrogen bonds. This displacement weakens the hydrogen bonds that hold the two polynucleotide chains together, leading to separation of these chains and thus initiating transcription (Blank and

Goodman 2008). The same authors also found that DNA-protein association could be elicited by magnetic fields (Lin et al 1998). We also tried to look for nCTCTn sequences in the upstream sequences of the genes studied by us; however we did not find the same in multiple copies and therefore the explanation given by Blank and Goodman (2008) probably is not relevant for our observations.

There are also reports on transient effects on calcium ion concentration of *Arabidopsis* when they are exposed to weak magnetic fields (65 μT) superimposed with an electromagnetic field having a frequency of 50 Hz (Pazur and Rassadina 2009). These authors explain their results on the basis of the ion-cyclotron resonance which has been described in the introduction in detail. A major drawback of the ion-cyclotron resonance model is that they take into account the presence of ELF magnetic field ($\mathbf{B}_{AC}$) (Extremely low frequency magnetic fields) as well as static magnetic fields ($\mathbf{B}_{DC}$) and their superimposition for the resulting response. Contradictorily, it has been shown that static magnetic fields alone can have the same effects as those observed with simultaneous application of AC/DC magnetic fields (Belyaev et al. 1994). As in our experiments the *Arabidopsis* seedlings were exposed only to static magnetic fields, and the responses were still there, our results cannot be explained on the basis of ion-cyclotron resonance model.

4.6 Magnetohomeostasis

An overview of the effects of the magnetic fields on various parameters of *Arabidopsis* indicates that the magnetic fields exert substantial influence on gene transcription, about 12-fold in case of *rbcl* (Fig. 4.5). However, when we analyze the effects of magnetic fields on some physiological processes that require a group of proteins and thus more genes, the effects become much smaller. Anthocyanin synthesis requires many genes, and the effects that we noticed for anthocyanin accumulation were almost half (about 6-fold in Fig. 4.5) as compared to the effects at the gene transcription level. Going further up at the organismic level, such as seedling growth, which is far more complex and requires the whole set of genes of the genome, the effects of magnetic fields seem to fade away completely, as has been noticed in the stimulus-response curves for hypocotyl length measurement in all the strains of plants studied. Similar observations were made by Harris et al. 2009, when testing the effects of magnetic fields of 50, 100 and 500 μT on hypocotyl growth. Contrary to this, when we examine a related phenomenon like suppression of hypocotyl growth by blue light requiring relatively lesser number of genes, we notice that the magnetic fields are able to influence this

parameter. It is evident from the Fig. 4.5 that such effects are minimal and in the example shown (green) in the figure the magnitude of effect is only about 2.5 fold.

It is reasonable to conclude that magnetoresponsiveness is most pronounced at the gene transcriptional level and that the responses are moderate in processes that require a fairly limited number of genes, e.g. pigment synthesis. However, elaborate and complex responses of *Arabidopsis*, e.g. extension growth of the hypocotyl, that depend upon large networks of different genes and many metabolic pathways, show hardly any effect of magnetic fields. It appears that such a large complex networks with variety of metabolic pathways are able to compensate for the dramatic increases and decreases of the gene transcripts elicited by different magnetic fields.

A somewhat comparable phenomenon has been noticed in bacterium *Shewanella oneidensis*. Investigators observed either up-regulation or down-regulation of 65 genes in the bacterium, when they were exposed to a static magnetic field of 14.1 T, in comparison to untreated cultures. However, such a treatment neither affected their growth in liquid medium nor the number of colony forming units on solid medium (Tsuchiya et al. 1999). It thus appears possible that the perturbances and imbalances created by magnetic fields at the gene transcription level are counterbalanced at the higher level of the metabolic machinery and finally obliterated completely at the organismic level. It may be concluded from these observations that *Arabidopsis* (and possibly even bacteria) manifest on the organismic level the capability of homeostasis, and with respect to magnetic perturbances "magnetohomeostasis".

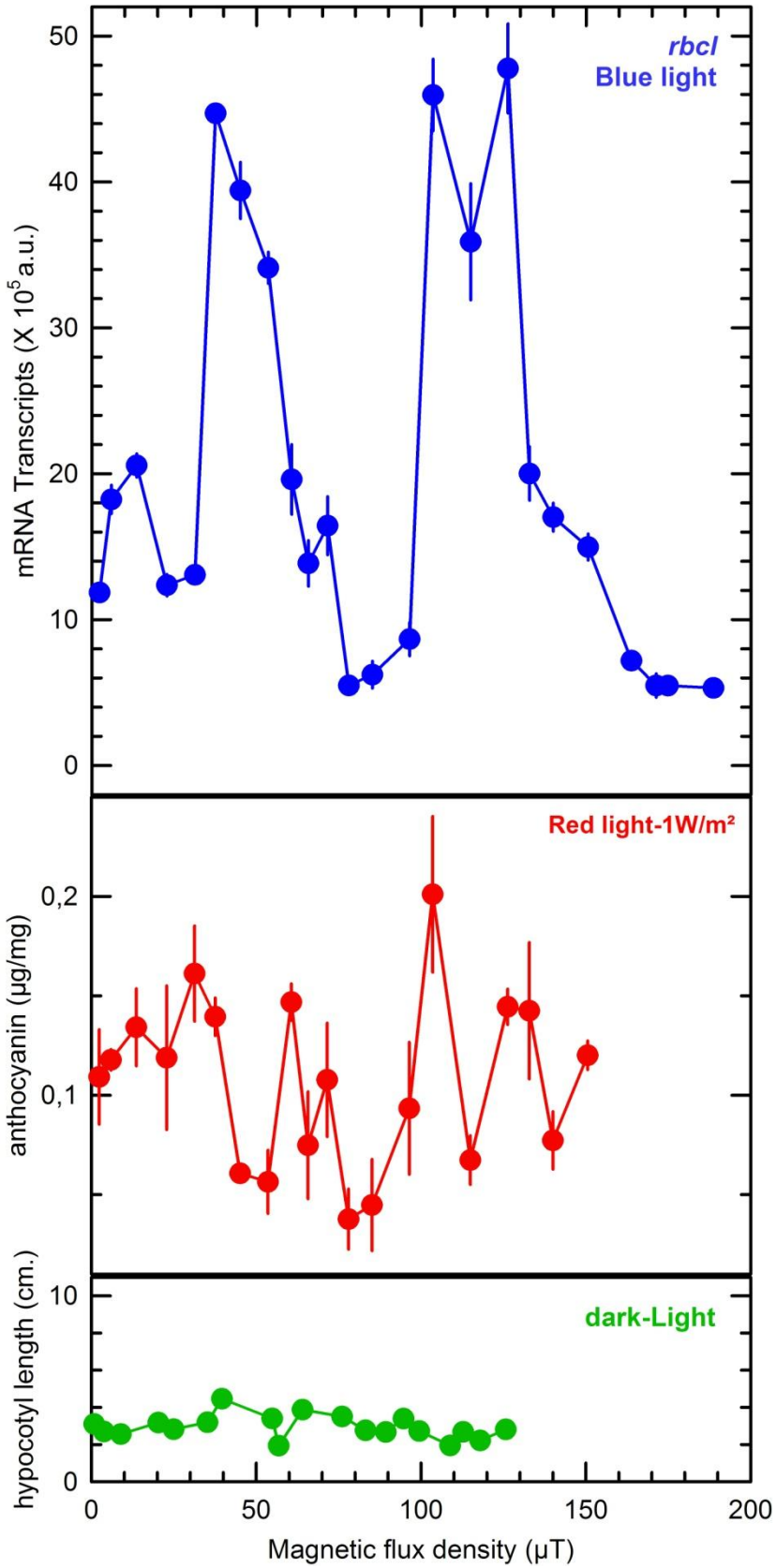

Fig 4.5: Magnetohomeostasis : Comparison of the effects of magnetic flux density on hypocotyl length (green), anthocyanin accumulation (red) and the gene expression (blue). The effects are maximal on gene transcription i.e. about 12-fold (*rbcl*), which are reduced to about 6-fold in case of anthocyanin accumulation and are further reduced to about 2.5-fold in case of suppression of hypocotyl length by blue light in *Arabidopsis*.

4.6 Role of cryptochromes in magnetoreception

Plant cryptochromes are responsible for various significant responses like accumulation of anthocyanins (Ahmad et al. 2007), extension growth of hypocotyls (Ahmad et al. 2002; Goto et al. 1993) which is elicited at the transcriptional level (Batschauer et al. 1996). Cryptochrome also has been targeted as the molecule that acts as receptor for the magnetic fields not only in plants (Ahmad et al. 2007) but also in animals (Ritz et al. 2000, Rodgers and Hore 2009). Strong support for cryptochrome-mediated UV-A/blue light dependent magnetosensitivity has come from the work on *Drosophila* (Gegear et al. 2008). While examining the magnetoresponsiveness in the wild type flies using a binary-choice behavioral assay, authors observed significant naive and trained responses to magnetic fields under white light. In the absence of UV-A/blue light the flies did not respond to the magnetic fields. Gegear and colleagues also tested the magnetosensitivity of CRY-deficient flies. Remarkably these mutant flies did not show any response to magnetic fields. Some indirect evidences supporting cryptochrome as magnetoreceptors have come from experiments on salamanders and bullfrog tadpoles. Experiments with salamanders showed that these animals also have the ability for magnetic field reception which is light dependent. Salamanders could orient normally only in short wavelength (upto 450 nm); when the wavelength was increased beyond 450 nm, they became disoriented. Under the exposure of light of wavelength of 500 nm and above, the animal's disorientation was shifted approximately 90° to the normal (Phillips and Borland 1992b). A comparable light-dependent magnetic 90° shift in orientation behavior has also been observed in bullfrog tadpoles (Phillips et al. 2010). In *Arabidopsis* also, the *Ler* seedlings show the spectacular response to magnetic fields. However, *Arabidopsis cry1cry2* double mutants retain the magnetoresponsiveness. But the magnitudes of effects in *cry1cry2* mutants are diminished to a large extent, indicating the primary role of cryptochromes in magnetoreception in *Arabidopsis* too. The important question that arises now is what is the magnetoreceptor in the CRY-deficient *Arabidopsis*? It is also clear that the absence of cryptochromes in *cry1cry2* mutant leads to changes in the stimulus-response curves. In this regard it is worthwhile to mention that our *cry1cry2* double mutants were not completely devoid of cryptochromes. They have the functional cryptochrome3 (CRY3) and possibly it is this cryptochrome that is mediating the response to magnetic fields in the absence of the two major cryptochromes. In *Drosophila* and in other animals the magnetic response is shown by a complex mechanism involving the cryptochromes in their eyes and the assimilation of the information presented by the cryptochromes by the neuronal network in their brain. In

contrast, *Arabidopsis* lack such a complex mechanism and it is possible that the changes in the magnetic fields are perceived by the CRY3 which results in the response without any complex assimilation of the magnetic information.

A comparison of transcription and translation of the large subunit of RuBisCO (RBCL) in *cry1cry2* double mutants and *phyAphyB* double mutants (Fig. 3.64 and 3.65) reveal that the phytochromes in *cry* mutants actually are masking the effects of magnetic fields. In contrast, the effects in *phy* mutants are far more pronounced under similar conditions, indicating that in the absence of major phytochromes the cryptochromes are more efficient in mediating the effects of magnetic fields. A similar phenomenon is observed in case of hypocotyl length. The cryptochromes in the absence of phytochromes in *phyAphyB* double mutants are able to manifest the effects of magnetic fields even under low fluence rate of blue light (Fig. 3.21), which is not the case in *Ler* seedlings (Fig. 3.13).

In contrast to light-mediated magnetoresponsiveness observed by others, we have observed the effects of magnetic fields even in darkness, though to a lesser extent. It therefore appears likely that magnetic fields elicit a response in *Arabidopsis* by more than one mechanism. The ion-interference mechanism may be responsible for overall transcriptional effects, as we have observed these also in darkness. However, these effects in turn may be magnified in light by the cryptochrome-mediated radical-pair mechanism.

In conclusion the questions raised by Galland and Pazur (2005), presented in the beginning of discussion can be answered partially. With respect to their first question, it is clear by our observations that *Arabidopsis* seedlings are actually responding to the variable magnetic flux densities. With regard to the second question, our results do not provide a clear picture and do not indicate towards any specific magnetoreceptor. The possibility of cryptochrome-mediated magnetoreception in *Arabidopsis* is weakened by the fact that the seedlings are showing the magnetoresponse even in darkness and in red light. On the other hand, as our results show a good correlation with the observations, which were described by Binhi (2001) on the basis of ion-interference mechanism, it appears that the major target of magnetic flux density could be the transcription complex as such. Finally, it seems that there is no obligate requirement of magnetic fields by the *Arabidopsis* seedlings for their survival as they did not show any sign of immortality at flux densities very close to zero magnetic flux density (0.8 μT).

5 References

Ahmad M, Cashmore AR (1993) HY4 gene of *Arabidopsis thaliana* encodes a protein with characteristics of a blue-light photoreceptor. *Nature* 366:162–166

Ahmad M, Cashmore AR (1997) The blue-light receptor cryptochrome 1 shows functional dependence on phytochromes A or phytochromes B in *Arabidopsis thaliana*. *Plant J.* 11:421–427

Ahmad M, Galland P, Ritz T, Wiltschko R, Wiltschko W (2007) Magnetic intensity affects crytochrome-dependent responses in *Arabidopsis thaliana*. *Planta* 225:615–624

Ahmad M, Jarillo JA, Smirnova O, Cashmore AR (1998) The CRY1 blue light photoreceptor of *Arabidopsis* interacts with phytochromes A *in vitro*. *Mol. Cell* 1:939–948

Ahmad M, Lin C, Cashmore AR (1995) Mutations throughout an *Arabidopsis* blue-light photoreceptor impair blue light-responsive anthocyanin accumulation and inhibition of hypocotyls elongation. *Plant J.* 8:653–658 (doi:10.1046/j.1365-313X.1995.08050653.x)

Akoyunoglou G (1964) Effect of a magnetic field on carboxydismutase. *Nature* 202:452–454

Aksenov SI, Bulychev AA, Grunina Tlu, Turovetskii VB (2000) Effect of a low frequency magnetic field on esterase activity and change in pH in wheat germ during swelling of wheat seeds. *Biofizika* 45:737–745

Alexander MP, Doijode SD (1995) Electromagnetic field: a novel tool to increase germination and seedling vigor of conserved onion (*Allium cepa* L.) and rice (*Oryza sativa* L.) seeds with low viability. *Plant Genet Resource Newslett.* 104:1–5

Alipov YD, Belyaev IY (1996) Difference in frequency spectrum of extremely-low-frequency effects on the genome conformational state of AB1157 and EMG2 *E. coli* cells. *Bioelectromagnetics* 17:384–387

Bauréus Koch CLM, Sommarin M, Persson BRR, Salford LG, Eberhardt JL (2003) Interaction between weak low frequency magnetic fields and cell membranes. *Bioelectromagnetics* 24:395–402

Bazylinski AD, Schlezinger DR, Howes BH, Frankel RB, Epstein SS (2000) Occurrence and distribution of diverse populations of magnetic protists in a chemically stratified coastal salt pond. *Chem. Geol*. 169:319–328

Bazylinski DA (2004) Magnetism and Biology: The Magnetotactic Bacteria. *Gravitational and Space Biology Bulletin* 17(2):115–125

Bazylinski DA, Frankel RB, Heywood BR, Mann S, King JW, Donaghay,PL and Hanson AK (1995) Controlled biomineralization of magnetite (Fe_3O_4) and greigite (Fe_3S_4) in a magnetotactic bacterium. *Applied Environmental Microbiology* 61:3232–3239.

Bazylinski, DA and Moskowitz, BM (1997) Microbial biomineralization of magnetic iron minerals: microbiology, magnetism and environmental significance. In: Geomicrobiology: interactions between microbes and minerals. (Banfield JF and Nealson KH, Eds.) Washington, DC: Mineralogical Society of America. *Reviews in Mineralogy* 35:181–223.

Begall S, Červený J, Neef J, Vojtech O, Burda H (2008) Magnetic alignment in grazing and resting cattle and deer. *Proc. Natl. Acad. Sci. USA* 105:13451–13455.

Begall S, Malkemper EP, Červený J, Nemec P, Burda H (2013) Magnetic alignment in mammals and other animals. *Mammalian Biology* 78:10–20

Belova NA, Lednev VV (2001a) Activation and inhibition of the gravitropic response in the flax stem segments exposed to the permanent magnetic field with magnetic density ranging from 0 to 350 T. *Biofizika* 46:118–121

Belyaev IY, Eriksson S, Nygren J, Torudd J, Harms-Ringdahl M (1999a) Effects of ethidium bromide on DNA loop organization in human lymphocytes measured by anomalous viscosity time dependence and single cell gel electrophoresis. *Biophys. Biochem. Acta* 1428:348–356

Belyaev IY, Alipov YD, Harms-Ringdahl M (1999b) Effects of weak ELF on *E. coli* cells and human lymphocytes: role of genetic, physiological and physical parameters, In: F. Bersani, editor. Electricity and magnetism in biology and medicine. NY: Kluwer Academic. 481–484

Belyaev IY, Matronchik AY, Alipov YD (1994) The effect of weak static magnetic and alternating magnetic fields on the genome conformational state of *E. coli* cells: the evidence for model of phase modulation of high frequency oscillations. In: Allen MJ (ed) Charge and field effects in biosystems, vol 4. World Scientific, Singapore. 174–184

Belyavskaya NA (2001) Ultrastructure and calcium balance in meristem cells of pea roots exposed to extremely low magnetic fields. *Adv. Space Res.* 28:645–650

Berden M, Zrimec A, Jerman I (2001) New biological detection system for weak ELF magnetic fields and testing of the paramagnetic resonance model (Lednev 1991). *Electro. Magnetobiol.* 20:27

Binhi VN (1997a) The mechanism of magnetosensitive binding of ions by some proteins. *Biophysics* 42:317–322

Binhi VN (1997b) Interference of ion quantum states within a protein explains weak magnetic field's effect on biosystems. *Electro and Magnetobiology* 16:203–214

Binhi VN, Alipov YD, Belyaev IY (2001) Effect of static magnetic field on *E. coli* cells and individual rotations of ion-protein complexes. *Bioelectromagnetics* 22:79–86

Birk GT, Lesch H, Konz C (2004) Solar wind induced magnetic field around the unmagnetized Earth. Astronomy & Astrophysics DOI, ms nr. Gb091

Blackman CF, Benane SG, Rabinowitz JR, House DE, Jones WT (1985) A role for the magnetic field in the radiation-induced efflux of calcium ions from brain tissue in vitro. *Bioelectromagnetics* 6:327–333

Blakemore RP (1982) Magnetotactic bacteria. *Annu. Rev. Microbiol.* 36:217–238

Blanchard JP, Blackman CP (1994) Clarification and amplification of an ion parametric resonance model for magnetic field interactions with biological systems. *Bioelectromagnetics* 15:217–238

Blank M, Goodman R (1997) Do electromagnetic fields interact directly with DNA? *Bioelectromagnetics* 18:111–115

Blank M, Goodman R (1999) Electromagnetic fields may act directly on DNA. *J. Cell Biochem.* 75:369–374

Blank M, Goodman R (2008) A mechanism for stimulation of biosynthesis by electromagnetic fields: charge transfer in DNA and base pair separation. *J. Cell Physiology* 214(1):20–26

Brown FA Jr, Chow CS (1975) Non-equivalence for bean seeds of clockwise and counterclockwise magnetic motion: a novel terrestrial adaptation? *Biol Bull* 148:370–379

Buchachenko AL, Kuznetsov DA (2008) Magnetic field affects enzymatic ATP synthesis. *J. Am. Chem. Soc.* 130:12868–12869

Busza A, Emery-Le M, Rosbash M, Emery P (2004) Roles of the two *Drosophila* cryptochrome structural domains in circadian photoreception. *Science* 204:1503–1506. (doi:10.1126/science.1096973)

Cain SD, Boles LC, Wang JH, Lohmann KJ (2005) Magnetic orientation and navigation in marine turtles, lobsters and molluscs: concepts and conundrums. *Integr. Comput. Biol.* 45:539–546. (doi:10.1093/icb/45.3.539)

Cashmore AR, Jarillo JA, Wu YJ, Liu D (1999) Cryptochromes: blue light receptors for plants and animals. *Science* 284:760–765. (doi:10.1126/science.284.5415.760)

Casal JJ (2000) Phytochromes, cryptochromes, phototropin: photoreceptor interactions in plants. *Photochem. Photobiol*. 71:1–11

Casal JJ, Mazzella MA (1998) Conditional synergism between cryptochrome 1 and phytochromes B is shown by the analysis of phyA, phyB and hy4 single, double and triple mutants in *Arabidopsis*. *Plant Physiol.* 118:19–25

Celestino C, Picazo ML, Toribio M, Alvare-Ude JA, Bardasano JL (1998) Influence of 50 Hz electromagnetic fields on recurrent embryogenesis and germination of cork oak somatic embryos. *Plant Cell Tissue Organ Cult.* 54:65–69

Chunxiao Xu, Xiao Yin, Yan Lv, Changzhe Wu, Yuxia Zhang, Tao Song (2012) A near-null magnetic field affects cryptochrome-related hypocotyl growth and flowering in *Arabidopsis. Advances in Space Research* 49:834–840

Cook DN, Ma D, Pon NG, Hearst JE (1992) Dynamics of DNA supercoiling by transcription in *Escherichia coli*. *Proc. Nat. Acad. Sci. USA* 89:10603-10607

Cook ES, Smith MJ (1964) Increase of trypsin activity. In: Barnothy MF (ed) Biological effects of magnetic fields. Plenum, New York. 246–254

Cremer-Bartels G, Krause K, Mitoskas G, Brodersen D (1984) Magnetic fields of the earth as additional Zeitgeber for endogenous rhythms? *Naturwissenschaften* 71:567–574

Dayal S, Singh RP (1986) Effect of seed exposure to magnetic field on the height of tomato plants. *Indian J Agric Sci* 56:483–486

Del Giudice E, Fleischmann M, Preparata G, Talpo G (2002) On the "unreasonable" effects of ELF magnetic fileds upon a system of ions. *Bioelectromagnetics* 23:522–530

Drobig J (1988) Saatgut im elektrmagnetischen Feld – zu einigen internationalen Untersuchungen. *Arch Acker-Pflanzenbau Bodenkd* 9:619–626

Durney CH, Rushforth CK, Anderson AA (1988) Resonant AC-DC magnetic fields: calculated response. *Bioelectromagnetics* 9:315–336

Eichwald C, Walleczek J (1996) Model for magnetic field effects on radical pair recombination in enzyme kinetics. *Biophys J.* 71:623–631

El-Din El-Assal S, Alonso-Blanco C, Peeters AJM, Wagemaker C, Weller JL, Koornneef M (2003) The role of cryptochrome 2 in flowering in *Arabidopsis*. *Plant Physiol.* 133:1504–1516. (doi:10.1104/pp.103. 029819)

Endo M, Mochizuki N, Suzuki T, Nagatani A (2007) CRYPTOCHROME2 in vascular bundles regulates flowering in *Arabidopsis*. *Plant Cell* 19:84–93

Exner V, Alexandre C, Rosenfeldt G, Alfarano P, Nater M, Caflisch A, Gruissem W, Batschauer A, and Hennig L (2010) A gain-of-function mutation of *Arabidopsis* CRYPTOCHROME1 promotes flowering. *Plant Physiology* 154:1633–1645

Foley LE, Gegear RJ, Reppert SM (2011) Human cryptochrome exhibits light dependent magnetosensitivity. *Nat. Commun*. 2:356

Fomichjova VM, Govorun RD, Danilov VI (1992a) Proliferation activity and cell reproduction in meristems of root seedlings of pea, flax and lentil under conditions of shielding the geomagnetic field. *Biofizika* 37:745–749

Fomichjova VM, Zaslavsky VA, Govorun RD, Danilov VI (1992b) Dynamics of RNA and protein synthesis in cells of root meristem of pea, flax and lentil under conditions of shielding the geomagnetic field. *Biofizika* 37:750–758

Frankel RB (1990) Iron biominerals: an overview. In: Frankel RB, Blakemore RP (eds) Iron biominerals. Plenum, New York. 1–6

Franklin KA, Larner VS, Whitelam GC (2005) The signal transducing photoreceptors of plants. *Int. J. Dev. Biol*. 49:653–664

Gajdardziska-Josifovska M, McClean RG, Schofield MA, Sommer CV, Kean WF (2001) Discovery of nanocrystalline botanical magnetite. *Eur. J. Mineral* 13:863–870

Gajdardziska-Josifovska M, Schofield MA, Robertson D, McClean R, Kean WF, Sommer C (2002) Botanical iron biominerals: electron diffraction and microscopy identification. *Microsc Microanal* 8:752–753

Galland, P and Pazur A (2005) Magnetoreception in plants: *J. Plant Res*. 118:371–389

Gao W, Liu Y, Zhou J, Pan H (2005) Effects of a strong magnetic field on bacterium *Shewanella oneidensis*: An assessment by using whole genome microarray. *Bioelectromagnetics* 26:558–563

García-Reina F, Arza-Pascual L (2001) Influence of a stationary magnetic field on water relations in lettuce seeds. I: theoretical considerations. *Bioelectromagnetics* 22:589–595

García-Reina F, Pascual L, Fundora IA (2001) Influence of a stationary magnetic field on water relations in lettuce seeds. Part II: experimental results. *Bioelectromagnetics* 22:596–602

Gegear RJ, Casselman A, Waddell S, Reppert SM (2008) Cryptochrome mediate light dependent magnetosensitivity in *Drosophila*. *Nature* 454:367–550. (doi:10.1038/ nature07183)

Giovani B, Byrdin M, Ahmad M, Brettel K (2003) Light-induced electron transfer in a cryptochrome blue-light photoreceptor. *Nature Struct. Biol.* 6:489–490

Gould, J. L., 2008, Animal navigation: the evolution of magnetic orientation. *Curr. Biol.* 18:482-482

Govorun RD, Danilov, Fomichjova VM, Beljavskaja NA, Zinchenko S (1992) Influence of geomagnetic field fluctuations and its shielding on early periods of higher plant germination. *Biofizika* 37:738–744

Grissom CB (1995) Magnetic field effects in biology: a survey of possible mechanisms with emphasis on radical-pair recombination. *Chem. Rev.* 95:3–24

Guo HW, Yang WY, Mockler TC, Lin CT (1998) Regulations of flowering time by *Arabidopsis* photoreceptors. *Science* 279:1360–1363

Halpern MH (1966) Effects of reproducible magnetic fields on the growth of cells in culture. NASDA CR-75121. Natl Astronaut Space Administration, Washington DC.

Halpern MH, van Dyke JH (1996) Very low magnetic fields: biological effects and their implications for space exploration. *Aerospace Med.* 37:281

Harris SR, Henbest KB, Maeda K, Pannel JR, Timmel CR, Hore PJ, Okamoto H (2009) Effect of magnetic fields on cryptochrome dependent responses in *Arabidopsis thaliana*. *J. R. Soc. Interface* 6:1196-1205. (doi:10.1098/rsif.2008.0519)

Hennig L, Funk M, Whitelam GC, Schafer E (1999) Functional interaction of cryptochrome 1 and phytochrome D. *Plant J.* 20:289–294

Heussen C, Nackerdien Z, Smit BJ, Böhm L (1987) Irradiation damage in chromatin isolated from V-79 Chinese hamster lung fibroblasts. *Radiat Res.* 110:84–94

Hirai T, Yoneda Y (2005) Transcriptional regulation of neuronal genes and its effect on neural functions: gene expression in response to static magnetism in cultured rat hippocampal neurons. *J. Pharmacol. Sci.* 98:219–224

Hsu DS, Zhao X, Zhao S, Kazantsev A, Wang RP, Todo T, Wei YF, Sancar A (1996) Putative human blue-light photoreceptors hCRY1and hCRY2 are flavoproteins. *Biochemistry* 35:13871–13877. (doi:10.1021/bi962209o)

Hughes RM, Vrana JD, Song J, Tucker CL (2012) Light-dependent, Dark-promoted interaction between *Arabidopsis* cryptochrome 1 and phytochromes B proteins. *The Journal of Biological Chemistry* 287:22165–22172

Imimoto M, Watanabe K, Fujiwara K (1996) Effects of magnetic flux density and direction of the magnetic field on growth and CO_2 exchange rate of potato plantlets in vitro. In: Kozai T (ed) Proceeding of the international symposium on plant production in closed ecosystem. Narita, Japan

Jiao Y et al. (2003) A genome-wide analysis of blue-light regulation of *Arabidopsis* transcription factor gene expression during seedling development. *Plant Physiol.* 133:1480–1493. (doi:10.1104/pp.103.029439)

Jiao Y, Lau OS, Deng XW (2007) Light-regulated transcriptional networks in higher plants. *Nat. Rev. Genet.* 8:217–230

Johnsen S, Lohmann KJ (2005) The physics and neurobiology of magnetoreception. *Nat. Rev. Neurosci.* 6:703–712. (doi:10.1038/nrn1745)

Johnsen S, Lohmann KJ (2008) Magnetoreception in animals. *Physics today* 29-35

Jones RL (1960) Response of growing plants to a uniform daily rotation. *Nature* 185:775

Juárez MT, Tauxe L, Gee JS, Pick T (1998) The intensity of the earth's magnetic field over the past 160 million years. *Nature* 394:878–881

Kalmijn AJ (1978) Electric and magnetic sensory world of sharks, skates, and rays. In: Hodgson FS, Mathewson RF (eds) Sensory biology of sharks, skates and rays. Office Naval Res, Arlington, VA, 507–528

Kanai S, Kikuno R, Toh H, Ryo H, Todo T (1997) Molecular evolution of the photolyase-blue-light photoreceptor family. *J. Mol. Evol.* 45:535–548. (doi:10.1007/PL00006258)

Kato R (1988) Effects of a magnetic field on the growth of primary roots of *Zea mays*. *Plant Cell Physiol.* 29:1215–1219

Kato R (1990) Effects of very low magnetic field on the gravitropic curvature of *Zea* roots. *Plant Cell Physiol.* 31:565–568

Kato R, Kamada H, Asashima M (1989) Effects of high and low magnetic fields on the growth of hairy roots of *Daucus carota* and *Atropa belladonna*. *Plant Cell Physiol.* 30:605–608

Kim ST, Heelis PF, Sancar A (1992) Energy transfer (deazaflavin → FADH2) and electron transfer (FADH2 → T < > T) kinetics in *Anacystis nidulans* photolyase. *Biochemistry* 31:11244–11248. (doi:10.1021/bi00160a040)

Kirschvink JL, Hagadorn JW (2000) A grand unified theory of biomineralization. In: Bäuerlein E (ed) The bio-mineralization of nano and micro-structure. Wiley, Weinheim, 139–150

Kirschvink JL, Kobayashi-Kirschvink A, Woodford BJ (1992) Magnetite biomineralization in the human brain. *Proc. Natl. Acad. Sci. USA* 89:7683–7687

Klar T, Pokorny R, Moldt J, Batschauer A, Essen LO (2007) Cryptochrome 3 from *Arabidopsis thaliana*: structural and functional analysis of its complex with a folate light antenna. *J. Mol. Biol.* 366:954–964. (doi:10. 1016/j.jmb.2006.11.066)

Kobayashi AK, Kirschvink JL, Nesson MH (1995) Ferromagnetism and EMFs. *Nature* 374:123

König HL, Krueger AP, Lang S, Sönning W (1981) Biological effects of environmental electromagnetism. Springer-Verlag, New York, Heidelberg, Berlin.

Krylov AV, Tarakanova GA (1960) Magnetotropism of plants and its nature. *Plant Physiol.* 7:156–160

Lednev VV (1991) Possible mechanism for the influence of weak magnetic fields on biological systems. *Bioelectromagnetics* 12:71–75

Liboff AR (1985) Geomagnetic cyclotron resonance in living cells. *Bio. Phys.* 9:99–102

Liboff AR (1997) Electric field ion cyclotron resonance. *Bioelectromagnetics* 18:85–87

Liboff AR, Cherng S, Jenrow KA, Bull A (2003) Calmodulin-dependent cyclic nucleotide phosphodiesterase activity is altered by 20 μT magnetostatic fields. *Bioelectromagnetics* 24:2–38

Liedvogel M, Maeda K, Henbest KB, Schleicher E, Simon T, Timmel CR, Hore PJ, Mouritsen H. (2007a) Chemical magnetoreception: bird cryptochrome 1a is

excited by blue light and forms long-lived radical-pairs. PLoS ONE 2(10): e1106. (doi:10.1371/journal.pone.0001106)

Liedvogel M, Mouritsen H (2010) Cryptochromes – a potential magnetoreceptor: what do we know and what do we want to know? *R. Soc. Interface* 7:147–S162 (doi:10.1098/rsif.2009.0411.focus)

Lin C (2000) Photoreceptors and regulation of flowering time. *Plant Physiol.* 123:39–50

Lin H, Goodman R, Shirley-Henderson (1994) Specific region of the c-myc promotor is responsive to electric and magnetic fields. *J. Cell. Biochem.* 54:281–288

Lin H, Han L, Blank M, Head M, Goodman R (1998) Magnetic field activation of protein-DNA binding. *J. Cell. Biochem.* 70:297–303

Lin C, Shalitin D (2003) Cryptochrome structure and signal transduction. *Annu. Rev. Plant Biol.* 54:469–496. (doi:10.1146/annurev.arplant.54.110901.160901)

Lohmann KJ, and Willows AOD **(**1987) Lunar-modulated geomagnetic orientation by a marine mollusk. *Science* 235:331–334

Lowenstam HA, Kirschvink JL (1985) Iron biomineralization a geobiological perspective. In: Kirschvink JL, Jones DS, MacFadden BJ (eds) Magnetite biomineralization and magnetoreception in organisms. Plenum, New York, 3–15

Malhotra K, Kim ST, Batschauer A, Dawut L, Sancar A (1995) Putative blue-light photoreceptors from *Arabidopsis thaliana* and *Sinapis alba* with a high degree of sequence homoloy to DNA photolyase contain the 2 photolyase cofactors but lack DNA-repair activity. *Biochemistry* 34:6892–6899. (doi:10.1021/bi00020a037)

Más P, Devlin PF, Panda S, Kay SA (2000) Functional interaction of phytochrome B and cryptochrome 2. *Nature* 408:207–211

Mathews S, Sharrock RA (1997) Phytochrome gene diversity. *Plant Cell Environ.* 20:666–671

McClean RG, Kean WF (1993) Contributions of wood ash magnetism to archaeomagnetic properties of fire pits and hearths. *Earth Planet Sci. Lett.* 119:387–394

McClean RG, Schofield MA, Kean WF, Sommer CV, Robertson DP, Toth D, Gajdardziska-Josifovska M (2001) Botanical iron minerals: correlation between nanocrystal structure and modes of biological self-assembly. *Eur. J. Mineral* 13:1235–1242

Merrill RT, Merrill, McElhinny (1998) The magnetic field of the Earth: paleomagnetism, the core, and the deep mantle. Academic Press Inc., U.S.

Miller JA, Serio GF, Howard RA, Bear JL, Evans JE, Kimball AP (1979) Subunit localizations of zinc (II) in DNA-dependent RNA polymerase from *Escherichia coli* B. *Biochim. Biophys. Acta* 579:291–297

Miyamoto Y, Sancar A (1998) Vitamin B2-based blue-light photoreceptors in the retinohypothalamic tract as the photoactive pigments for setting the circadian

clock in mammals. *Proc. Natl. Acad. Sci. USA* 95:6097–6102. (doi:10.1073/pnas.95.11.6097)

Mockler TC, Guo H, Yang H, Duong H, Lin C (1999) Antagonistic actions of *Arabidopsis* cryptochromes and phytochrome B in the regulation of floral induction. *Development* 126:2073–2082

Mohr H (1994) Coaction between pigment systems. In Photomorphogenesis in Plants (Kendrick RE, Kronenberg GHM eds.). Dordrecht: Kluwer Academic Publishers. 353–373

Möller A, Sagasser S, Wiltschko W, Schierwater B (2004) Retinal cryptochrome in a migratory passerine bird: a possible transducer for the avian magnetic compass. *Naturwissenschaften* 91:585–588

Mouritsen H, Janssen-Bienhold U, Liedvogel M, Feenders G, Stalleicken J, Dirks P, Weiler R (2004) Cryptochromes and neuronal-activity markers colocalize in the retina of migratory birds during magnetic orientation. *Proc. Nat. Acad. Sci. USA* 101:14294–14299

Mullins JM, Penafiel LM, Juutilainen J, Litovitz TA (1999) Dose-response of electromagnetic field-enhanced ornithine decarboxylase activity. *Bioelectrochem Bioenerg.* 48:193–199

Murray RW (1962) The response of the ampullae of Lorenzini of elasmobranchs to electrical stimulation. *J. Exp. Biol.* 39:119–128

Nanush'yan ER, Murashev VV (2003) Induction of multinuclear cells in the apical meristems of *Allium cepa* by geomagnetic field outrages. *R. J. Plant Physiol.* 50:522–526

Neff MM, Chory J (1998) Genetic interactions between phytochrome A, phytochrome B and cryptochrome 1 during *Arabidopsis* development. *Plant Physiol.* 118:27–36

Negishi Y, Hashimoto A, Tsushima M, Dobrota C, Yamshita M, Nakamura T (1999) Growth of pea epicotyl in low magnetic field: implication for space research. *Adv. Space Res.* 23:2029–2032

Neves M, Glielmo M, Martins JL, Lins U (2003) Interaction of magnetotactic bacteria with flagellated protozoa: induced magnetotaxis. *Acta Microsc.* 12(B):11–12

Nodwell LM, Price NM (2001) Direct use of inorganic colloidal iron by marine mixotrophic phytoplankton. *Limnol. Oceanogr.* 46:765–777

Nossol B, Buse G, Silny J (1993) Influence of weak static and 50 Hz magnetic fields on the redox activity of cytochrome-C oxidase. *Bioelectromagnetics* 14:361–372

Novitsky YI, Novitskaya GV, Kocheshova TK, Nechiporenko GA, Dobrovol'skii MV (2001) Growth of green onions in a weak permanent magnetic field. *Russ. J. Plant Physiol.* 48:709–715

Oliveriusová L, Nemec P, Králová Z, Sedlácekn F (2012) Magnetic compass orientation in two strictly subterranean rodents: learned or species-specific innate directional

preference. *The Journal of Experimental Biology* 215: 3649-3654. (doi:10.1242/jeb.069625)

Palmer JD (1963) Organismic spatial response in very weak spatial magnetic fields. *Nature* 198:1061–1062

Park HW, Kim ST, Sancar A, Deisenhofer J (1995) Crystal structure of DNA photolyase from *Escherichia coli*. *Science* 268:1866–1872. (doi:10.1126/science.7604260)

Payne G, Sancar A (1990) Absolute action spectrum of E-$FADH_2$ and E-$FADH_2$-MTHF forms of *Escherichia coli* DNA photolyase. *Biochemistry* 29:7715–7727. (doi:10.1021/bi00485a021)

Pazur A (2004) Characterization of weak magnetic field effects in an aqueous glutamic acid solution by nonlinear dielectric spectroscopy and voltametry. *Biomagn. Res .Technol.* 2:8–19

Pazur A and Rassadina V (2009) Transient effect of weak electromagnetic fields on calcium ion concentration in *Arabidopsis thaliana*. *Bmc Plant Biology* 9:47

Phillips JB, Borland SC (1992b) Behavioral evidence for use of a light-dependent magnetoreception mechanism by a vertebrate. *Nature* 359:142–144

Phillips JB, Jorge PE, Muheim R (2010) Light-dependent magnetic compass orientation in amphibians and insects: candidate receptors and candidate molecular mechanisms *J. R. Soc. Interface* 7:241–256 (doi: 10.1098/rsif.2009.0459.focus)

Pittman UJ (1963a) Effects of magnetism on seedling growth of cereal plants. *Biomedical Sci. Inst.* 1:117–122

Pittman UJ (1963b) Magnetism and plant growth. I. Effects on germination and early growth of cereal seeds. *Can. J. Plant Sci.* 43:513–51

Pittman UJ (1964) Magnetism and plant growth. II. Effects on root growth of cereals. *Can. J. Plant Sci.* 44:283–287

Pokorny R, Klar T, Hennecke U, Carell T, Batschauer A, Essen LO (2008) Recognition and repair of UV lesions in loop structures of duplex DNA by DASH-type cryptochrome. *Proc. Natl. Acad. Sci. USA* 105:21023–21027

Portaccio M, De Luca P, Durante D, Grano V, Rossi S, Bencivenga U, Lepore M, Mita DG (2005) Modulation of the catalytic activity of free and immobilized peroxydase by extremely low frequency electromagnetic fields: dependence on frequency. *Bioelectromagnetics* 26:145–152

Quail PH (2007a) Phytochrome interacting factors, in Light and Plant Development. (G. Whitelam and K. Halliday eds.). Blackwell Publishing, Oxford. 81–105

Quail PH (2007b) Phytochrome-regulated gene expression. *J. Integr. Plant Biol.* 49:11–20

Quirin S (2005) Solar wind hammers the ozone layer. *Nature* doi:10.1038/news050228-12

Reed JW, Nagatani A, Elich TD, Fagan M, Chory J (1994) Phytochrome A and phytochrome B have overlapping but distinct functions in *Arabidopsis* development. *Plant Physiol.* 104:1139–1149

Ritz T, Adem S, Schulten K (2000) A model for vision-based magnetoreception in birds. *Biophys. J.* 78:707–718

Rockwell NC, Su YS, Lagarias JC (2006) Phytochrome structure and signaling mechanisms. *Annu. Rev. Plant Biol.* 57:837–858

Rodgers CT, Hore PJ (2009) Chemical magnetoreception in birds: The radical pair mechanism. *Proc. Natl. Acad. Sci. USA.* 106:353–360

Rosen AD (1996) Inhibition of calcium channel activation in GH3 cells by static magnetic field. *Biochim. Biophys. Acta* 1282:149–155

Rosen AD (2003) Mechanism of action of moderate-intensity static magnetic fields on biological systems. *Cell Biochem. Biophys.* 39:163–174

Sandweiss J (1990) On the cyclotron resonance model of ion transport. *Bioelectromagnetics* 11:203–205

Scaiano JC, Cozens FL, McLean J (1994) Model for the rationalization of magnetic field effects in vivo. Application of the radical-pair mechanism to biological systems. *Photochem. Photobiol.* 59:585–589

Schaefer E, Nagy F (2006) Photomorphogenesis in Plants and Bacteria. Springer, Dordrecht, The Netherlands

Schulten K, Staerk H, Weller A, Werner HJ, Nickel B (1976) Magnetic field dependence of the geminate recombination of radical ion pairs in polar solvents. *Z. Phys. Chem. NF* 101:371–390

Schulten K, Swenberg CE, Weller A (1978) A biomagnetic sensory mechanism based on magnetic field modulated coherent electron spin motion. *Z. Phys. Chem. NF* 111:1–5

Selby CP, Sancar A (2006) A cryptochrome/photolyase class of enzymes with single-stranded DNA-specific photolyase activity. *Proc. Natl. Acad. Sci. USA* 103:17696–17700

Semm P, Schneider T, Volirath L (1960) Effects of an Earth-strength magnetic field on electrical activity of pineal cells. *Nature* 288:607–615

Shimizu E, Matsuda-Honjyo Y, Samoto H, Saito R, Nakajima Y, Nakayama Y, Kato N, Yamazaki M, Ogata Y (2004) Static magnetic fields-induced bone sialoprotein (BSP) expression is mediated through FGF2 response element and pituitary-specific transcription factor-1 motif. *J. Cell. Biochem.* 91:118–1196

Shinomura T, Nagatani A, Hanzawa A, Kubota M, Watanabe M et al., (1996) Action spectra for phytochrome A and B-specific photoinduction of seed germination in *Arabidopsis thaliana*. *Proc. Natl. Acad. Sci. USA* 93:8129–8133

Smith S (1987) Calcium cyclotron resonance and diatom mobility. *Bioelectromagnetics* 8:215–227

Smith SD, McLeod BR, Liboff AR (1995) Testing the ion cyclotron resonance theory of electromagnetic field interaction with odd and even harmonic tuning for cations. *Bioelectrochem. Bioenerg.* 38:161–167

Solov'yov IA, Chandler DE, Schulten K (2007) Magnetic field effects in *Arabidopsis thaliana* cryptochrome 1. *Biophys. J.* 92:2711–2726. (doi:10.1529/ biophysj.106.097139)

Song SH, Dick B, Penzkofer A, Pokorny R, Batschauer A, Essen O (2006) Absorption and fluorescence spectroscopic characterization of cryptochrome 3 from *Arabidopsis thaliana*. *J. Photochem. Photobiol. B.* 85:1–16

Ssawostin PW (1930a) Magnetophysiologische Untersuchungen. I. Die Rotationsbewegung des Plasmas in einem konstanten magnetischen Kraftfelde. *Planta* 11:683–726

Ssawostin PW (1930b) Magnetwachstumreaktionen bei Pflanzen. *Planta* 12:327–330

Stanewsky R (2002) Clock mechanisms in *Drosophila*. *Cell Tissue Res.* 309:11–26. (doi:10.1007/s00441-002-0569-0)

Suh WC, Leirmo S, Record Jr MT (1992) Roles of $Mg2^{+}$ in the mechanism of formation and dissociation of open complexes between Escherichia coli RNA polymerase and the lambda PR promoter: kinetic evidence for a second open complex requiring $Mg2^{+}$. *Biochemistry* 31:7815–7825

Stivers JT, Harris TK, Mildvan AS (1997) Vaccinia DNA topoisomerase I: evidence supporting a free rotation mechanism for DNA supercoil relaxation. *Biochemistry* 36:5212–5222.

Tarduno JA, Cottrell RD, Watkeys MK, Hofmann A, Doubrovine PV, Mamajek EE, Liu D, Sibeck DG, Neukirch LP, Usui Y (2010) Geodynamo, solar wind and magnetopause 3.4 to 3.45 billion years ago. *Science* 327:1238–1240

Torres de Araujo FF, Pires MA, Frankel RB, Bicudo CEM (1986) Magnetite and magnetotaxis in algae. *Biophys. J.* 50:375–378

Tsuchchiya K, Okuno K, Ano T, Tanaka K, Takahashi H, Shoda M (1999) High magnetic field enhances stationary phase-specific transcription activity of *Escherichia coli*. *Bioelectrochem. Bioenergitics* 40:383–387

Tuinstra R, Greenebaum B, Goodman EM (1997) Effects of magnetic fields on cell-free transcription in *E. coli* and *Hela* extracts. *Bioelectrochem. Bioenergitics* 43:7-12

Usami T, Mochizuki N, Kondo M, Nishimura M, Nagatani A (2004) Cryptochromes and phytochromes synergistically regulate *Arabidopsis* root greening under blue light. *Plant Cell Physiol.* 45:1798–1808

Va´cha M, Drstkova D, Puzova T. (2008) Tenebrio beetles use magnetic inclination compass. *Naturwissenschaften* 95:761–765. (doi:10.1007/s00114-008-0377-9)

Vakharia DN, Davariya RL, Parameswaran M (1991) Influence of magnetic treatment on groundnut yield and yield attributes. *Ind. J. Plant Physiol.* 34:131–136

Wajnberg E, Acosta-Avalos D, Cambraia Alves O, Ferreira de Oliveira J, Srygley RB, Esquivel DMS (2010) Magnetoreception in eusocial insects: an update. *J. R. Soc. Interface* 7:207–225

Walleczek J (1995) Magnetokinetic effects on radical pairs: a paradigm for magnetic field interactions with biological systems at lower than thermal energy. *Adv. Chem.* 250:395–420

Whitelam G, Halliday K (2007) Light and Plant Development. Blackwell Publishing, Oxford.

Wiltschko R, Wiltschko W (1995) Magnetic orientation in animals. Springer, Berlin Heidelberg New York

Wiltschko R, Wiltschko W (2006) Magnetoreception. *BioEssays* 28:157–168.

Wiltschko W (1968) Uber den Einfluss statischer Magnetfelder auf die Zugorientierung der Rotkehlchen (*Erithacus rubecula*). *Z. Tierpsychol.* 25:537–558.

Wiltschko W, Wiltschko R (1981) Disorientation of inexperienced young pigeons after transportation in total darkness. *Nature* 291:433–434

Wiltschko W, Wiltschko R (2005) Magnetic orientation and magnetoreception in birds and other animals. *J. Comp. Physiol. A.* 191:675–693. (doi:10.1007/s00359-005-0627-7)

Worczak M, Wadelton K, Davis JC, Paul AL, Meisel MW (2007) Effects of high magnetic fields on *in vitro* transcription. Proceedings of the 2nd International Workshop on Materials Analysis and proceedings in Magnetic Fields (Grenoble, France) eds. Torbet J, Rivoirard S, Beaugnon E (CNRS Grenoble) 67–70

Yang HQ, Tang, RH Cashmore AR (2001) The signaling mechanism of *Arabidopsis* CRY1 involves direct interaction with COP1. *Plant Cell* 13:2573–2587

Yang HQ, Wu YJ, Tang RH, Liu D, Liu Y, Cashmore AR (2000) The C termini of *Arabidopsis* cryptochromes mediate a constitutive light response. *Cell* 103:815–827. (doi:10.1016/S0092-8674(00)00184-7)

Yoshii T, Ahmad M, Helfrich-Föster C (2009) Cryptochrome mediates light-dependent magnetosensitivity of *Drosophila's* circadian clock. *PLoS Biol.* 7, e1000086. (doi:10.1371/journal.pbio.1000086)

Zhadin MN (2001) Review of Russian literature on biological action of DC and low-frequency AC magnetic fields. *Bioelectromagnetics* 22:27–45

Zhadin MN, Novikov VV, Barnes FS, Pergola NF (1998) Combined action of static and alternating magnetic fields on ionic current in aqueous glutamic acid solution. *Bioelectromagnetics* 19:41–45

Zhu H, Sauman I, Yuan Q, Casselman A, Emery-Le M, Emery P, Reppert SM (2008) Cryptochromes define a novel circadian clock mechanism in monarch butterflies that may underlie sun compass navigation. *PLoS Biol.* 6(1): e4. (doi:10.1371/journal.pbio.0060004)

Acknowledgements

I am indebted to Prof. Dr. Paul Galland for providing me the opportunity to pursue my doctoral research under his able guidance. The valuable discussions with him in person and in the group seminars have immensely helped me to complete this work. Prof. Galland has always been and will remain a motivating force for me in my academic pursuit.

I wish to thank each and every member of the group for providing me a very hospitable atmosphere at the workplace in the very new country. I must mention that in the period of my stay I never felt like a foreign member in the group. I would like to thank Völker Fries for training me in the techniques used in the experimental work. My gratitude is also for Marco Goettig who has been a great helping hand in performing my experiments. My thanks are also due for Dr. Franz Grolig who guided me in the protein quantification methodology. I thank Christian for helping me in my protein quantification experiments. I feel thankful to Michaela for the final formatting of the thesis. I am also thankful to Fan Wu for providing me the photographs to be included in thesis. I thank Sigrid Volk for preparing culture plates for me. I am thankful to Agnes for providing me the seeds of the different strains of *Arabidopsis* on time.

I acknowledge the support of Prof. Dr. Alfred Batschauer and his group members for using his lab and equipments at the time of need. I would also like to thank Prof. Dr. Uwe Maier for granting me the permission to use the mastercycler for performing the quantitative PCR.

I would like to thank Prof. Dr. Paul Galland, Prof. Dr. Alfred Batschauer, Prof. Dr. Hans-Ulrich Mösch and PD Dr. Markus Braun for agreeing to assess my thesis as the committee members.

I wish to thank my parent organization, Kirori Mal College in India for providing me the study leave for pursuing higher studies in Germany. My special thanks to Dr. Anita Kamra from zoology department, in the college and to one of my friend, Dr. Rajbir for motivating me for this work.

Last but not the least I owe my deepest gratitude to my Parents, wife and my children, Khushi and Prasanna without whose blessings and support I could not have pursued my research here.

Erklärung

ich versichere, dass ich meine Dissertation

“Magnetoreception in *Arabidopsis thaliana*: Effects of geomagnetic fields on transcription and translation”

selbstständig, ohne unerlaubte Hilfe angefertigt und mich dabei keiner anderen als der von mir ausdrücklich bezeichneten Quellen und Hilfen bedient habe.

Die Dissertation wurde in der jetzigen oder einer ähnlichen Form noch bei keiner anderen Hochschule eingereicht und hat noch keinen sonstigen Prüfungszwecken gedient.

Marburg, den_____ _____

(Sunil Kumar Dhiman)

Curriculum Vitae

Name: Sunil Kumar Dhiman

Date of Birth: 02.06.1971

Natonality: Indian

Place of Birth: Rae Bareli, India

Parents: Mr. S L Dhiman and Mrs. Sheetla Devi

Married to: Mrs. Sarita Dhiman

Children: Two, Khushi (Daughter-12 yr) and Prasanna (son-7 yr)

Professions Undertaken: Since 2000 as Assistant Professor at BS level I have taught in Department of Botany, University of Delhi, K.M.C., University Enclave, New Delhi and continuing even now. From 1996 to 2000 taught as Assistant Professor at BS and MS level in Department of Botany, CCS University, J. V. C., Baraut, UP, India

Educational Qualification

Doctoral Research: On the topic "Magnetoreception in *Arabidopsis thaliana*: Effects of geomagnetic fields on transcription and translation", in AG Prof. Dr. Paul Galland, Faculty of Biology, Philipps-Universität Marburg, Germany.

M.Phil. (1996): Department of Botany, University of Delhi, New Delhi-110007. India**.**
Title-"Pre-fertilization Aspects of Embryology in Angiosperm: An Overview

M.Sc.(1994): Department of Botany, University of Delhi, New Delhi-110007. India.

B.Sc.(1992): Department of Botany, Kirori Mal College, University of Delhi, New Delhi-110007. India

Scholarships-awarded: Junior Research Fellowship in June-1994 conducted jointly by Council for scientific and Industrial Research (CSIR) and University Grant Commission (UGC) New Delhi, India. The Fellowship is awarded for five years.

Additional Duties: Being members of Sports and Garden Committees at Kirori Mal College, Delhi University, I have worked for the betterment of the Cricket and Badminton as well as the Garden at the College. I have also been Staff Advisor to the Botanical Society,

Kirori Mal College, Delhi University for three years, whereby I have organized various academic and cultural functions.

I have also been Secretary to Residents Welfare Association (RWA) of my Colony in New Delhi for four years. At this position I have worked for the plantation of the colony, improvement of Parks, establishment of playground for kids, improvement of sanitation facilities by the Delhi government and organization of festivals on various occasions within the colony.

Conferences and Workshops

1. Participated in **Botaniker Tagung 2013** held in Berlin, Germany on 30th September - 4th October, and gave a taik.

2. Participated in **12th. Gravimeeting 2011** held in Erlangen, Germany on 1-2 December 2011, and gave an oral presentation.

3. Participated in **Plant Biology Congress 2012** held in Freiburg, Germany on July 29-August 3, 2012

4. Participated in **11th. Gravimeeting 2011** held in Erlangen, Germany on 1-2 December 2011, and gave an oral presentation.

5. Participated in **Botaniker Tagung 2011** held in Berlin, Germany on 18th-23rd September, and presented a poster.

6. Participated in **12th International Symposium on Spin and Magneic Field Effects in Chemistry and Related Phenomena (SCM2011)** held in Noordwijk, Netherlands on 15th- 20th May 2011, and presented a poster.

7. Participated in National Workshop on "**Recent Techniques in Structural and Functional Genomics**", held at CIMAP, Lucknow, UP, India (Dec 15-24, 2006).

8. Attended National symposium on **"Emerging Trends in Biotechnology"** Department of Biochemistry, University of Delhi, DBC, New Delhi (Nov 16-17, 2006).